AD_____

Award Number: DAMD17-00-1-0415

TITLE: Functional Analysis of the ErbB4 Receptor Tyrosine Kinase

PRINCIPAL INVESTIGATOR: David J. Riese II, Ph.D.

CONTRACTING ORGANIZATION: Purdue Research Foundation
West Lafayette, Indiana 47907-1063

REPORT DATE: July 2002

TYPE OF REPORT: Annual Summary

PREPARED FOR: U.S. Army Medical Research and Materiel Command
Fort Detrick, Maryland 21702-5012

REPORT DOCUMENTATION PAGE

Form Approved
OMB No. 074-0188

1. AGENCY USE ONLY (Leave blank)	2. REPORT DATE	3. REPORT TYPE AND DATES COVERED
	July 2002	Annual Summary (1 Jul 01 - 30 Jun 02)

4. TITLE AND SUBTITLE
Functional Analysis of the ErbB4 Receptor Tyrosine Kinase

5. FUNDING NUMBERS
DAMD17-00-1-0415

6. AUTHOR(S)
David J. Riese II, Ph.D.

7. PERFORMING ORGANIZATION NAME(S) AND ADDRESS(ES)
Purdue Research Foundation
West Lafayette, Indiana 47907-1063

E-Mail: driese@purdue.edu

8. PERFORMING ORGANIZATION REPORT NUMBER

9. SPONSORING / MONITORING AGENCY NAME(S) AND ADDRESS(ES)
U.S. Army Medical Research and Materiel Command
Fort Detrick, Maryland 21702-5012

10. SPONSORING / MONITORING AGENCY REPORT NUMBER

11. SUPPLEMENTARY NOTES
Report contains color

12a. DISTRIBUTION / AVAILABILITY STATEMENT
Approved for Public Release; Distribution Unlimited

12b. DISTRIBUTION CODE

13. ABSTRACT ***(Maximum 200 Words)***

My laboratory studies the signaling network comprised of the epidermal growth factor (EGF) family of peptide hormones and the ErbB family of receptor tyrosine kinases. We are particularly interested in elucidating the roles that these hormones and receptors play in breast cancer and in developing reagents that target these hormones and receptor and may be use in diagnosing or treating breast cancer. In part due to the generous support of this career development award, we have made progress on four fronts. (1) We have identified and characterized novel small-molecule EGFR antagonists. Some of these hold promise as breast tumor imaging agents specific for tumors that overexpress EGFR. (2) We have used a set of constitutively active ErbB4 mutants to determine that ErbB4 signaling inhibits the proliferation of non-malignant and malignant human mammary cell lines. This suggests that ErbB4 may be a mammary-specific tumor suppressor. (3) We have characterized four novel EGF family hormones. (4) Moreover, we have made mutants of two EGF family hormones that have enabled us to identify residues critical for activation of ErbB4 signaling by these hormones. These data may lead to synthetic, specific ErbB4 agonists and antagonists that could be used to define the role of ErbB4 in breast cancer or could be used to prevent breast cancer.

14. SUBJECT TERMS	15. NUMBER OF PAGES
Breast Cancer, EGFR, ErbB2, HER2, Neu, ErbB4, EGF, Neuregulins, Heregulins	85
	16. PRICE CODE

17. SECURITY CLASSIFICATION OF REPORT	18. SECURITY CLASSIFICATION OF THIS PAGE	19. SECURITY CLASSIFICATION OF ABSTRACT	20. LIMITATION OF ABSTRACT
Unclassified	Unclassified	Unclassified	Unlimited

Table of Contents

Introduction

My laboratory studies the signaling network comprised of the epidermal growth factor (EGF) family of peptide hormones and the ErbB family of receptor tyrosine kinases. We are particularly interested in elucidating the roles that these hormones and receptors play in breast cancer and in developing reagents that target these hormones and receptor and may be use in diagnosing or treating breast cancer. In part due to the generous support of this career development award, we have made progress on four fronts. (1) We have identified and characterized novel small-molecule EGFR antagonists. Some of these hold promise as breast tumor imaging agents specific for tumors that overexpress EGFR. (2) We have used a set of constitutively active ErbB4 mutants to determine that ErbB4 signaling inhibits the proliferation of non-malignant and malignant human mammary cell lines. This suggests that ErbB4 may be a mammary-specific tumor suppressor. (3) We have characterized four novel EGF family hormones. (4) Moreover, we have made mutants of two EGF family hormones that have enabled us to identify residues critical for activation of ErbB4 signaling by these hormones. These data may lead to synthetic, specific ErbB4 agonists and antagonists that could be used to define the role of ErbB4 in breast cancer or could be used to prevent breast cancer.

Report Body

1. Characterize putative inhibitors of ErbB family receptor tyrosine kinases. We have screened novel quinazolines and novel analogs of lavendustin A to identify novel, specific inhibitors of ErbB family receptor tyrosine kinases. This is the first step in developing novel breast tumor imaging agents that identify the most aggressive tumors by targeting tumor cells that overexpress EGFR or ErbB2. These experiments are being performed in collaboration with the laboratory of Dr. Mark Cushman at Purdue University and the laboratory of Dr. Henry VanBrocklin at the Lawrence Berkeley National Laboratory.

The results of the screen of the lavendustin A analogs are described in a research article published in the *Journal of Medicinal Chemistry*. A copy of this paper can be found in the appendix (Mu, *et al*). The results of the efforts of my laboratory are noted in Figure 1. To summarize, while several of the lavendustin A analogs inhibit the EGFR tyrosine kinase domain, none are as potent as analogs that are in clinical trials as antitumor agents. Furthermore, the lavendustin A analogs exhibit tubulin polymerization IC_{50} values that are approximately the same as the EGFR tyrosine kinase IC_{50} values. Moreover, the DNA synthesis IC_{50} values are approximately the same for MCF-7 (EGF-independent) and MCF-10A (EGF-dependent) cells. These data suggest that the lavendustin A analogs are not specific for the EGFR and hold little promise as tumor imaging agents specific for tumors that overexpress EGFR.

The results of the screen of the quinazolines analogs are shown in Figure 2. To summarize, several quinazolines are potent, specific inhibitors of the EGFR tyrosine kinase domain. We hope that some of these molecules are suitable for radiolabeling with radioactive fluorine or bromine in order to use in positron emission tomography scanning. Dr. Van Brocklin and I preparing a manuscript that describes these results.

These experiments were supported in part by an NIH grant to Dr. Riese (R21CA080770). However, this grant expired 3/31/01 and this grant is not renewable. Dr. VanBrocklin and I were recently awarded an NIH R01 grant to support our efforts to screen additional quinazolines analogs (R01CA079823). Dr. Cushman and I are continuing to apply for grants to support our efforts to screen additional lavendustin A analogs.

2. Define ErbB4 coupling to biological responses. We have generated three constitutively active mutants of the ErbB4 receptor tyrosine kinase that exhibit ligand-independent kinase activity and ligand-independent tyrosine phosphorylation (Figure 3-4). These results are described in a paper that was recently published in *Cell Growth and Differentiation.* A copy of this paper can be found in the appendix (Penington, *et al*). We are expressing these mutants in variety of cellular and organismal contexts to define the functional role of ErbB4 signaling. Obviously, we are particularly interested in the role of ErbB4 signaling in breast cancer.

These mutants, unlike constitutively active ErbB2/HER2/Neu mutants, do NOT cause anchorage independence, increased growth rates, increased saturation densities, or a loss of contact inhibition in a fibroblast cell line (Figures 5-7). These results are described in a paper that was recently published in *Cell Growth and Differentiation.* A copy of this paper can be found in the appendix (Penington, *et al*).

These data suggest that ErbB2 and ErbB4 play distinct roles in mammary tumorigenesis. Indeed, we have generated preliminary data indicating that ErbB4 overexpression in the SKBR3 human breast tumor cell line causes EGF and NRG to inhibit cellular DNA synthesis (Figure 8). Furthermore, the Q646C ErbB4 mutant is coupled to reduced colony formation on plastic in

human mammary and prostate cell lines (Figure 9-12). These data suggest that ErbB4 may be a tumor suppressor and that reduced ErbB4 expression and signaling plays a causative role in mammary and prostate tumorigenesis. Later this summer we intend to submit a paper that describes inhibition of colony formation of prostate tumor cell lines by the constitutively active Q646C ErbB4 mutant. Additional experiments to evaluate the effect of ErbB4 signaling on mammary and prostate tumor cell line proliferation, differentiation, and malignant phenotype are underway. Moreover, in collaboration with Dr. William Muller at McMaster University, we are generating transgenic mice that express the constitutively active ErbB4 Q646C mutants in the mammary epithelium. These mice will enable us to test our ErbB4 tumor suppressor hypothesis *in vivo*.

These experiments are being supported by a USAMRMC BCRP Idea grant (DAMD-17-00-1-0416) and a USAMRMC PCRP New Investigator grant (DAMD-17-02-1-0130) to Dr. Riese as well as by undergraduate research fellowships to Mr. Eric Williams and Ms. Ianthe Bryant.

3. Characterize biological responses to recombinant neuregulins. We have developed a system to express and purify novel recombinant neuregulins, which are members of the EGF family of peptide hormones. We have identified the patterns of ErbB family receptor tyrosine phosphorylation and signaling that are activated by each of these four recombinant neuregulins. Neuregulin 2alpha (NRG2α) and neuregulin2beta (NRG2β) are both ErbB3 agonists, but neuregulin3 (NRG3) and neuregulin4 (NRG4) are not (Figure 13). NRG2β is the most potent ErbB4 agonist whereas NRG3 and NRG4 are more modest ErbB4 agonists and NRG2α is a weak ErbB4 agonist (Figure 14 and Figure 15). These results are described in a manuscript that has been accepted for publication by *Oncogene* pending revision. A copy of the revised manuscript is attached to this document (Hobbs, *et al*). These experiments have been supported in part by an NIH grant to Dr. Riese (R21CA80770). However, this grant expired 3/31/01 and this grant is not renewable.

4. Identify and characterize the ErbB4 binding domain of neuregulin2β (NRG2β). NRG2α and NRG2β are splicing isoforms of the same gene. NRG2β is a potent ErbB4 agonist, whereas NRG2α is not (Figure 14 and Figure 15). We have generated mutants of NRG2α and NRG2β to identify amino acid residues that are sufficient and necessary for activation of ErbB4 signaling by NRG2 isoforms. We have determined that Phe45 of NRG2β is necessary and sufficient for activation of ErbB4 tyrosine phosphorylation by NRG2 (Figure 16 and Figure 17). These results are described in a draft of a manuscript being prepared for submission. These give us important clues as to how binding of EGF family hormones to ErbB4 is specified. These clues are the first steps in our attempts to generate specific synthetic or recombinant ErbB4 agonists and antagonists. Such molecules will be useful in probing ErbB4 function and may be useful in staging or treating breast and prostate cancers. These experiments have been supported in part by an NIH grant to Dr. Riese (R21CA80770) and an NIH sabbatical leave fellowship to Dr. Robert P. Hammer of Louisiana State University (F33CA85049). However, both of these grants have expired and neither is renewable. This fall Dr. Hammer and I intend to submit a new application for an NCI R01 grant to support these experiments.

Key Research Accomplishments

Task 1

- Screened novel lavendustin A analogs for inhibition of EGFR, ErbB2, and ErbB4 tyrosine kinase activity and for inhibition of EGFR coupling to cell proliferation.
- Screened novel quinazolines for inhibition of EGFR, ErbB2, and ErbB4 tyrosine kinase activity and for inhibition of EGFR coupling to cell proliferation.

Task 2

- Generated a set of three constitutively active ErbB4 mutants and demonstrated that these mutants do not malignantly transform the growth of a rodent fibroblast cell line.
- In preliminary experiments, we have demonstrated that one of the constitutively active ErbB4 mutants appears to be coupled to reduced colony formation and reduced cell proliferation in the MCF-10A human mammary epithelial cell line and in a panel of human prostate tumor cell lines. Additional experiments to evaluate the consequences of ErbB4 signaling on cellular function are underway.

Task 3

- Developed a system to express and purify recombinant neuregulins.
- Assayed recombinant neuregulins for stimulation of ErbB family receptor tyrosine phosphorylation.

Task 4

- Generated putative NRG2α "gain of function" and NRG2β "loss of function" mutants.
- Assayed NRG2α and NRG2β mutants for activation of ErbB4 tyrosine phosphorylation.
- Determined that NRG2β Phe45 is sufficient and necessary (within the context of NRG2) for activation of ErbB4 tyrosine phosphorylation.

Reportable Outcomes

Task 1

- We published a manuscript in the *Journal of Medicinal Chemistry* that describes the results of our screen of the lavendustin A analogs. A copy of this publication is included in the appendix of this report (Mu, *et al*).
- We submitted a pending grant application to NCI/NIH for additional funding to support our efforts to synthesize and screen novel lavendustin A analogs (Dr. Mark Cushman, PI).
- An application made to NCI/NIH for additional resources to support our efforts to synthesize and screen novel quinazolines has been selected for funding (R01C079823, Dr. Henry VanBrocklin, PI).

Task 2

- We published a manuscript in *Cell Growth and Differentiation* that describes the construction and analysis of three constitutively active ErbB4 mutants. A copy of this publication is included in the appendix of this report (Penington, *et al*).
- Mr. Desi Penington wrote and successfully defended a master's degree thesis entitled "Construction and analysis of constitutively-active mutants of the ErbB4 receptor tyrosine kinase" that is based on the results of the studies described in Task 2. Mr. Penington received his M.S. in August 2001.
- An application made to the USAMRMC PCRP for a New Investigator Award to support our efforts to analyze ErbB4 function in prostate cancer cells has been selected for funding (DAMD-17-02-1-0130, Dr. David J. Riese II, PI).
- We were awarded an undergraduate research fellowship by the American Association of Colleges of Pharmacy to support our efforts to analyze ErbB4 function in prostate cancer cells (Mr. Eric Williams, PI; Dr. David J. Riese II , mentor).
- We were awarded an undergraduate research fellowship by the American Society for Microbiology to support our efforts to analyze ErbB4 function in breast and prostate cancer cells (Ms. Ianthe Bryant, PI; Dr. David J. Riese II, mentor).

Task 3

- A manuscript that describes the expression and purification of recombinant neuregulins has been accepted pending revision by *Oncogene*. This manuscript also describes the patterns of ErbB family receptor signaling that are stimulated by each neuregulin. A copy of the revised manuscript is included in the appendix of this report (Hobbs, *et al*).

Task 4

- We are preparing a manuscript that describes the construction and functional analyses of the NRG2 mutants.

Conclusions

We have made significant progress on all four of our goals. We have screened and novel quinazolines and lavendustin A analogs to identify EGFR tyrosine kinase inhibitors that may be suitable for the development of novel tumor imaging agents. We are continuing to screen additional quinazolines analogs. We have generated three constitutively-active ErbB4 mutants that are enabling us to elucidate ErbB4 functions. We have characterized the patterns of ErbB family receptor signaling stimulated by four novel NRGs. We have identified an amino acid residue critical for activation of ErbB4 signaling by NRG2.

References

Hobbs, S.S., S.L. Coffing, A.T.D. Le, E.M. Cameron, E.E. Williams, M. Andrew, E.N. Blommel, R.P. Hammer, H. Chang, and D.J. Riese II. "Neuregulin isoforms exhibit distinct patterns of ErbB family receptor activation." *Oncogene*, accepted pending revision.

Mu, F., S.L. Coffing, D.J. Riese II, R.L. Geahlen, P. Verdier-Pinard, E. Hamel, J. Johnson, and M. Cushman. "Design, synthesis, and biological evaluation of a series of Lavendustin A analogues that inhibit EGFR and Syk tyrosine kinases, as well as tubulin polymerization." *J. Med. Chem.* **44**: 441-452 (2001).

Penington, D.J., I. Bryant, and D.J. Riese II. "Constitutively active ErbB4 and ErbB2 mutants exhibit distinct biological activities." *Cell Growth Diff.* **13**: 247-256 (2002).

Appendices: List of Documents (75 pages total)

Figure 1. *Lavendustin A analogs inhibit tubulin polymerization, syk tyrosine kinase activity, EGFR tyrosine kinase activity, and MCF-7 (EGF-independent) and MCF-10A (EGF-dependent) cellular DNA synthesis.* From Mu, *et al., J. Med. Chem.* **44**: 441-452 (2001).

Figure 2. *Quinazoline analogs specifically inhibit EGFR tyrosine kinase activity, and MCF-10A (EGF-dependent) cellular DNA synthesis.* Unpublished data.

Figure 3. *Q646C, H647C, and A648C ErbB4 mutants exhibit increased kinase activity.* From Penington, *et al., Cell Growth Diff.* **13**: 247-256 (2002).

Figure 4. Q646C, H647C, and A648C mutants exhibit increased *ligand-independent tyrosine phosphorylation.* From Penington, *et al., Cell Growth Diff.* **13**: 247-256 (2002).

Figure 5. *Constitutively active ErbB4 mutants do not cause anchorage independence in FR3T3 fibroblasts.* From Penington, *et al., Cell Growth Diff.* **13**: 247-256 (2002).

Figure 6. *Constitutively active ErbB4 mutants do not cause an increase in growth rate or an increase in saturation density in fibroblasts.* From Penington, *et al., Cell Growth Diff.* **13**: 247-256 (2002).

Figure 7. *Constitutively active ErbB4 mutants do not cause a loss of contact inhibition (focus formation) in FR3T3 fibroblasts.* From Penington, *et al., Cell Growth Diff.* **13**: 247-256 (2002).

Figure 8. *Overexpression of ErbB4 in the SKBR3 human breast tumor cell line causes inhibition of DNA synthesis by EGF and NRG.* Unpublished data.

Figure 9. *The constitutively active Q646C ErbB4 mutant inhibits colony formation by the MCF10A human mammary epithelial cell line.* Unpublished data.

Figure 10. *The constitutively active Q646C ErbB4 mutant inhibits colony formation by the DU145 human prostate tumor cell line.* Unpublished data.

Figure 11. *The constitutively active Q646C ErbB4 mutant inhibits colony formation by the PC-3 human prostate tumor cell line.* Unpublished data.

Figure 12. *The constitutively active Q646C ErbB4 mutant specifically inhibits colony formation by the PC-3, DU-145, and LNCaP human prostate tumor cell lines.* Unpublished data.

Figure 13. *Neuregulin (NRG) isoforms differentially activate receptor tyrosine phosphorylation in the BaF3/ErbB2+ErbB3 cell line.* From Hobbs, *et al.*, *Oncogene*, accepted pending revisions.

Figure 14. *In the CEM/ErbB4 cell line, Neuregulin2beta (NRG2β) is a potent ErbB4 ligand, but Neuregulin2alpha (NRG2α) is not.* From Hobbs, *et al.*, *Oncogene*, accepted pending revisions.

Figure 15. *Increased Neuregulin2alpha (NRG2α) concentrations stimulate minimal ErbB4 tyrosine phosphorylation in the CEM/ErbB4 cell line.* From Hobbs, *et al.*, *Oncogene*, accepted pending revisions.

Figure 16. *NRG2β Phenylalanine 45 is necessary for stimulation of ErbB4 tyrosine phosphorylation.* Unpublished data.

Figure 17. *Substitution of phenylalanine for lysine at position 45 is sufficient to cause NRG2α to stimulate abundant ErbB4 tyrosine phosphorylation.* Unpublished data.

Journal Article (36 pages). Hobbs, S.S., S.L. Coffing, A.T.D. Le, E.M. Cameron, E.E. Williams, M. Andrew, E.N. Blommel, R.P. Hammer, H. Chang, and D.J. Riese II. "Neuregulin isoforms exhibit distinct patterns of ErbB family receptor activation." *Oncogene*, accepted pending revision.

Journal Article (12 pages). Mu, F., S.L. Coffing, D.J. Riese II, R.L. Geahlen, P. Verdier-Pinard, E. Hamel, J. Johnson, and M. Cushman. "Design, synthesis, and biological evaluation of a series of Lavendustin A analogues that inhibit EGFR and Syk tyrosine kinases, as well as tubulin polymerization." *J. Med. Chem.* **44**: 441-452 (2001).

Journal Article (10 pages). Penington, D.J., I. Bryant, and D.J. Riese II. "Constitutively active ErbB4 and ErbB2 mutants exhibit distinct biological activities." *Cell Growth Diff.* **13**: 247-256 (2002).

Figure 1. *Lavendustin A analogs inhibit tubulin polymerization, syk tyrosine kinase activity, EGFR tyrosine kinase activity, and MCF-7 (EGF-independent) and MCF-10A (EGF-dependent) cellular DNA synthesis.*

Table 1. Inhibitory Activities of Lavendustin A Analogues

	IC_{50} (μM)					
compd	MGM[a]	tubulin[b]	Syk[c]	EGFR[d]	MCF 7 DNA[e]	MCF 10A DNA[f]
4	8.7 ± 0.4	3.6 ± 0.7	NT[g]	14 ± 10	11 ± 4	14 ± 3
13a	14.8 ± 1.4	3.6 ± 1	5	10 ± 4	9 ± 3	11 ± 3
13b	0.35 ± 0.05	4.0 ± 0.4	5	4 ± 2	12 ± 4	10 ± 1
13c	7.6 ± 2.4	4.2 ± 0.5	45	35 ± 11	7 ± 0	6 ± 1
13d	15.4	4.2 ± 0.8	50	>100	14 ± 0	11 ± 2
13e	15.5	3.2 ± 0.6	25	8 ± 4	17 ± 4	17 ± 4
13f	10.0 ± 0.95	3.2 ± 0.7	25	46 ± 13	13 ± 2	9 ± 1
13g	20.4	4.5 ± 1	5	~300	16 ± 3	15 ± 2
13h	19.5	2.1 ± 0.4	1.5	>50	14 ± 3	16 ± 5
13i	16.0 ± 0.55	3.6 ± 0.3	NT[g]	15 ± 6	11 ± 5	7 ± 0.0
13j	13.2 ± 0.3	5.0 ± 1	28	1 ± 0.4	2 ± 0.2	2 ± 0.0
13k	2.7 ± 0.1	>40	50	35 ± 7	1 ± 0.3	3 ± 0.5
13l	11.2 ± 1.4	5.3 ± 0.9	8	4 ± 1	10 ± 3	6 ± 0.7
13m	>100	>40	NT[g]	[h]	>50	NT[g]
18a	8.8 ± 1.7	6.2 ± 1	18	>100	16 ± 3	34 ± 9
18b	6.4 ± 1.2	4.9 ± 0.9	5	>200	3 ± 1	7 ± 2
18c	5.3 ± 1.3	5.7 ± 1	35	33 ± 5	0.4 ± 0.1	3 ± 1
23	12.1 ± 0.8	6.9 ± 1	>100	~500	5 ± 1	6 ± 1

[a] Mean graph midpoint for growth inhibition of all human cancer cell lines (approximately 55) successfully tested. [b] IC_{50} values for inhibition of tubulin polymerization. [c] IC_{50} values for in vitro inhibition of Syk PTK. [d] IC_{50} values for inhibition of EGFR phosphorylation in BaF3 mouse lymphoid cells. [e] IC_{50} values for inhibition of DNA synthesis in MCF 7 cells. [f] IC_{50} values for inhibition of DNA synthesis in MCF-10A cells. [g] NT, not tested. [h] Stimulates EGFR tyrosine phosphorylation.

From Mu, *et al.*, *J. Med. Chem.* **44**: 441-452 (2001).

Figure 2. *Quinazoline analogs specifically inhibit EGFR tyrosine kinase activity, and MCF-10A (EGF-dependent) cellular DNA synthesis.*

Quinazolines

IC50 values for receptor phosphorylation (kinase activity) (all values in nM)

Drug	EGFR Ptyr Mean ± S.E.	n	ErbB2 Ptyr Mean ± S.E.	n	ErbB4 Ptyr Mean ± S.E.	n
JL1089	11.1 ± 3.7 (n= 3)	######## ± ######## (n= 0)	######## ± ######## (n= 0)
JL1093	2.1 ± 0.5 (n= 10)	143 ± 52 (n= 6)	49 ± 16 (n= 4)
JL2027	3.2 ± 0.8 (n= 10)	215 ± 87 (n= 5)	50 ± 19 (n= 4)
JL2037	>50 ± ###### (n= 2)	######## ± ###### (n= 0)	######## ± ###### (n= 0)
JL2049	10.9 ± 2.6 (n= 6)	######## ± ######## (n= 0)	######## ± ######## (n= 0)
JL2059	4.6 ± 2.0 (n= 4)	69 ± 10 (n= 3)	59 ± 29 (n= 5)
JL2063	6.6 ± 1.6 (n= 7)	231 ± 92 (n= 5)	>100 ± ###### (n= 3)
JL2067	19.1 ± 2.9 (n= 5)	######## ± ######## (n= 0)	######## ± ######## (n= 0)
JL2103	0.8 ± 0.2 (n= 4)	######## ± ######## (n= 0)	######## ± ######## (n= 0)
JL2107	1.2 ± 0.2 (n= 4)	######## ± ######## (n= 0)	######## ± ######## (n= 0)
JL4083	12.8 ± 3.5 (n= 5)	######## ± ######## (n= 0)	######## ± ######## (n= 0)
JL4085	143 ± 21 (n= 4)	######## ± ######## (n= 0)	######## ± ######## (n= 0)
JL4125	112.2 ± ###### (n= 5)	######## ± ######## (n= 0)	######## ± ######## (n= 0)
JL4127	47.5 ± 8.7 (n= 5)	######## ± ######## (n= 0)	######## ± ######## (n= 0)
JL4137	6.2 ± 2.3 (n= 4)	######## ± ######## (n= 0)	######## ± ######## (n= 0)
JL4139	5.1 ± 1.1 (n= 4)	######## ± ######## (n= 0)	######## ± ######## (n= 0)
AG02142	4.9 ± 0.4 (n= 3)	######## ± ######## (n= 0)	######## ± ######## (n= 0)
AG02143	6.1 ± 0.5 (n= 3)	######## ± ######## (n= 0)	######## ± ######## (n= 0)

Quinazolines

IC50 values for cellular DNA synthesis (all values in nM)

Drug	MCF-10A Mean ± S.E.	n	MCF-7 Mean ± S.E.	n	MDA-MB-231 Mean ± S.E.	n	MDA-MB-453 Mean ± S.E.	n	MCF-7/MCF-10A Ratio
JL1089	585 ± 108 (n= 7)	2433 ± 61 (n= 6)	2217 ± 164 (n= 6)	1725 ± 232 (n= 4)	0.2406
JL1093	316 ± 61 (n= 13)	1600 ± 100 (n= 3)	4600 ± 1021 (n= 3)	3200 ± 1320 (n= 3)	0.1966
JL2027	78 ± 12 (n= 25)	1695 ± 169 (n= 15)	1911 ± 156 (n= 9)	1557 ± 260 (n= 7)	0.0461
JL2037	>3000 ± ###### (n= 5)	######## ± ###### (n= 0)	######## ± ######## (n= 0)	######## ± ######## (n= 0)	#VALUE!
JL2049	489 ± 87 (n= 7)	>7000 ± ###### (n= 6)	>9000 ± ###### (n= 5)	3067 ± 491 (n= 5)	0.0974
JL2059	153 ± 25 (n= 12)	1571 ± 263 (n= 7)	3100 ± 650 (n= 5)	1925 ± 544 (n= 4)	0.0974
JL2063	186 ± 23 (n= 11)	1453 ± 88 (n= 3)	2533 ± 145 (n= 3)	2633 ± 944 (n= 3)	0.1311
JL2067	1634 ± 160 (n= 3)	4717 ± 1014 (n= 6)	5140 ± 1308 (n= 5)	2175 ± 709 (n= 4)	0.3464
JL2103	175 ± 24 (n= 3)	1962 ± 387 (n= 5)	######## ± ######## (n= 0)	######## ± ######## (n= 0)	0.0875
JL2107	106 ± 8 (n= 3)	1038 ± 402 (n= 4)	######## ± ######## (n= 0)	######## ± ######## (n= 0)	0.0996
JL4083	179 ± 31 (n= 6)	1950 ± 260 (n= 4)	######## ± ######## (n= 0)	######## ± ######## (n= 0)	0.0916
JL4085	141 ± 17 (n= 16)	1101 ± 656 (n= 3)	######## ± ######## (n= 0)	######## ± ######## (n= 0)	0.1281
JL4125	402 ± 85 (n= 7)	2100 ± 265 (n= 3)	######## ± ######## (n= 0)	######## ± ######## (n= 0)	0.1916
JL4127	425 ± 103 (n= 8)	1525 ± 125 (n= 4)	######## ± ######## (n= 0)	######## ± ######## (n= 0)	0.2764
JL4137	118 ± 16 (n= 7)	1445 ± 414 (n= 3)	######## ± ######## (n= 0)	######## ± ######## (n= 0)	0.0815
JL4139	96 ± 16 (n= 16)	1620 ± 254 (n= 5)	1900 ± 213 (n= 6)	867 ± 371 (n= 3)	0.0607
AG02142	128 ± 25 (n= 4)	######## ± ######## (n= 0)	######## ± ######## (n= 0)	######## ± ######## (n= 0)	#DIV/0!
AG02143	135 ± 32 (n= 4)	######## ± ######## (n= 0)	######## ± ######## (n= 0)	######## ± ######## (n= 0)	#DIV/0!

Unpublished data

Figure 3. *Q646C, H647C, and A648C ErbB4 mutants exhibit increased kinase activity.*

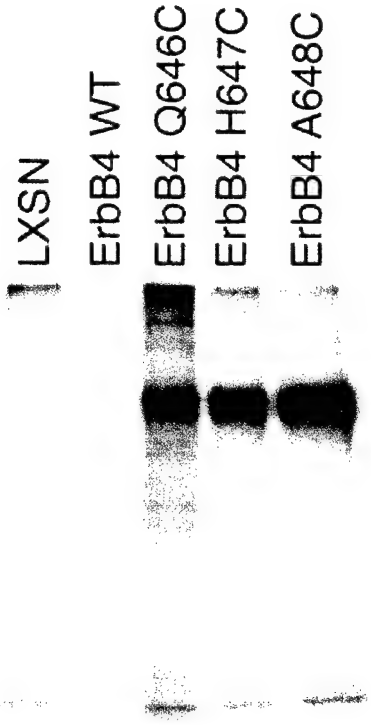

Fig. 2. Q646C, H647C, and A648C mutants exhibit increased *in vitro* kinase activity. Equal amounts of protein lysates (1000 μg) from PA317 cells that stably express wild-type ErbB4 or the ErbB4 mutants (Q646C, H647C, and A648C) were immunoprecipitated with an anti-ErbB4 rabbit polyclonal antibody. Lysates from PA317 cells that express the LXSN vector served as the negative control. Kinase reactions were performed on the immunoprecipitates in the presence of [γ-^{32}P]ATP. The products were resolved by SDS-PAGE. The gel was dried overnight and exposed to X-ray film for ~20 h to visualize the products of the kinase reactions.

From Penington, *et al.*, *Cell Growth Diff.* **13**: 247-256 (2002).

Figure 4. *Q646C, H647C, and A648C mutants exhibit increased ligand-independent tyrosine phosphorylation.*

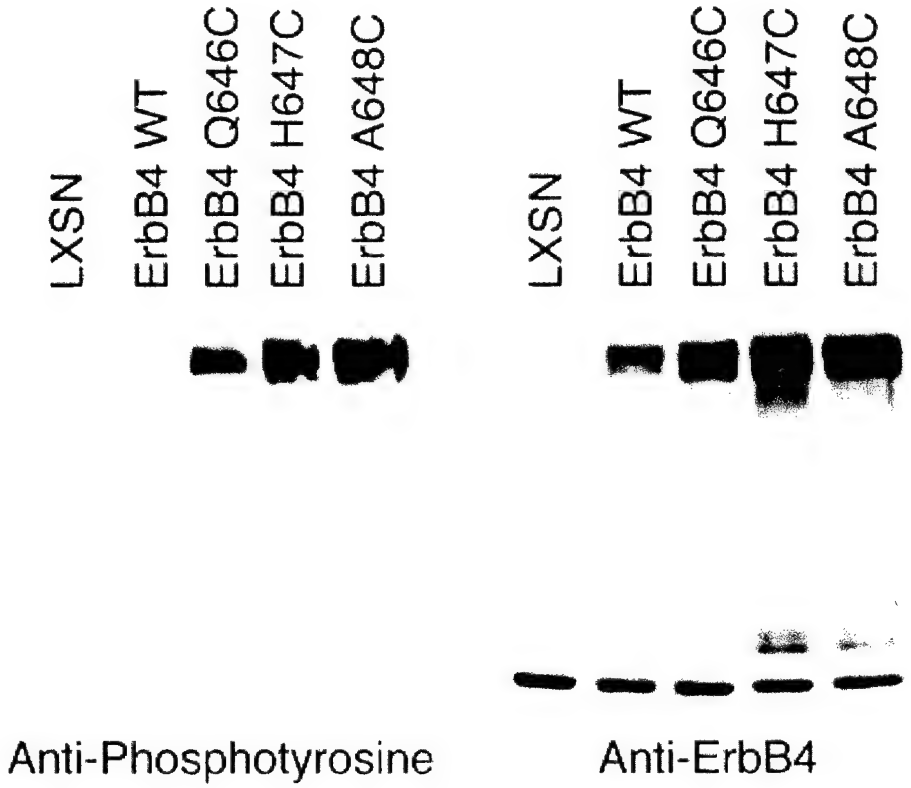

Fig. 1. ErbB4 mutants are constitutively tyrosine phosphorylated. ErbB4 expression and tyrosine phosphorylation were assayed in PA317 cells infected with retroviruses that direct the expression of wild-type ErbB4 or the ErbB4 mutants. Cells infected with the LXSN recombinant retrovirus vector control served as the negative control. Lysates were prepared from each of the cell lines, and ErbB4 was immunoprecipitated from 1000 μg of each lysate. Samples were resolved by SDS-PAGE, electroblotted to nitrocellulose, and immunoblotted with an anti-phosphotyrosine antibody (*left panel*). The blot was then stripped and probed with an anti-ErbB4 rabbit polyclonal antibody (*right panel*). The band at the *top* of the blots represents ErbB4.

From Penington, *et al.*, *Cell Growth Diff.* **13**: 247-256 (2002).

Figure 5. *Constitutively active ErbB4 mutants do not cause anchorage independence in FR3T3 fibroblasts.*

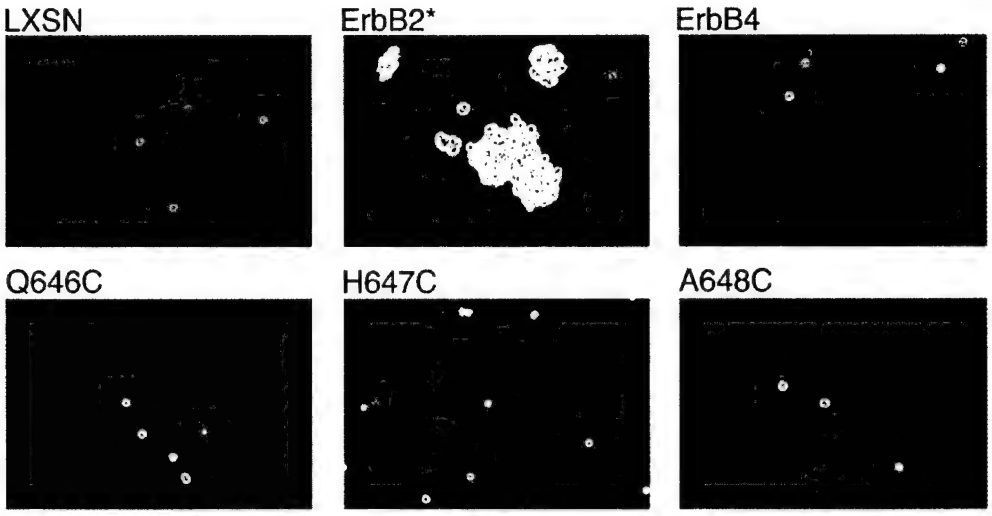

Fig. 4. Constitutively active ErbB4 receptors do not induce growth in semisolid medium. FR3T3 cells that stably express the LXSN vector control, the constitutively active ErbB2 mutant (ErbB2*), wild-type ErbB4, or the constitutively active ErbB4 mutants (Q646C, H647C, and A648C) were seeded in semisolid medium at a density of $2 \cdot 10^4$ cells/ml in 60-mm dishes. The cells were incubated for 10 days, after which images were recorded by photomicroscopy. Images shown are representative of those obtained in three independent experiments.

From Penington, *et al.*, *Cell Growth Diff.* **13**: 247-256 (2002).

Figure 6. *Constitutively active ErbB4 mutants do not cause an increase in growth rate or an increase in saturation density in fibroblasts.*

Fig. 5. Constitutively active ErbB4 mutants do not increase the growth rate of FR3T3 fibroblasts. FR3T3 cells that express the LXSN vector control, the constitutively active ErbB2* mutant, wild-type ErbB4, or the constitutively active ErbB4 mutants (Q646C, H647C, and A648C) were plated at a density of $2 \cdot 10^4$ cells in 60-mm dishes (700 cells/cm^2) and were incubated for 1–10 days. Cells were counted daily to assess growth rates and saturation densities. The means for three independent experiments; *bars*, SE.

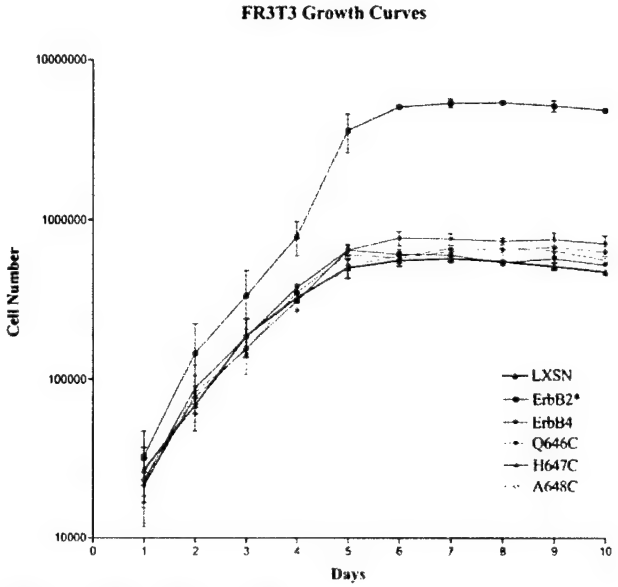

From Penington, *et al.*, *Cell Growth Diff.* **13**: 247-256 (2002).

Figure 7. *Constitutively active ErbB4 mutants do not cause a loss of contact inhibition (focus formation) in FR3T3 fibroblasts.*

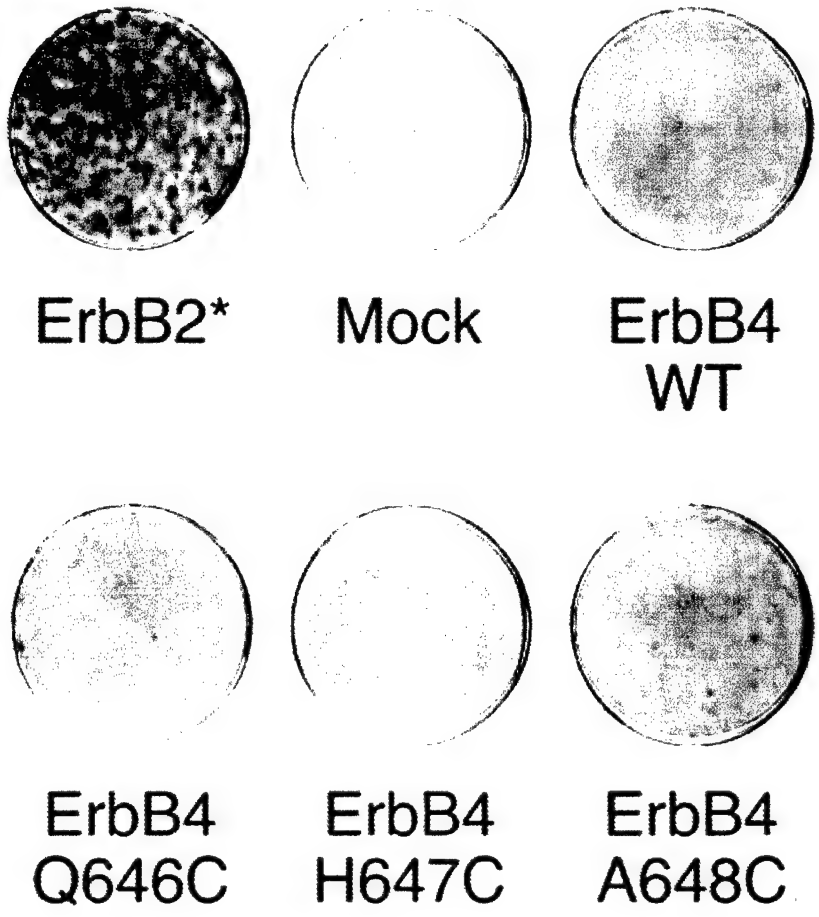

Fig. 3. Constitutively active ErbB4 receptors do not induce a loss of contact inhibition. FR3T3 fibroblasts infected with the LXSN (vector control) retrovirus, the wild-type ErbB4 retrovirus, the constitutively active ErbB2* retrovirus, or the constitutively active ErbB4 mutant retroviruses were assayed for loss of contact inhibition (focus formation).

From Penington, *et al.*, *Cell Growth Diff.* **13**: 247-256 (2002).

Figure 8. *Overexpression of ErbB4 in the SKBR3 human breast tumor cell line causes inhibition of DNA synthesis by EGF and NRG.*

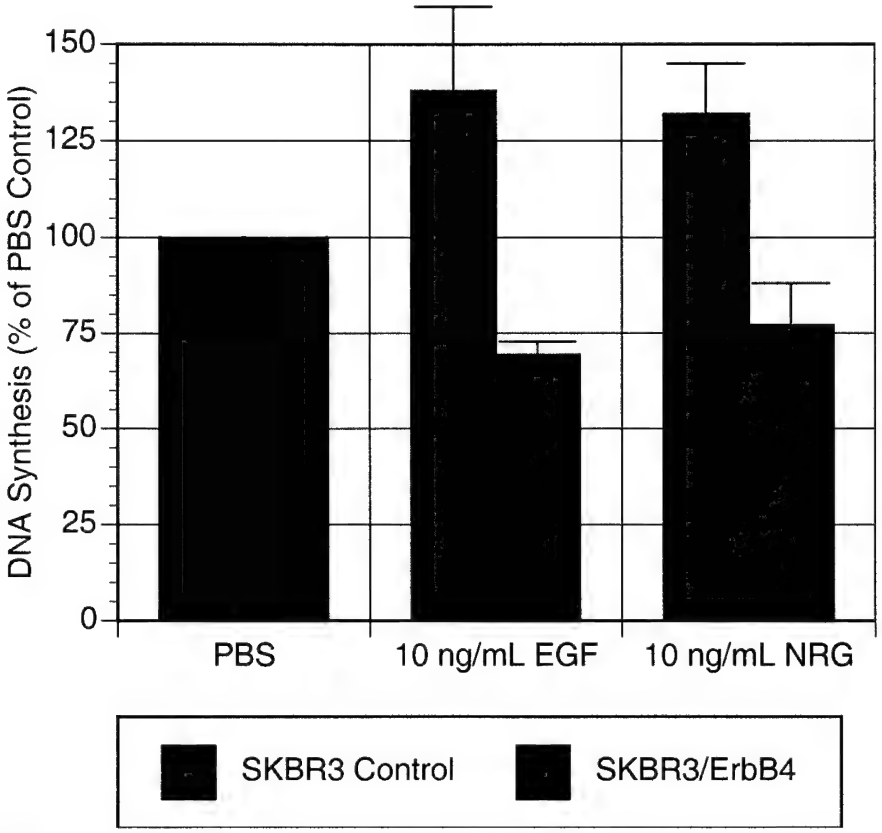

Unpublished data.

Figure 9. *The constitutively active Q646C ErbB4 mutant inhibits colony formation by the MCF10A human mammary epithelial cell line.*

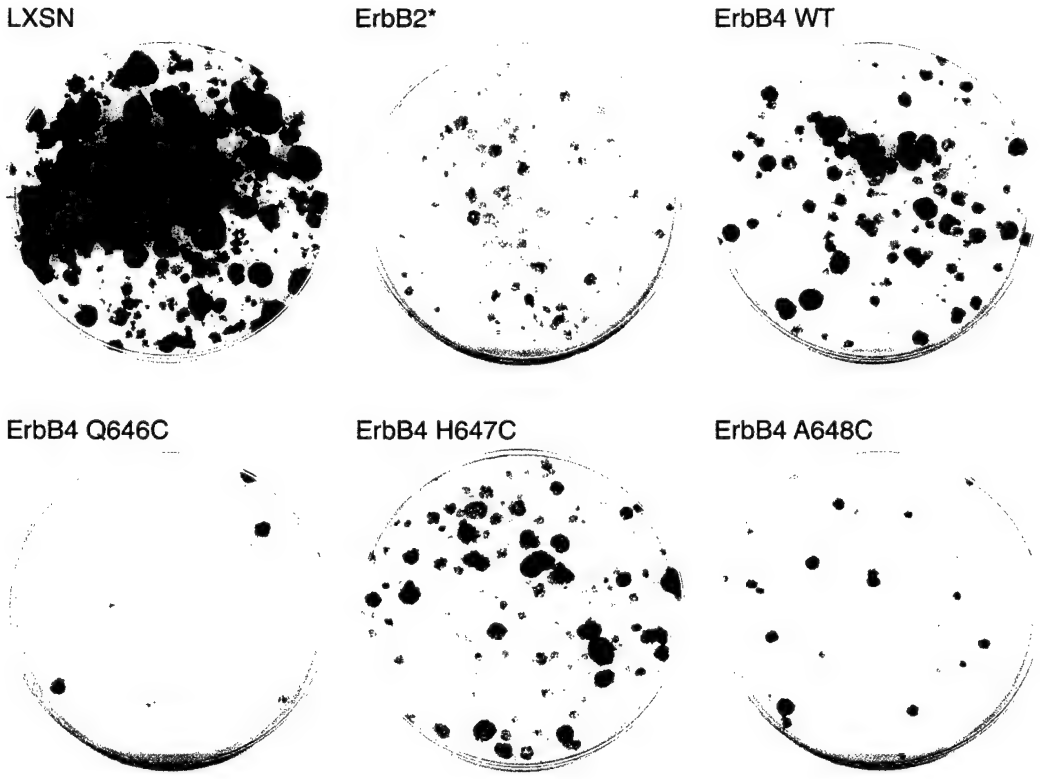

Unpublished data.

Figure 10. *The constitutively active Q646C ErbB4 mutant inhibits colony formation by the DU145 human prostate tumor cell line.*

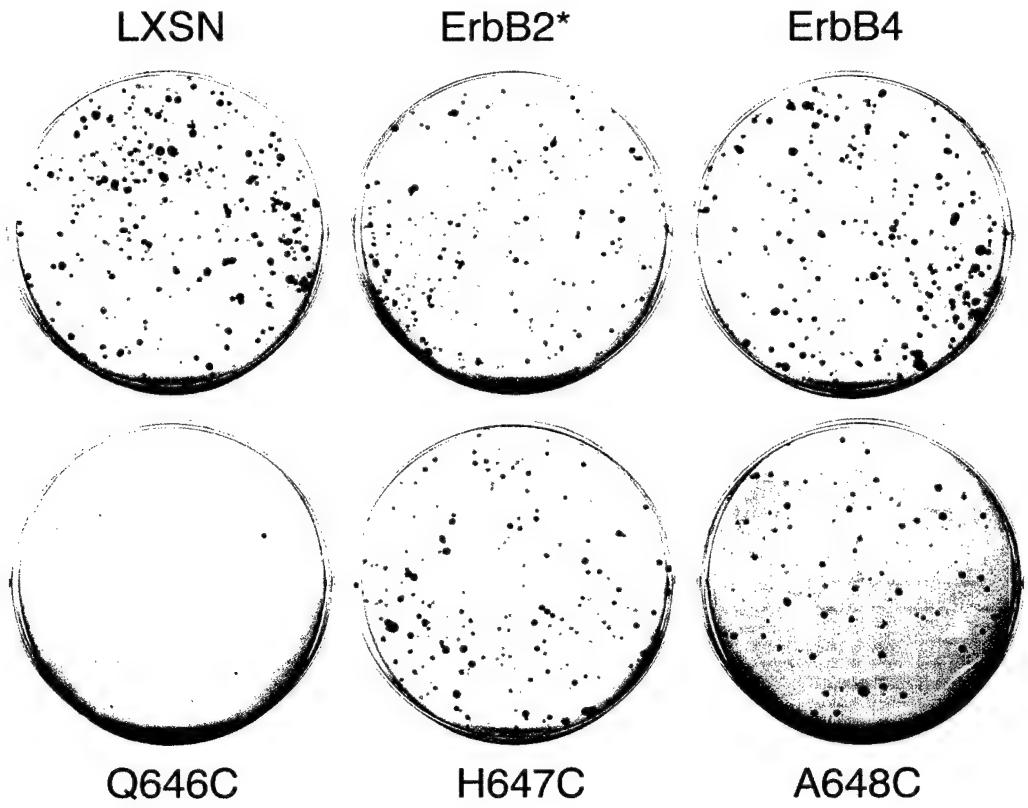

Unpublished data.

Figure 11. *The constitutively active Q646C ErbB4 mutant inhibits colony formation by the PC-3 human prostate tumor cell line.*

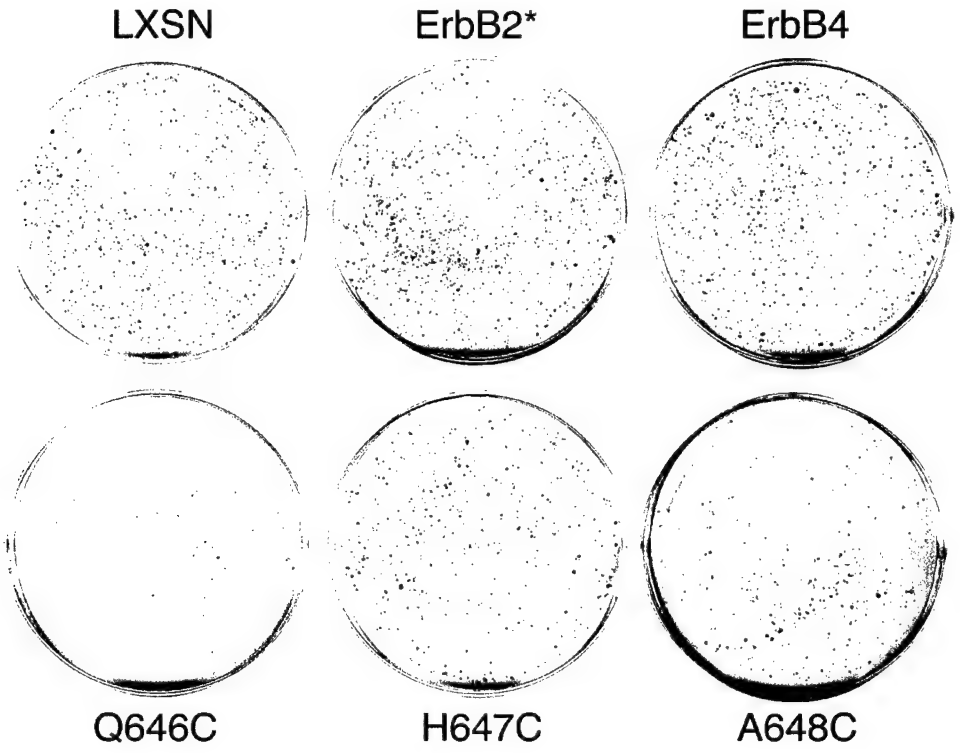

Unpublished data.

Figure 12. *The constitutively active Q646C ErbB4 mutant specifically inhibits colony formation by the PC-3, DU-145, and LNCaP human prostate tumor cell lines.*

Viral Titers (CFU/mL)

C127

plated	7/11/01	7/25/01	10/4/01	11/7/01	11/30/01	7/3/02	7/10/02	7/12/02
LXSN	3.00E+05	4.10E+05	1.50E+05	2.00E+05		5.24E+06	7.04E+05	6.24E+05
ErbB2*	6.30E+04	9.60E+04	2.60E+04	5.40E+04		7.14E+05	3.71E+05	4.14E+05
LXSN/ErbB4	6.50E+04	1.40E+05	2.30E+04	4.10E+04	5.30E+04	1.45E+05	1.90E+05	1.17E+05
646	7.60E+04	1.10E+05	2.10E+04	5.00E+04	4.60E+04	4.95E+05	6.92E+05	1.18E+06
647	8.50E+04	1.20E+05	2.90E+04	5.10E+04		4.72E+05	7.51E+05	1.08E+06
648	1.50E+04	3.10E+04	1.70E+04	1.60E+04		7.41E+04	1.41E+05	2.82E+05
646 Kin-				1.40E+04	1.10E+04			

PC-3

plated	7/11/01	7/25/01	10/4/01	11/7/01	11/30/01	7/3/02	7/10/02	7/12/02
LXSN	1.10E+04	9.00E+04	4.00E+04	1.25E+05		2.57E+05	2.24E+05	3.32E+04
ErbB2*	3.60E+03	1.10E+04	8.10E+03	2.30E+04		3.64E+04	6.99E+04	3.18E+04
LXSN/ErbB4	4.40E+03	1.70E+04	1.40E+04	2.60E+04	3.50E+04	1.53E+04	4.27E+04	9.23E+03
646	2.70E+02	9.70E+02	5.30E+02	2.10E+03	4.20E+03	1.60E+04	4.06E+04	1.15E+04
647	4.50E+03	1.90E+04	1.10E+04	3.40E+04		3.89E+04	1.01E+05	8.06E+04
648	1.20E+03	5.60E+03	2.00E+03	5.90E+03		1.28E+04	2.61E+04	1.72E+04
646 Kin-				9.70E+03	4.30E+04			

DU-145

plated	7/11/01	7/25/01	10/4/01	11/7/01	11/30/01	7/3/02	7/10/02	7/12/02
LXSN	1.90E+04	1.20E+05	2.50E+04	2.00E+04		2.47E+05	1.31E+05	1.96E+04
ErbB2*	4.70E+03	2.20E+04	4.20E+03	2.30E+03		5.20E+04	6.85E+04	3.91E+04
LXSN/ErbB4	4.90E+03	2.20E+04	8.70E+03	2.00E+03	7.60E+03	1.07E+04	4.08E+04	5.67E+03
646	1.30E+02	5.00E+02	1.30E+02	1.30E+02	6.00E+02	7.00E+03	4.13E+03	2.70E+03
647	4.50E+03	1.80E+04	2.70E+03	2.30E+03		6.03E+04	3.43E+04	6.00E+04
648	1.30E+03	8.00E+03	2.50E+03	5.70E+02		1.51E+04	1.29E+04	1.89E+04
646 Kin-				9.00E+02	3.70E+03			

LNCaP

plated					11/30/01	7/3/02	7/10/02	7/12/02
LXSN								
ErbB2*								
LXSN/ErbB4					2.10E+04			
646					2.00E+03			
647								
648								
646 Kin-					1.90E+04			

Viral Titer Ratios

PC-3/C127 Ratio

7/11/01	7/25/01	10/4/01	11/7/01	11/30/01	7/3/02	7/10/02	7/12/02	Average	Std. Error	n
3.7	22.0	26.7	62.5		4.9	31.8	5.3	22.4	8.0	7
5.7	11.5	31.2	42.6		5.1	18.8	7.7	17.5	5.4	7
6.8	12.1	60.9	63.4	66.0	10.6	22.4	7.9	31.3	9.6	8
0.4	0.9	2.5	4.2	9.1	3.2	5.9	1.0	3.4	1.1	8
5.3	15.8	37.9	66.7		8.2	13.5	7.5	22.1	8.5	7
8.0	18.1	11.8	36.9		17.2	18.5	6.1	16.6	3.9	7
			69.3	390.9				230.1	160.8	2

DU145/C127 Ratio

7/11/01	7/25/01	10/4/01	11/7/01	11/30/01	7/3/02	7/10/02	7/12/02	Average	Std. Error	n
6.3	29.3	16.7	10.0		4.7	18.6	3.1	12.7	3.5	7
7.5	22.9	16.2	4.3		7.3	18.5	9.4	12.3	2.6	7
7.5	15.7	37.8	4.9	14.3	7.4	21.5	4.8	14.2	4.0	8
0.2	0.5	0.6	0.3	1.3	1.4	0.6	0.2	0.6	0.2	8
5.3	15.0	9.3	4.5		12.8	4.6	5.6	8.1	1.6	7
8.7	25.8	14.7	3.6		20.4	9.1	6.7	12.7	3.0	7
			6.4	33.6				20.0	13.6	2

LNCaP/C127 Ratio

11/30/01	7/3/02	7/10/02	7/12/02	Average	Std. Error	n
				#DIV/0!	#DIV/0!	0
				#DIV/0!	#DIV/0!	0
39.6				39.6	#DIV/0!	1
4.3				4.3	#DIV/0!	1
				#DIV/0!	#DIV/0!	0
				#DIV/0!	#DIV/0!	0
172.7				172.7	#DIV/0!	1

Unpublished data.

Figure 13. *Neuregulin (NRG) isoforms differentially activate receptor tyrosine phosphorylation in the BaF3/ErbB2+ErbB3 cell line.*

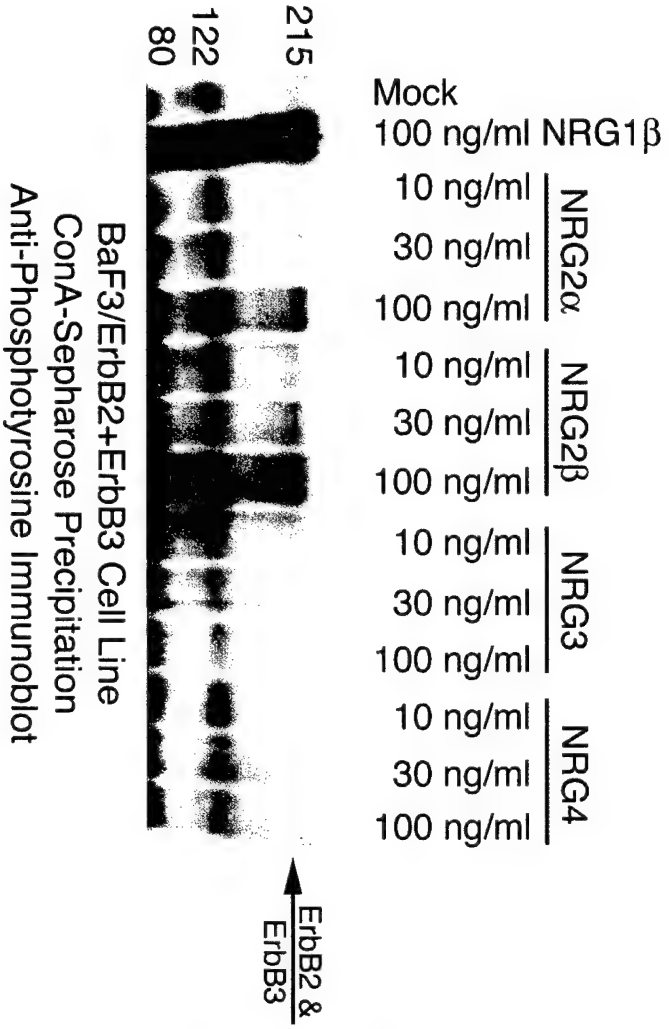

From Hobbs, *et al.*, *Oncogene*, accepted pending revisions.

Figure 14. *In the CEM/ErbB4 cell line, Neuregulin2beta (NRG2β) is a potent ErbB4 ligand, but Neuregulin2alpha (NRG2α) is not.*

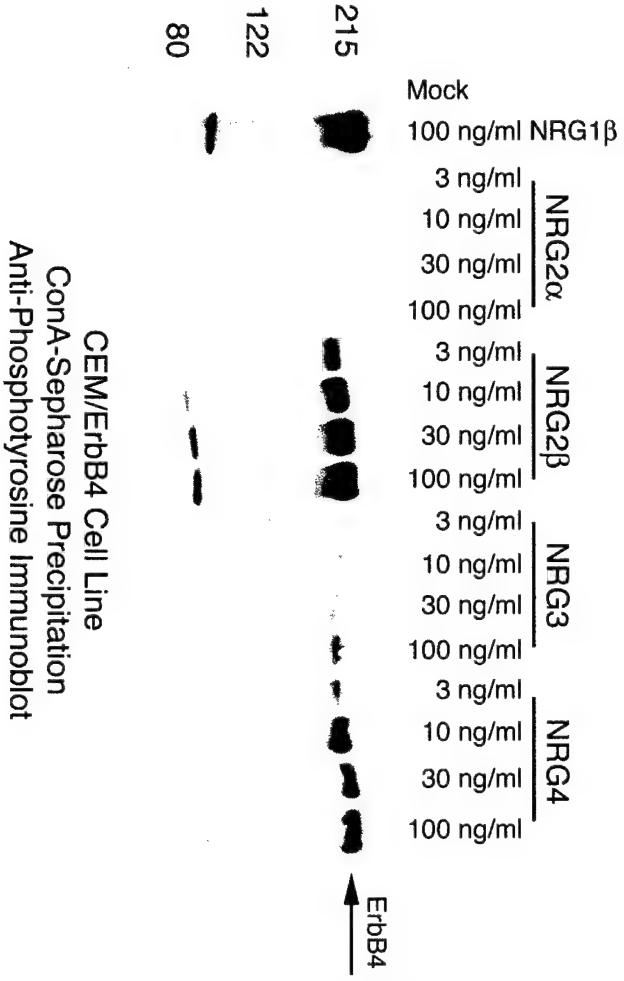

From Hobbs, *et al.*, *Oncogene*, accepted pending revisions.

Figure 15. *Increased Neuregulin2alpha (NRG2α) concentrations stimulate minimal ErbB4 tyrosine phosphorylation in the CEM/ErbB4 cell line.*

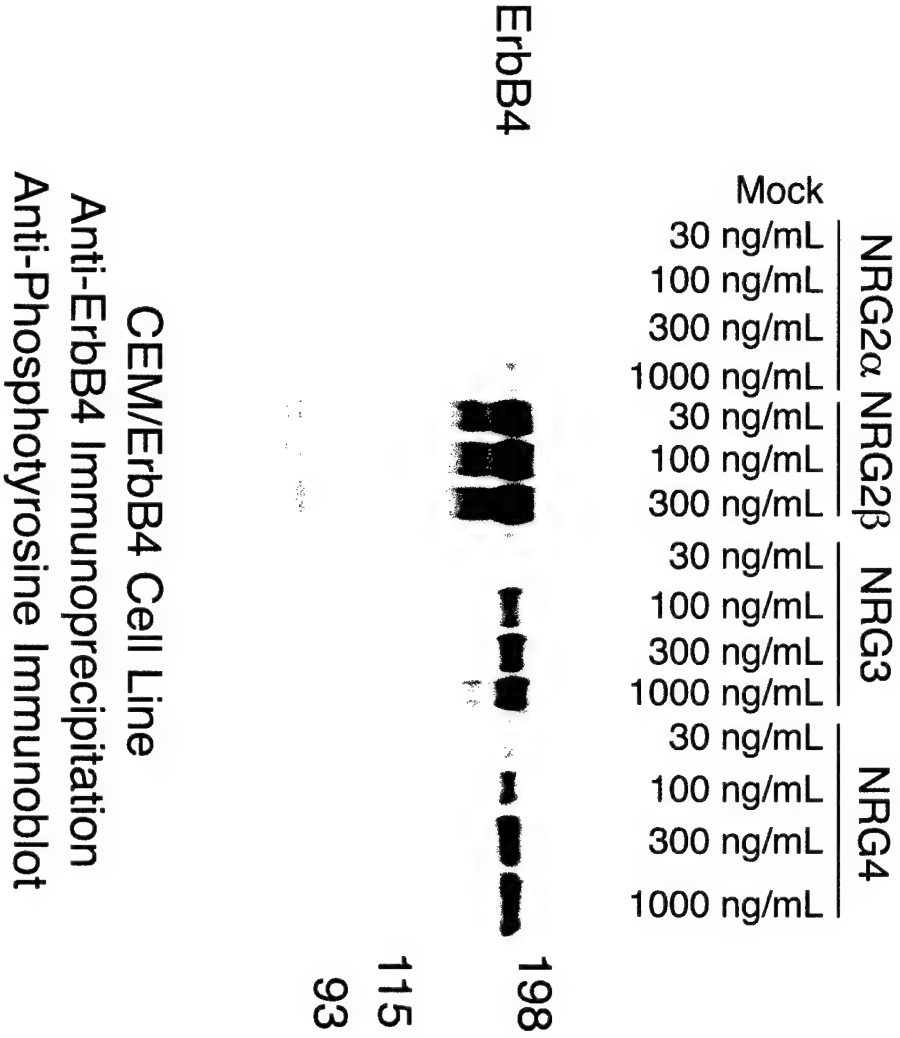

From Hobbs, *et al.*, *Oncogene*, accepted pending revisions.

Figure 16. *NRG2β Phenylalanine 45 is necessary for stimulation of ErbB4 tyrosine phosphorylation.*

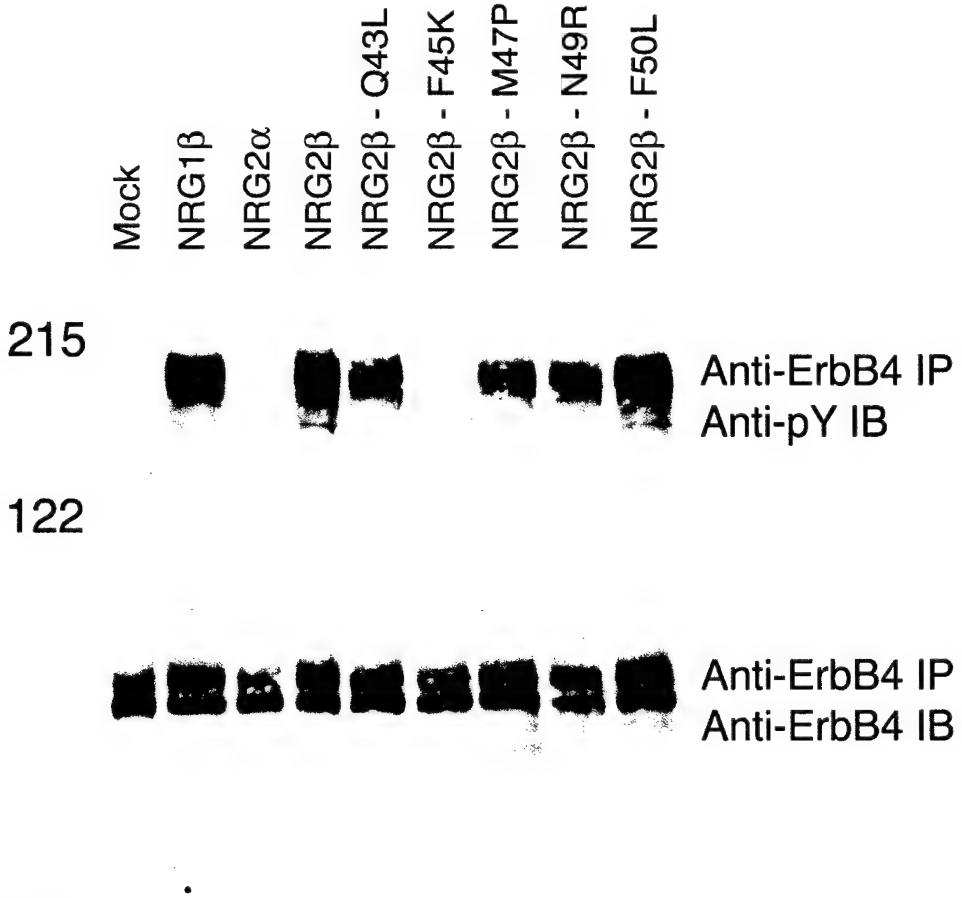

Unpublished data.

Figure 17. *Substitution of phenylalanine for lysine at position 45 is sufficient to cause NRG2α to stimulate abundant ErbB4 tyrosine phosphorylation.*

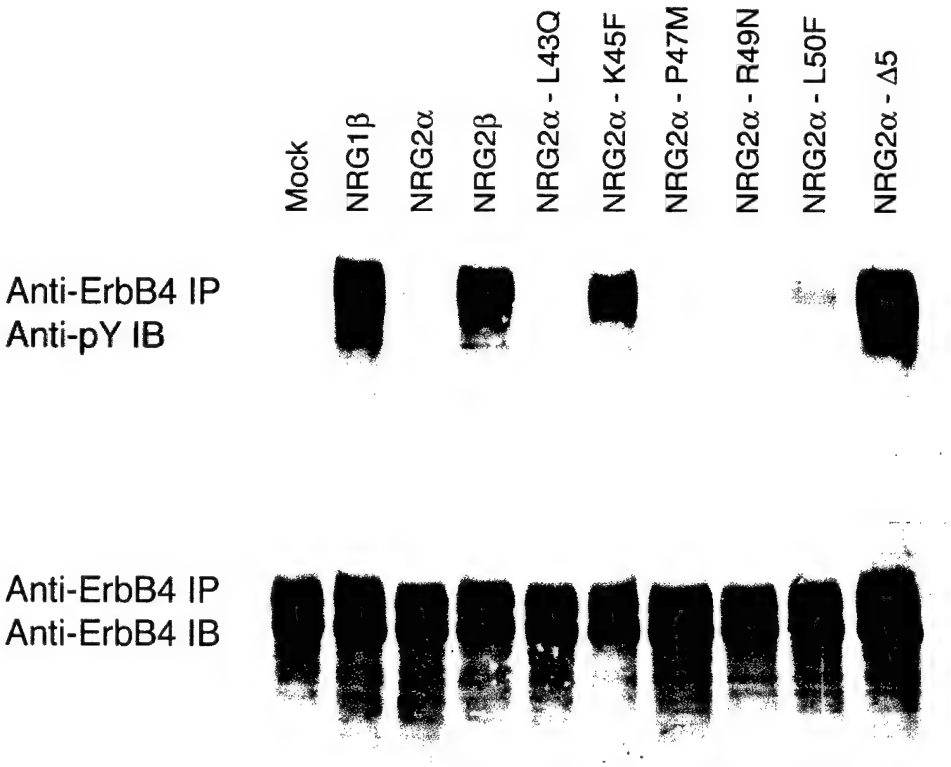

Unpublished data.

Neuregulin Isoforms Exhibit Distinct Patterns of ErbB Family Receptor Activation

S.S. Hobbs, S.L. Coffing, A.T.D. Le, E.M. Cameron, E.E. Williams, M. Andrew, E.N. Blommel, R.P. Hammer[1], H. Chang[2], and D.J. Riese II[3]

Department of Medicinal Chemistry and Molecular Pharmacology
Purdue University School of Pharmacy
West Lafayette, Indiana 7907-1333 USA

[1]Department of Chemistry
Louisiana State University
Baton Rouge, Louisiana 70803-1804 USA

[2]Bristol-Myers Squibb Pharmaceutical Research Institute
P.O. Box 5400
Princeton, NJ 08543-5400

Running Title: Receptor activation by NRG isoforms

Keywords: Heregulins, Neuregulins, ErbB3, ErbB4, HER3, HER4

[3]Corresponding Author:
David J. Riese II
Dept. of Medicinal Chemistry and Molecular Pharmacology
Purdue University
1333 RHPH, Room 224D
West Lafayette, IN 47907-1333 USA
Tel: 765-494-6091
FAX: 765-494-1414
Email: driese@purdue.edu

Abstract

During the last decade, several novel members of the Epidermal Growth Factor family of peptide growth factors have been identified. Most prominent among these are the Neuregulins or Heregulins. To date, four different Neuregulin genes have been identified (Neuregulin1-4) and several different splicing isoforms have been identified for at least two of these genes (Neuregulin1 and Neuregulin2). While Neuregulin1 isoforms have been extensively studied, comparatively little is known about Neuregulin3, Neuregulin4, or the Neuregulin2 isoforms. Indeed, there has been no systematic comparison of the activities of these molecules. Here we demonstrate that Neuregulin2alpha and Neuregulin2beta stimulate ErbB3 tyrosine phosphorylation and coupling to biological responses. In contrast, Neuregulin3 and Neuregulin4 fail to activate ErbB3 signaling. Furthermore, Neuregulin2beta, but not Neuregulin2alpha, stimulates ErbB4 tyrosine phosphorylation and coupling to biological responses. Finally, both Neuregulin3 and Neuregulin4 stimulate modest amounts of ErbB4 tyrosine phosphorylation. However, whereas Neuregulin3 stimulates a modest amount of ErbB4 coupling to biological responses, Neuregulin4 fails to stimulate ErbB4 coupling to biological responses. This suggests that there are qualitative as well as quantitative differences in ErbB family receptor activation by Neuregulin isoforms.

Introduction

The Epidermal Growth Factor (EGF) family of peptide hormones consists of approximately twenty different proteins encoded by at least ten different genes [Reviewed in 1-3]. These peptide growth factors are agonists for the four ErbB family receptors, including the Epidermal Growth Factor Receptor (EGFR), ErbB2 (HER2/Neu), ErbB3 (HER3), and ErbB4 (HER4) [Reviewed in 2-4]. Deregulated signaling by this network has been implicated in the genesis and progression of several types of human malignancies, including tumors of the breast, ovary, prostate, pancreas, lung, and brain [Reviewed in 3, 5-7].

During the last decade, several novel members of the EGF family have been identified and characterized. Most notable among these proteins are the Neuregulins (NRGs), also known as the Heregulins (HRGs) or Neu Differentiation Factors (NDFs) [8-13]. Currently, there are four known Neuregulin genes, NRG1 through NRG4. NRG1 and NRG2 encode multiple splicing isoforms; these are denoted as either alpha or beta isoforms depending on the sequence of the EGF homology domain.

Difficulties in the expression and purification of Neuregulin isoforms have hampered efforts to characterize the functions of these ligands. Nonetheless, several fundamental principles have emerged: (1) both the alpha and beta isoforms of NRG1 are ErbB3 ligands [14-17]; (2) the NRG1 beta isoform is a higher affinity ligand for ErbB4 than is the NRG1 alpha isoform [17-18]; (3) NRG3 and NRG4 are ErbB4 ligands [12-13, 17]. However, some of these experiments have been performed *in vitro* using recombinant receptor fragments and synthetic hormones or hormones expressed from bacteria. Other experiments have been performed using a variety of cultured cell lines. Thus, it has been difficult to compare the results that appear in different reports. Indeed, there has been no report of a systematic functional comparison of NRG2 alpha, NRG2 beta, NRG3, and NRG4.

Thus, a careful analysis of the published literature reveals a number of fundamental questions concerning NRG function. (1) Do the alpha and beta isoforms of NRG2 behave similarly to the corresponding NRG1 isoforms? (2) Are NRG3 and NRG4 agonists for ErbB3? (3) Given the large number of ErbB4 agonists among the NRGs, are the different agonists for ErbB4 functionally distinct? In this report we describe a novel method for easily expressing and purifying recombinant, bioactive NRGs. We present data indicating that NRG2 alpha (NRG2α) and NRG2 beta (NRG2β) are functionally distinct. We also present data indicating that NRG3 and NRG4 are ErbB4 agonists but do not appear to be ErbB3 agonists. Finally, we present data indicating that the different NRG ErbB4 agonists cause differential coupling of ErbB4 to biological responses. This is some of the most compelling evidence to date that different direct agonists for the same ErbB family receptor may be functionally distinct.

Results

Recombinant NRGs Can Be Expressed In Insect Cells. Several groups have expressed recombinant EGF family peptide hormones in *E. coli*. Advantages of this strategy include yield and suitability of the protein for structural analysis by NMR or X-ray crystallography. One disadvantage of this strategy is that the purification and refolding strategies may be cumbersome. Another is that the proteins lack the glycosylation present in proteins expressed in eukaryotic cells. Other groups have generated synthetic EGF family peptide hormones. A significant disadvantage of this strategy is the expense. Thus, we sought to produce recombinant NRG2α, NRG2β, NRG3, and NRG4 using an insect cell expression system (Invitrogen). The advantages of this system are that the yield is reasonable (~ 300 μg purified protein/liter of insect cell culture), the expense is modest (~$200/mg purified protein), the purification strategy is straightforward, there is no need to refold the protein following purification, and the protein is glycosylated.

We began by subcloning a portion of the NRG cDNAs into the insect cell vector pMT-BiP-V5HisB (Invitrogen). Others and we have previously reported the cloning of the NRG2α and NRG2β cDNAs [10-11]. The NRG3 cDNA [12] was isolated from a human cDNA library and the NRG4 cDNA [13] was isolated from a mouse cDNA library. The regions of these cDNAs encoding the EGF homology domain and surrounding sequences (NRG2α: Ser247 to Asp328; NRG2β: Ser247 to Lys314; NRG3: Ser284 to Gln360; NRG4: Thr3 to Asn60) were subcloned into the conditional insect cell expression vector pMT-BiP-V5HisB (Invitrogen). The inserts were cloned in frame with the vector sequences that encode the upstream BiP secretion signal and the downstream V5 and polyhistidine epitope tags (Figure 1a). The predicted sequences of the recombinant NRGs encoded by these expression constructs are shown in Figure

1b. The amino acid sequences of the NRG3 and NRG4 regions are identical to those reported in the literature [12-13].

We cotransfected the S2 Schneider insect cell line (American Type Culture Collection) with the NRG constructs and pCoHygro, a plasmid that directs the expression of the hygromycin resistance gene (Invitrogen). Transfected S2 cells were selected using hygromycin and were pooled to generate stable cell lines. A one-liter culture of each cell line was expanded to a density of 10^7 cells/ml and resuspended in serum-free insect cell medium (Gibco/BRL/Life Technologies) supplemented with 1 mM $CuSO_4$ to induce recombinant NRG expression from the pMT-BiP-V5His constructs. The recombinant NRGs were purified and concentrated by ultrafiltration, dialysis, and chromatography using ProBond Ni^{2+} beads.

We quantified the absolute concentrations of the NRG preparations by immunoblotting using an anti-V5 antibody (Invitrogen). A 53-kDa positive control peptide (Positope – Invitrogen) was used as the standard (Figure 2). Each NRG appeared as a heterogeneous mixture of at least three isoforms with distinct mobilities. Overall, the apparent molecular weights of the NRG isoforms is a little less than those predicted from the amino acid sequences (NRG2α - 12,500 Da; NRG2β –10,900 Da; NRG3 – 12,200 Da; NRG4 – 9,700 Da); however, the relative apparent molecular weights are in agreement with those predicted from the amino acid sequences. (NRG2α and NRG3 have higher apparent molecular weights than NRG2β and NRG2β has a higher apparent molecular weight than NRG4.) Finally, the multiple isoforms of each NRG were resolved to a single, tightly focused band by treatment with peptide N-glycosidase F (data not shown). This suggests that these isoforms represent differentially glycosylated species.

We digitized the immunoblots and quantified the bands for each NRG. We quantified all of the bands for those NRGs that exhibited multiple isoforms. We used these values to construct a dose response curve of best fit for each NRG. These curves were used in conjunction with the dose response curve of best fit for the positope control to calculate the concentration of each NRG stock. We also quantified the relative concentrations of the NRG preparations by ELISA using an anti-V5 antibody (Invitrogen) and the ABC ELISA kit (Pierce). Recombinant NRG yields were typically 300 μg from a 1 L culture of insect cells.

Recombinant NRGs differentially stimulate ErbB3 tyrosine phosphorylation. We assessed the interactions of the recombinant NRGs with ErbB family receptors by first assaying induction of ErbB3 tyrosine phosphorylation by the NRG isoforms. ErbB3 lacks tyrosine kinase activity and ErbB2 is an orphan receptor for which there is no known ligand. Consequently, we assayed ligand induction of ErbB3 tyrosine phosphorylation in mouse BaF3 lymphoid cells (which lack endogenous EGFR, ErbB2, and ErbB4 expression) that we had engineered to express ErbB2 and ErbB3 (BaF3/ErbB2+ErbB3) [19]. The recombinant NRG1β positive control (EGF homology domain; R&D Systems) stimulates abundant ErbB2 and ErbB3 tyrosine phosphorylation (Figure 3). Both NRG2α and NRG2β stimulate more modest amounts of ErbB3 tyrosine phosphorylation, nonetheless indicating that these growth factors are ligands for ErbB3. In contrast, neither NRG3 nor NRG4 stimulate detectable ErbB3 tyrosine phosphorylation.

Recombinant NRGs differentially stimulate ErbB4 tyrosine phosphorylation. We assayed induction of ErbB4 tyrosine phosphorylation by the NRG isoforms using a human CEM

lymphoid cell line (which lacks endogenous ErbB receptor expression [20]) engineered to express ErbB4 [20]. The NRG1β positive control and NRG2β stimulate abundant ErbB4 tyrosine phosphorylation, whereas NRG4 stimulates a moderate amount of ErbB4 tyrosine phosphorylation and NRG3 stimulates a modest amount of ErbB4 tyrosine phosphorylation (Figure 4). NRG2α fails to stimulate any detectable ErbB4 tyrosine phosphorylation (Figure 4).

Increasing NRG2α concentrations fail to stimulate ErbB4 tyrosine phosphorylation (Figure 4). We were concerned that the failure of NRG2α to stimulate ErbB4 tyrosine phosphorylation was due to a relatively modest difference in the affinities of NRG2α and NRG2β for ErbB4. Consequently, we stimulated CEM/ErbB4 cells with greater concentrations of NRG2α. In Figure 5 we show that 1000 ng/mL NRG2α stimulates little ErbB4 tyrosine phosphorylation. In contrast, ErbB4 tyrosine phosphorylation reaches saturation at a NRG2β concentration of approximately 30 ng/mL and a NRG3 and NRG4 concentration of approximately 300 ng/mL. Thus, the dissociation constant (K_d) of NRG3 and NRG4 for ErbB4 appears to be approximately 10 times greater than the K_d of NRG2β for ErbB4. Furthermore, if the failure of NRG2α to stimulate abundant ErbB4 tyrosine phosphorylation is due to the decreased affinity of NRG2α for ErbB4, the K_d of NRG2α for ErbB4 must be more than 30 times greater than the K_d of NRG2β for ErbB4.

Recombinant NRGs differentially stimulate ErbB family receptor coupling to biological responses. We assayed induction of ErbB3 coupling to biological responses in the BaF3/ErbB2+ErbB3 cell line and the BaF3/EGFR+ErbB4 cell line. BaF3 cells are dependent upon interleukin-3 (IL3) for survival and proliferation. However, we have previously shown that ligands for ErbB3 induce IL3-independent survival, but not proliferation, in BaF3/ErbB2+ErbB3

cells [19]. Furthermore, we have previously shown that ligands for EGFR or ErbB4 induce IL3-independent proliferation in BaF3/EGFR+ErbB4 cells [19, 21].

Here we demonstrate that NRG2α and NRG2β, as well as the NRG1β positive control, induce IL3-independent survival in BaF3/ErbB2+ErbB3 cells (Figure 6). Furthermore, NRG3 fails to induce IL3 independence in BaF3/ErbB2+ErbB3 cells and NRG4 induces minimal IL3 independence in these cells. These results are largely consistent with the ErbB3 tyrosine phosphorylation data that suggest that NRG2α and NRG2β are ligands for ErbB3, whereas NRG3 and NRG4 are not ligands for ErbB3 (Figure 3).

We also demonstrate that NRG2β and the NRG1β positive control induce IL3-independent proliferation in BaF3/EGFR+ErbB4 cells (Figure 6). In contrast, NRG3 induces IL3-independent survival (not proliferation) in BaF3/EGFR+ErbB4 cells and both NRG2α and NRG4 induce minimal IL3 independence in these cells. The results of the IL3 independence assays indicate that NRG2β, but not NRG2α, is an ErbB4 agonist, which is in line with the ErbB4 tyrosine phosphorylation data with NRG2α and NRG2β (Figure 4 and Figure 5).

NRG3 and NRG4 fail to stimulate ErbB4 tyrosine phosphorylation in BaF3/EGFR+ErbB4 cell lines. Despite the fact that 100 ng/mL NRG3 or NRG4 stimulates ErbB4 tyrosine phosphorylation (Figure 4 and Figure 5), 100 ng/mL NRG3 or NRG4 fail to stimulate ErbB4 coupling to biological responses to the extent that NRG2β does (Figure 6). Furthermore, despite the fact that identical concentrations of NRG3 and NRG4 stimulate similar levels of ErbB4 tyrosine phosphorylation (Figure 5), NRG3 stimulates a greater level of IL3 independence in the BaF3/EGFR+ErbB4 cell line than does NRG4 (Figure 6). In an attempt to resolve these discrepancies, we stimulated BaF3/EGFR+ErbB4 cells with the various NRG

isoforms and assayed both EGFR and ErbB4 tyrosine phosphorylation by receptor immunoprecipitation and antiphosphotyrosine immunoblotting. In Figure 7 we show that 100 ng/mL NRG1β or NRG2β stimulates EGFR and ErbB4 tyrosine phosphorylation, but 100 ng/mL NRG2α, NRG3, or NRG4 does not. Indeed, even 1000 ng/mL NRG3 or NRG4 does not stimulate EGFR or ErbB4 tyrosine phosphorylation (Figure 8). These data are consistent with the IL3 independence data (Figure 6) and suggest that EGFR inhibits stimulation of ErbB4 tyrosine phosphorylation and coupling to downstream signaling events by NRG3 and NRG4.

Discussion

In this work we demonstrate that recombinant NRGs can be expressed in insect cells and that these molecules retain biological and biochemical activities. This is a significant advance since methods traditionally used to generate EGF family peptide hormones are cumbersome or expensive. Indeed, this methodology will facilitate functional analyses of NRGs by site-directed mutagenesis. While this strategy has been used to analyze the function of some EGF family hormones, most notably EGF itself [Reviewed in 22-23], such analyses of NRGs have been limited to binding studies done using NRGs expressed in phage display systems [24-25]. Undoubtedly, studies facilitated by the ready availability of NRG mutants will reveal new insights into the nature of the interactions between EGF family peptide growth factors and their cognate ErbB family receptor tyrosine kinases.

The studies presented here also represent the initial systematic functional comparison of NRG2α, NRG2β, NRG3, and NRG4. Here we show that NRG2α and NRG2β stimulate ErbB3 tyrosine phosphorylation (in the context of ErbB2 and ErbB3 coexpression), whereas NRG3 and NRG4 do not. These results are consistent with the published observation that NRG alpha and beta isoforms are ligands for ErbB3 [16-18, 26-27]. However, these results contrast with the observation that a recombinant NRG2α fusion protein fails to compete with radiolabeled NRG1β for binding to recombinant ErbB2-ErbB3 heterodimers [17]. Of course the physiologic relevance of preformed recombinant ErbB2-ErbB3 heterodimers is unclear and it was noted by the authors that the NRG fusion proteins have reduced affinity for their native receptors [24]. Our results are consistent with the published observation that a recombinant NRG3 fusion protein fails to compete with radiolabeled NRG1β for binding to a recombinant ErbB3 fusion protein [17]. However, the observation that NRG3 stimulates ErbB2 and ErbB3 tyrosine phosphorylation in 32D cells devoid of endogenous ErbB family receptors [28] contrasts with

our results. Of course, coexpression of ErbB2 and ErbB3 in 32D cells permits EGF stimulation of receptor coupling to IL3 independence and mitogenesis [26]. This calls into question the utility of the 32D model system for defining ligand-receptor interactions. Regardless, we conclude that NRG2α and NRG2β are functionally distinct from NRG3 and NRG4.

We also show that NRG2β is a potent agonist of ErbB4 tyrosine phosphorylation, whereas NRG3 and NRG4 stimulate modest levels of ErbB4 tyrosine phosphorylation and NRG2α fails to stimulate ErbB4 tyrosine phosphorylation (Figure 4 and Figure 5). These results are consistent with the observation that NRG beta isoforms are more potent and higher affinity ligands for ErbB4 than are NRG alpha isoforms [15, 17-18, 26-27]. These data are also consistent with the observation that NRG3 and NRG4 are both ErbB4 ligands [12, 13, 17]. However, these data also suggest that NRG2β is a more potent ligand for ErbB4 than are NRG4 and NRG3. It should be noted that ErbB4 tyrosine phosphorylation reaches saturation following stimulation with 30 ng/mL NRG2β, 300 ng/mL NRG3, or 300 ng/mL NRG4. Thus, some of the functional difference between NRG2β and NRG3 or NRG4 appears to be due to the higher affinity of NRG2β for ErbB4. Indeed, the affinity of NRG3 for ErbB4 is reported to be less than one-tenth the affinity of NRG2β for ErbB4 [17]. Similarly, the affinity of NRG4 for ErbB4 is reported to be approximately one-tenth the affinity of NRG1β for ErbB4 [13].

NRG2α and NRG2β stimulate IL3 independent survival in BaF3/ErbB2+ErbB3 cells, whereas NRG3 and NRG4 do not stimulate IL3 independence in these cells (Figure 6). These results are consistent with the observation that NRG alpha and beta isoforms stimulate coupling of ErbB2 and ErbB3 to biological responses [16, 26-27]. These results are also consistent with the tyrosine phosphorylation data shown in Figure 3. NRG3 does not stimulate any IL3 independence in the BaF3/ErbB2+ErbB3 cells (Figure 6), consistent with the tyrosine

phosphorylation data shown in Figure 3. NRG4 also fails to stimulate ErbB3 tyrosine phosphorylation in the BaF3/ErbB2+ErbB3 cells (Figure 3). However, NRG4 stimulates a modest amount of IL3 independence in these cells (Figure 6). It is possible that the IL3 independence assay is a more sensitive measure of ligand-induced receptor signaling than is antiphosphotyrosine immunoblotting. Indeed, we have previously shown that the ligand concentration required for saturated levels of ErbB receptor tyrosine phosphorylation in BaF3 cells is approximately 10-fold greater than the ligand concentration required for saturated levels of IL3 independence in the same cell lines [19].

NRG2β stimulates IL3-independent proliferation in BaF3/EGFR+ErbB4 cell lines, whereas NRG2α stimulates minimal IL3 independence (Figure 6). This is consistent with the tyrosine phosphorylation data shown in Figures 4 and 5. More intriguing are the observations that 100 ng/mL NRG3 stimulates only IL3-independent survival and that 100 ng/mL NRG4 stimulates minimal IL3 independence (Figure 6). We were concerned that we were not using a sufficient concentration of NRG3 or NRG4 in these IL3 independence assays. However, even 1000 ng/mL NRG3 or NRG4 failed to stimulate IL3-independent proliferation in the BaF3/EGFR+ErbB4 cells (data not shown). Thus, we attempted to explain these results by assaying ligand-induced receptor tyrosine phosphorylation in the BaF3/EGFR+ErbB4 cells (Figure 7 and Figure 8). These experiments reveal that NRG2α, NRG3, and NRG4 stimulate minimal receptor tyrosine phosphorylation in the BaF3/EGFR+ErbB4 cells. This is consistent with the relative inactivity of these ligands in the IL3 independence assay using these cells. Furthermore, the high basal (ligand-independent) level of receptor tyrosine phosphorylation in these cells (Figure 7 and Figure 8) may account for the small amount of IL3-independence stimulated by NRG2α (which is presumably not a potent ErbB4 agonist).

We are left trying to explain why NRG3 and NRG4 stimulate much lower levels of ErbB4 tyrosine phosphorylation (Figure 7 and Figure 8) and ErbB receptor coupling to biological responses in the BaF3/EGFR+ErbB4 cells (Figure 6) than would be expected from the ErbB4 tyrosine phosphorylation data obtained from the CEM/ErbB4 cells (Figure 4 and Figure 5). A simple, non-mechanistic explanation is that EGFR inhibits ligand-induced ErbB4 tyrosine phosphorylation. However, we have previously shown that ErbB2 or ErbB3 expression does not quantitatively modulate ErbB4 tyrosine phosphorylation stimulated by betacellulin or NRG1β [29]. Nonetheless, it is possible that inhibition of ligand-induced ErbB4 signaling is specific for EGFR, NRG3, or NRG4.

A more attractive, mechanistic explanation is that the EGFR-ErbB4 heterodimers stimulated by NRG3 and NRG4 treatment are in a different conformation that results in less receptor tyrosine phosphorylation than the EGFR-ErbB4 heterodimers stimulated by NRG2β. There are precedents for differential receptor tyrosine kinase dimerization, tyrosine phosphorylation, and coupling to downstream events. The bovine papillomavirus (BPV) E5 protein is a membrane-bound agonist for the platelet derived growth factor receptor (PDGFR) and stimulates PDGFR dimerization, tyrosine phosphorylation, and PDGFR-dependent malignant growth transformation of fibroblasts [Reviewed in 30]. However, there are BPV E5 mutants that stimulate PDGFR tyrosine phosphorylation yet fail to couple to PDGFR-dependent growth transformation [31-32]. Similarly, mutation of different ErbB2 extracellular juxtamembrane amino acids residues to cysteine results in ErbB2 disulfide-linked dimers that exhibit high levels of ErbB2 tyrosine phosphorylation yet fail to cause malignant growth transformation of fibroblasts [33].

Thus, we hypothesize that in BaF3/EGFR+ErbB4 cells, NRG3 and NRG4 stimulate EGFR and ErbB4 phosphorylation on different or a smaller number of tyrosine residues than does NRG2β. These hypotheses are consistent with several published observations. In the MDA-MB-453 breast tumor cell line, NRG1β and NRG2β stimulate ErbB2 and ErbB3 tyrosine phosphorylation to similar extents, but only NRG1β causes differentiation of these cells and the two growth factors cause differential recruitment of SH2 domain-containing proteins to the phosphorylated ErbB2 and ErbB3 and differential activation of gene transcription [34, 35]. Similarly, betacellulin, NRG1β, NRG2β, and NRG3 induce qualitatively different patterns of ErbB4 tyrosine phosphorylation, as revealed by 2-dimensional peptide mapping [36].

Our data suggest that regulation of ErbB family receptor signaling by EGF family hormones occurs at multiple levels. NRG2α and NRG2β are more potent ErbB3 agonists than are NRG3 and NRG4 (Figure 3 and Figure 6). Furthermore, NRG2β is a potent ErbB4 agonist, whereas NRG3 and NRG4 are less potent ErbB4 agonists and NRG2α directly stimulates minimal ErbB4 signaling (Figures 4-8). To a first approximation, these differences in activity of the various NRGs and other EGF family hormones (Figure 9) reflect the different affinities of these hormones for ErbB family receptors [17, Reviewed in 1-3]. Consequently, differential ligand activation of signaling by a specific ErbB family receptor is in part a function of quantitative differences in the affinities of the various ligands for the particular receptor.

However, this quantitative model cannot explain all of the data presented here. The dissociation constant (K_d) of NRG2α and ErbB4 is reported to be 20-50 fold greater than the K_d of NRG2β and ErbB4 [17, 26-27]. Yet, whereas 3 ng/mL NRG2β stimulates a modest amount of ErbB4 tyrosine phosphorylation, 300 ng/mL NRG2α fails to stimulate ErbB4 tyrosine phosphorylation and 1000 ng/mL NRG2α stimulates only a very small amount of ErbB4 tyrosine

phosphorylation (Figure 4 and Figure 5). Furthermore, whereas NRG3 and NRG4 stimulate detectable amounts of ErbB4 tyrosine phosphorylation in CEM/ErbB4 cells, at the same ligand concentrations they fail to stimulate detectable amounts of ErbB4 tyrosine phosphorylation in BaF3/EGFR+ErbB4 cells. In contrast, NRG2β stimulates abundant ErbB4 tyrosine phosphorylation in both cell lines. These observations suggest that there are qualitative differences in activation of ErbB4 signaling and coupling to downstream signaling events by the various NRG isoforms. Published data suggest that these qualitative differences between the NRG isoforms reflect ligand-induced ErbB4 tyrosine phosphorylation on different tyrosine residues and consequent differential receptor coupling to downstream signaling pathways. This would explain the functional differences of the NRG isoforms seen in this study. One of our future challenges will be to formally test whether there are qualitative differences in the activities of the ErbB4 ligands and to identify the mechanism for these differences. Another challenge will be to develop a model that explains the interactions of EGF family hormones with ErbB family receptors and that accounts for these qualitative differences in the activities of the ErbB4 ligands.

Materials and Methods

Cell Lines and cell culture. The S2 Schneider insect cells were purchased from the American Type Culture Collection. The CEM/ErbB4 cells [20] were a generous gift of Dr. Gregory D. Plowman, Exelixis Pharmaceuticals. The BaF3/ErbB2+ErbB3 and BaF3/EGFR+ErbB4 cell lines have been described previously [19]. All cell lines were maintained according to vendor instructions or published procedures [19, 20, 29].

Plasmids and plasmid construction. The insect cell conditional expression vector pMT-BiP-V5HisB and the pCoHygro plasmid were purchased from Invitrogen. We isolated NRG2α, NRG2β, NRG3, and NRG4 clones from human, rat, and mouse cDNA libraries. The regions of the cDNA clones that encode the EGF homology domain of the NRG isoforms were amplified by PCR and were subcloned by standard molecular biology techniques into the BglII and SacII sites of pMT-BiP-V5HisB. The upstream primer used to amplify the rat NRG2α sequences has the following sequence: 5'-CTCGAGAGATCTTCGGGGCACGCCCGGAAGTG-3'. The downstream primer has the following sequence: 5'-CTCGAGCCGCGGATTCAAATCCAAGGTGCTTGG-3'. The amplified sequences encode Ser247 to Asp328 [10-11]. The upstream primer used to amplify the rat NRG2β sequences has the following sequence: 5'-CTCGAGAGATCTTCGGGGCACGCCCGGAAGTG-3'. The downstream primer has the following sequence: 5'-CTCGAGCCGCGGCTTCTGGTACAGCTCCTC-3'. The amplified sequences encode Ser247 to Lys314 [10-11]. The upstream primer used to amplify the human NRG3 sequences has the following sequence: 5'-CTCGAGAGATCTTCCGAGCACTTCAAACCCTG-3'. The downstream primer has the following sequence: 5'-CTCGAGCCGCGGCTGCCTTTGATAAACTTCTTCACTCTCC-3'.

The amplified sequences encode Ser284 to Gln360 [12]. The upstream primer used to amplify the mouse NRG4 sequences has the following sequence: 5'-CTCGAGAGATCTACAGATCACGAGCAGCC-3'. The downstream primer has the following sequence: 5'- CTCGAGCCGCGGATTACTTTCGCTTGGGATGCTGG -3'. The amplified sequences encode Thr3 to Asn60 [13]. The inserts were subcloned in frame with the upstream BiP secretion signal encoded by pMT-BiP-V5HisB and in frame with the downstream V5 and polyhistidine epitope tags encoded by pMT-BiP-V5HisB.

Generation and purification of recombinant NRGs. The NRG clones were co-transfected into the S2 cells along with the plasmid pCoHygro, which carries the hygromycin resistance gene. Transfections were performed using a calcium phosphate transfection kit (Invitrogen) according to vendor instructions. Transfected cells were selected using 300 U/ml hygromycin B (Cellgro) and stably transfected cells appeared approximately 14 days after the beginning of selection.

Hygromycin-resistant cells were pooled, expanded, and frozen for archival purposes. Transfected cells were seeded in a 1 L culture at a density of $2x10^6$ cells/mL. Cells were maintained until they reached a density of $1x10^7$ cells/mL. At that point cells were collected by centrifugation and seeded at a density of $2x10^7$ cells/mL in serum-free medium (Gibco/BRL/Life Technologies) supplemented with 1 mM $CuSO_4$. Cells were maintained for five days in serum-free medium to permit recombinant NRG expression and secretion into the culture medium.

The insect cells were collected from the culture media by centrifugation. The conditioned media supernatants were transferred into a fresh container and clarified by filtration through a 0.22 μM filter. The NRGs present in the conditioned medium were concentrated

approximately 30-fold by ultrafiltration using a 5000 M.W.C.O. filter (Amicon). The concentrated NRGs were dialyzed against PBS using a 5000 M.W.C.O. membrane (Pierce) to remove low-molecular weight impurities. The NRGs were purified by incubating the samples with ProBond Ni^{2+} beads (Invitrogen), which bind proteins tagged with polyhistidine. The NRGs were eluted from the beads using 500 mM imidazole. We removed the imidazole from the eluates by dialysis against PBS using a 500 M.W.C.O. membrane (Pierce). The dialyzed proteins were then concentrated to a final volume of 2-5 ml by ultrafiltration using a 5000 M.W.C.O. filter (Amicon).

Anti-V5 immunoblotting. Anti-V5 immunoblotting was used to quantify the concentrations of the recombinant NRG samples. Samples were resolved by SDS-PAGE using a 20% acrylamide gel. Resolved samples were electroblotted onto nitrocellulose. The blots were probed using an anti-V5 mouse monoclonal antibody (Invitrogen). Primary antibody binding was detected using a goat anti-mouse antibody conjugated to horseradish peroxidase (Pierce). Secondary antibody binding was visualized by chemiluminescence (Amersham). The positope recombinant protein (Invitrogen) was analyzed in parallel as a control for V5 immunoblotting and as a standard for quantification.

The resulting immunoblot was digitized using a UMAX Astra 2400S flatbed scanner and the image was cropped using Adobe Photoshop. The bands were quantified using NIH Image for Macintosh software. We generated a dose-response line of best fit for each recombinant NRG using Microsoft Excel. The coefficients of correlation exceeded 0.96. These curves were used to calculate the concentration of each recombinant NRG stock.

Anti-V5 ELISA. The concentration of the NRG2α, NRG3, and NRG4 preparations were determined relative to the concentration of the NRG2β preparation by ELISA using an anti-V5 monoclonal antibody (Invitrogen) and the ABC ELISA kit (Pierce). Polyvinyl chloride (PVC) 96-well assay plates were seeded with 1 ng/well, 3 ng/well, and 10 ng/well of NRG2β and 3 μL/well, 10 μL/well, and 30 μL/well of several dilutions of the other NRGs in a total volume of 100 μl/well. The plates were incubated for 1 hour at room temperature to allow for protein binding to the wells. The wells were then washed three times with 200 μL tris-buffered saline supplemented with 0.05% Tween-20 (TBS-T). Non-specific binding of the antibody to the wells was blocked by incubating the wells for one hour at room temperature with 100 μL TBS/1% bovine serum albumin (Sigma). Next, 100 μL of the mouse-anti-V5 monoclonal antibody (0.2 μg/ml - Invitrogen) was added to each well and the plates were incubated for 30 minutes at room temperature. The wells were then washed three times with 200 μL TBS-T and 100 μL of a biotinylated anti-mouse antibody (1.5 μg/mL – Pierce) was added to each well. The plates were incubated for 30 minutes at room temperature. The wells were washed three times with 200 μL TBS-T. An avidin/biotinylated alkaline phosphatase complex (100 μL) was added to each well and the plates were incubated for 30 minutes at room temperature. The wells were washed three times with 200 μL TBS-T, after which 100 μl of TBS-T was added to each well and the plates were incubated for 5 minutes at room temperature. The TBS-T was removed and 100 μl of the alkaline phosphatase substrate, p-nitrophenyl phosphate (1 mg/mL solution dissolved in diethanolamine- Pierce), was added to each well. The plates were incubated until the appropriate amount of substrate had been dephosphorylated, which is evident from the yellow color of the product. The reactions were terminated by adding 25 μL 2 M NaOH to each well. Finally, the

amount of product in each well was determined by measuring absorbance at 405 nm using a SpectrFluor Plus plate reader (Tecan).

The amount of product was plotted as a function of sample stock volume for NRG2α, NRG3, and NRG4. These dose-response curves were compared to a standard dose-response curve generated using NRG2β to determine the relative concentration of the NRG2α, NRG3, and NRG4 stocks.

Stimulation and analysis of ErbB family receptor tyrosine phosphorylation. We analyzed ligand-induced ErbB family receptor tyrosine phosphorylation in CEM/ErbB4, BaF3/ErbB2+ErbB3, and BaF3/EGFR+ErbB4 cells using procedures published previously [10, 19, 21, 29, 37, 38]. Briefly, approximately 10^7 cells were stimulated for 7 minutes on ice with ligand, after which the cells were lysed in an isotonic lysis buffer supplemented with the nonionic detergent NP40. Nuclei and debris were collected from the lysates by centrifugation and the supernatants were transferred to a fresh tube. The protein content of the lysates was analyzed using a modified Bradford assay (Pierce). ErbB family receptors were precipitated from the lysates using Concanavlin A-sepharose, which binds to glycoproteins. ErbB family receptors were also precipitated from the lysates using an anti-EGFR mouse monoclonal antibody (Santa Cruz Biotechnology), or an anti-ErbB4 rabbit polyclonal antibody (Santa Cruz Biotechnology).

The precipitates were resolved by SDS-PAGE using a 7.5% acrylamide gel. The resolved samples were electroblotted onto nitrocellulose. The blots were probed using an anti-phosphotyrosine mouse monoclonal antibody (Upstate Biotechnology). Primary antibody binding was detected using a goat anti-mouse antibody conjugated to horseradish peroxidase (Pierce). Secondary antibody binding was visualized by chemiluminescence (Amersham).

Stimulation and analysis of ErbB family receptor coupling to IL3 independence. We analyzed ligand-induced ErbB family receptor coupling to IL3 independence in BaF3/ErbB2+ErbB3 and BaF3/EGFR+ErbB4 cells using procedures published previously [10, 19, 21, 29, 37, 38]. Briefly, cells were seeded in 24 well dishes at a density of 10^5 cells/mL in medium lacking interleukin3 (IL3), in medium supplemented with IL3, or in medium lacking IL3 but supplemented with a recombinant NRG. Cells were incubated for 96 hours, afterwhich viable cells were counted using a hemacytometer. If the viable cell density was greater than 10^5 cells/mL, the cells were judged to be proliferating. If the viable cell density was between 10^4 and 10^5 cells/mL, the cells were judged to be surviving. If the viable cells density was below 10^4 cells/mL, the cells were judged to be dying.

Acknowledgements

S.S.H. was supported by an NIH predoctoral training grant (T32GM008737). E.M.C. was supported by undergraduate research fellowships from the Carroll County (Indiana) Cancer Society and the American Foundation for Pharmaceutical Education. E.E.W. was supported by an undergraduate research fellowship from the American Association of Colleges of Pharmacy and Merck. R.P.H. was supported by an NIH sabbatical leave fellowship (F33CA085049). We also acknowledge additional support from the NIH (R21CA080770 to D.J.R.) the U.S. Army Medical Research and Materiel Command (DAMD17-00-1-0415 and DAMD17-00-1-0416 to D.J.R.), the Indiana Elks Foundation (to D.J.R.), and the American Cancer Society (IRG-58-006 to the Purdue Cancer Center).

References

1. Kumar, R. and Vadlamudi, R.K. (2000). *J. Clin. Ligand Assay*, **23**, 233-237.

2. Gullick, W.J. (2001). *Endocrine-Related Cancer*, **8**, 75-82.

3. Yarden, Y., and Sliwkowski, M.X. (2001). *Nature Revs. Mol. Cell. Biol.*, **2**, 127-137.

4. Schlessinger, J. (2000). *Cell*, **103**, 211-225.

5. Stern, D.F. (2000). *Breast Cancer Res.* **2**, 176-183.

6. Normanno, N., Bianco, C., DeLuca, A., and Salomon, D.S. (2001). *Frontiers Biosci.* **6**, d685-d707.

7. Ozawa, F., Friess, H., Tempia-Caliera, A., Kleeff, J., and Buchler, M.W. (2001). *Teratogen. Carcinogen. Mutagen.*, **21**, 27-44.

8. Holmes, W.E., Sliwkowski, M.X., Akita, R.W., Henzel, W.J., Lee, J., Park, J.W., Yansura, D., Abadi, N., Raab, H., Lewis, G.D., Shepard, H.M., Kuang, W.-J., Wood, W.I., Goeddel, D.V., and Vandlen, R.L. (1992). *Science*, **256**, 1205-1210.

9. Wen, D., Peles, E., Cupples, R., Suggs, S.V., Bacus, S.S., Luo, Y., Trail, G., Hu, S., Silbiger, S.M., Ben Levy, R., Koski, R.A., Lu, H.S., and Yarden, Y. (1992). *Cell*, **69**, 559-572.

10. Chang, H., Riese, D.J. II, Gilbert, W., Stern, D.F., and McMahan, U.J. (1997). *Nature*, **387**, 509-512.

11. Carraway, K.L. III, Weber, J.L., Unger, M.J., Ledesma, J., Yu, N., Gassmann, M., and Lai, C. (1997). *Nature*, **387**, 512-516.

12. Zhang, D., Sliwkowski, M.X., Mark, M., Frantz, G., Akita, R., Sun, Y., Hillan, K., Crowley, C., Brush, J., and Godowski, P.J. (1997). *Proc. Natl. Acad. Sci. USA*, **94**, 9562-9567.

13. Harari, D., Tzahar, E., Romano, J., Shelly, M., Pierce, J.H., Andrews, G.C., and Yarden, Y. (1999). *Oncogene*, **18**, 2681-2689.

14. Kita, Y.A., Barff, J., Luo, Y., Wen, D., Brankow, D., Hu, S., Liu, N., Prigent, S.A., Gullick, W.J., and Nicolson, M. (1994). *FEBS Lett.*, **349**, 139-143.

15. Lu, H.S., Chang, D., Philo, J.S., Zhang, K., Narhi, L.O., Liu, N., Zhang, M., Sun, J., Wen, J., Yanagihara, D., Karunakaran, D., Yarden, Y., and Ratzkin, B. (1995). *J. Biol. Chem.*, **270**, 4784-4791.

16. Pinkas-Kramarski, R., Shelly, M., Glathe, S., Ratzkin, B.J., and Yarden, Y. (1996). *J. Biol. Chem.*, **271**, 19029-19032.

17. Jones, J.T., Akita, R.W., and Sliwkowski, M.X. (1999). *FEBS Lett.*, **447**, 227-231.

18. Tzahar, E., Levkowitz, G., Karungaran, D., Yi, L., Peles, E., Lavi, S., Chang, D., Liu, N., Yayon, A., Wen, D., and Yarden, Y. (1994). *J. Biol. Chem.*, **269**, 25226-25233.

19. Riese, D.J. II, van Raaij, T.M., Plowman, G.D., Andrews, G.C., and Stern, D.F. (1995). *Mol. Cell. Biol.*, **15**, 5770-5776.

20. Plowman, G.D., Green, J.M., Culouscou, J.-M., Carlton, G.W., Rothwell, V.M., and Buckley, S. (1993). *Nature*, **366**, 473-475.

21. Riese, D.J. II, Bermingham, Y., van Raaij, T.M., Buckley, S., Plowman, G.D., and Stern, D.F. (1996). *Oncogene*, **12**, 345-353.

22. Groenen, L.C., Nice, E.C., and Burgess, A.W. (1994). *Growth Factors* **11**, 235-237.

23. Boonstra, J., Rijken, P., Humbel, B., Cremers, F., Verkeij, A., and van Bergen en Henegouwen, P. (1995). *Cell Biol. Intl.* **19**, 413-430.

24. Jones, J.T., Ballinger, M.D., Pisacane, P.I., Lofgren, J.A., Fitzpatrick, V.D., Fairbrother, W.J., Wells, J.A., and Sliwkowski, M.X. (1998). *J. Biol. Chem.* **273**, 11667-11674.

25. Ballinger, M.D., Jones, J.T., Lofgren, J.A., Fairbrother, W.J., Akita, R.W., Sliwkowski, M.X., and Wells, J.A. (1998). *J. Biol. Chem.* **273**, 11675-11684.

26. Pinkas-Kramarski, R., Shelly, M., Guarino, B.C., Wang, L.M., Lyass, L., Alroy, I., Alamandi, M., Kuo, A., Moyer, J.D., Lavi, S., Eisenstein, M., Ratzkin, B.J., Seger, R., Bacus, S.S., Pierce, J.H., Andrews, G.C., and Yarden, Y. (1998). *Mol. Cell. Biol.*, **18**, 6090-6091. Correction: *Mol. Cell. Biol.*, **19**: 8695 (1999).

27. Pinkas-Kramarski, R., Shelly, M., Guarino, B.C., Wang, L.M., Lyass, L., Alroy, I., Alamandi, M., Kuo, A., Moyer, J.D., Lavi, S., Eisenstein, M., Ratzkin, B.J., Seger, R., Bacus, S.S., Pierce, J.H., Andrews, G.C., and Yarden, Y. (1999). *Mol. Cell. Biol.*, **19**, 8695.

28. Hijazi, M.M., Young, P.E., Dougherty, M.K., Bressette, D.S., Cao, T.T., Pierce, J.H., Wong, L.M., Alimandi, M., and King, C.R. (1998). *Int. J. Onc.*, **13**, 1061-1067.

29. Feroz, K., Williams, E., and Riese, D.J. II. (2002). *Cell. Signal.* **14**, 793-798.

30. Drummond-Barbosa, D., and DiMaio, D. (1997). *Biochim. Biophys. Acta* **1332**, M1-M17.

31. Nilson, L.A., Gottlieb, R.L., Polack, G.W., and DiMaio, D. (1995). *J. Virology* **69**, 5869-5874.

32. Klein, O., Polack, G.W., Surti, T., Kegler-Ebo, D., Smith, S.O., and DiMaio, D. (1998). *J. Virology* **72**, 8921-8932.

33. Burke, C.L, and Stern, D.F. (1998). *Mol. Cell. Biol.* **18**, 5371-5379.

34. Sweeney Crovello, C., Lai, C., Cantley, L.C., and Carraway, K.L. III. (1998). *J. Biol. Chem.* **273**, 26954-26961.

35. Sweeney, C., Fambrough, D., Huard, C., Diamonti, A.J., Lander, E.S., Cantley, L.C., and Carraway, K.L. III. (2001). *J. Biol. Chem.* **276**, 22685-22698.

36. Sweeney, C., Lai, C., Riese, D.J. II, Diamonti, A.J., Cantley, L.C., and Carraway, K.L. III. (2000). *J Biol. Chem.* **276**, 19803-19807.

37. Riese, D.J. II, Kim, E.D., Elenius, K., Buckley, S., Klagsbrun, M., Plowman, G.D., and Stern, D.F. (1996). *J. Biol. Chem.* **271**, 20047-20052.

38. Riese, D.J. II, Komurasaki, T., Plowman, G.D., and Stern, D.F. (1998). *J. Biol. Chem.* **273**, 11288-11294.

39. Riese, D.J. II and Stern, D.F. (1998). *Bioessays* **20**, 41-48.

Figure 1. *The NRG cDNAs were subcloned into the conditional insect cell expression vector pMT-BiP-V5-His.* (a) The inserts were cloned in frame with the regions of the vector that encode the BiP signal sequence and the V5 and polyhistidine epitope tags. (b) The amino acid sequences of the NRG inserts are noted. The consensus EGF homology domain of each NRG is underlined. The six conserved cysteine residues are denoted by larger type.

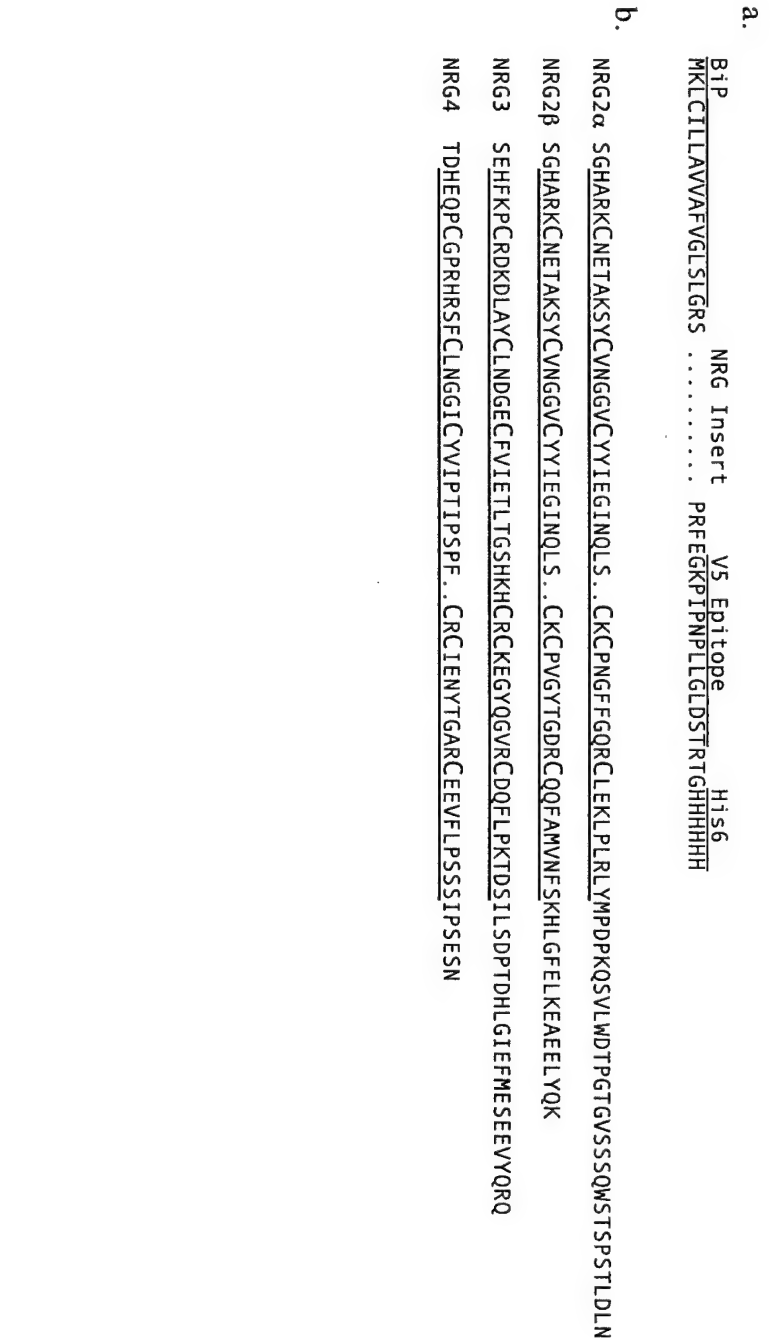

Figure 2. *Anti-V5 immunoblotting can be used to assess the relative concentrations of the NRG isoforms.* Dilutions were prepared for each recombinant NRG stock. Various volumes were resolved by SDS-PAGE using a 20% acrylamide gel. The resolved proteins were electroblotted onto nitrocellulose and the resulting blot was probed using an anti-V5 monoclonal antibody. Antibody binding was visualized using an HRP-conjugated anti-mouse secondary antibody and chemiluminescence. Defined amounts (10 ng, 30 ng, and 100 ng) of the positope recombinant peptide (Invitrogen) were used as a positive control for V5 immunoblotting and as a standard for quantification. Positions of molecular weight markers are indicated.

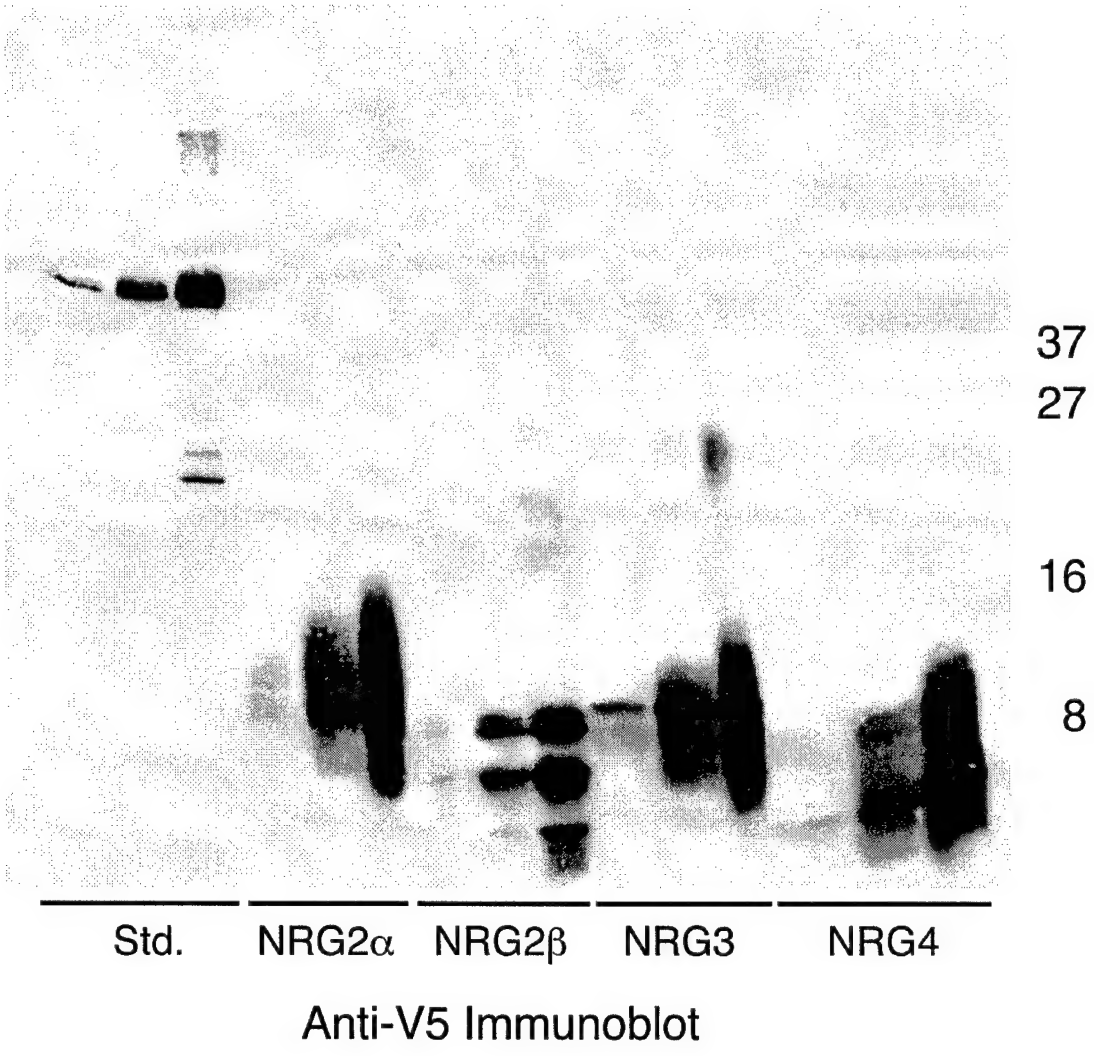

Figure 3. *NRG2α and NRG2β, but not NRG3 and NRG4, stimulate ErbB2 and ErbB3 tyrosine phosphorylation in BaF3/ErbB2+ErbB3 cells.* BaF3/ErbB2+ErbB3 cells were stimulated with NRG2α, NRG2β, NRG3, and NRG4 as noted below. NRG1β was used as a positive control and the NRG solvent (PBS) was used as a negative (mock) control. Cells were lysed and the ErbB receptors were precipitated using ConcanavalinA-sepharose. Precipitates were resolved by SDS-PAGE and the resolved proteins were electroblotted onto nitrocellulose. The blots were probed with an anti-phosphotyrosine monoclonal antibody. Antibody binding was visualized using an HRP-conjugated anti-mouse secondary antibody and chemiluminescence. Positions of molecular weight markers are indicated.

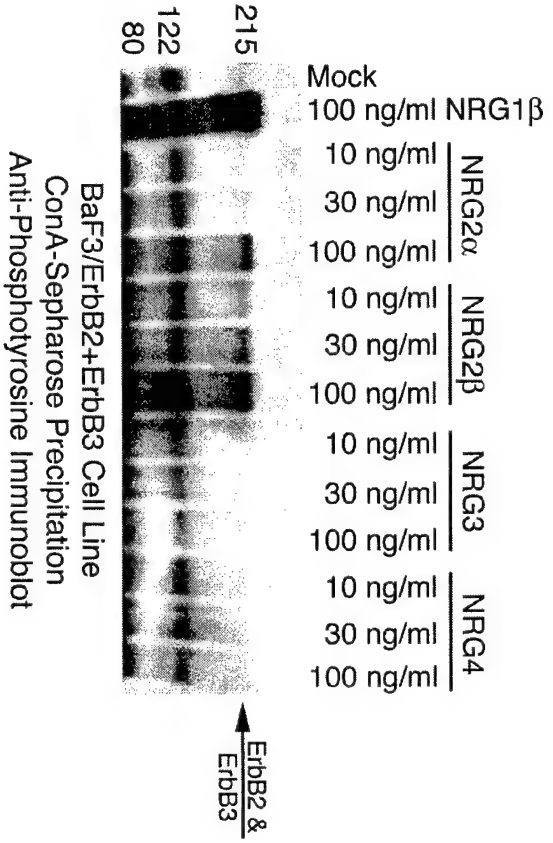

Figure 4. *NRG isoforms stimulate distinct levels of ErbB4 tyrosine phosphorylation in CEM/ErbB4 cells*. CEM/ErbB4 cells were stimulated with NRG2α, NRG2β, NRG3, and NRG4 as noted below. NRG1β was used as a positive control and the NRG solvent (PBS) was used as a negative (mock) control. Cells were lysed and ErbB4 was precipitated using ConcanavalinA-sepharose. Precipitates were resolved by SDS-PAGE and the resolved proteins were electroblotted onto nitrocellulose. The blots were probed with an anti-phosphotyrosine monoclonal antibody. Antibody binding was visualized using an HRP-conjugated anti-mouse secondary antibody and chemiluminescence. Positions of molecular weight markers are indicated.

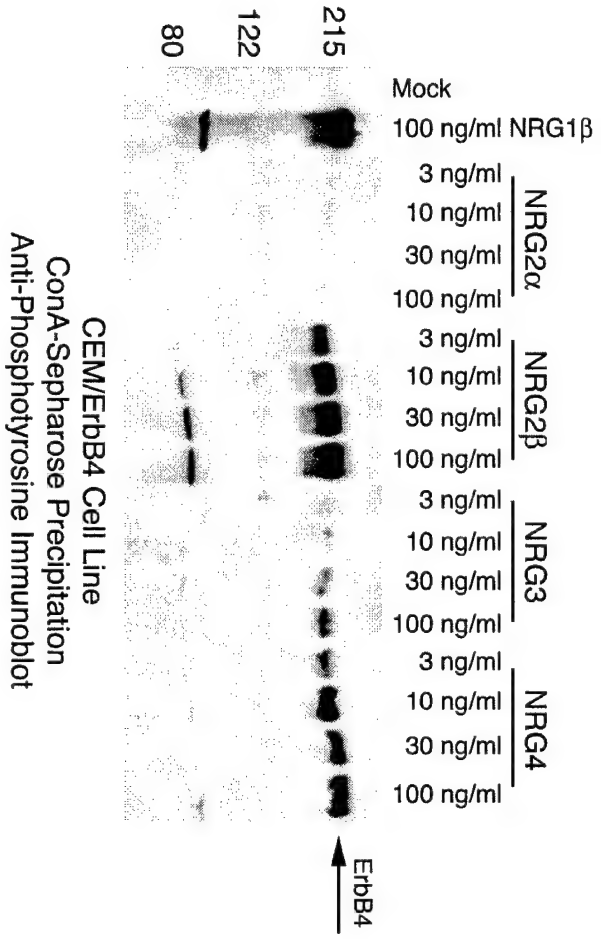

Figure 5. *Increased NRG2α concentrations fail to stimulate ErbB4 tyrosine phosphorylation in CEM/ErbB4 cells.* CEM/ErbB4 cells were stimulated with NRG2α, NRG2β, NRG3, and NRG4 as noted below. NRG1β was used as a positive control and the NRG solvent (PBS) was used as a negative (mock) control. Cells were lysed and ErbB4 was precipitated using an antibody specific for ErbB4. Precipitates were resolved by SDS-PAGE and the resolved proteins were electroblotted onto nitrocellulose. The blots were probed with an anti-phosphotyrosine monoclonal antibody. Antibody binding was visualized using an HRP-conjugated anti-mouse secondary antibody and chemiluminescence. Positions of molecular weight markers are indicated.

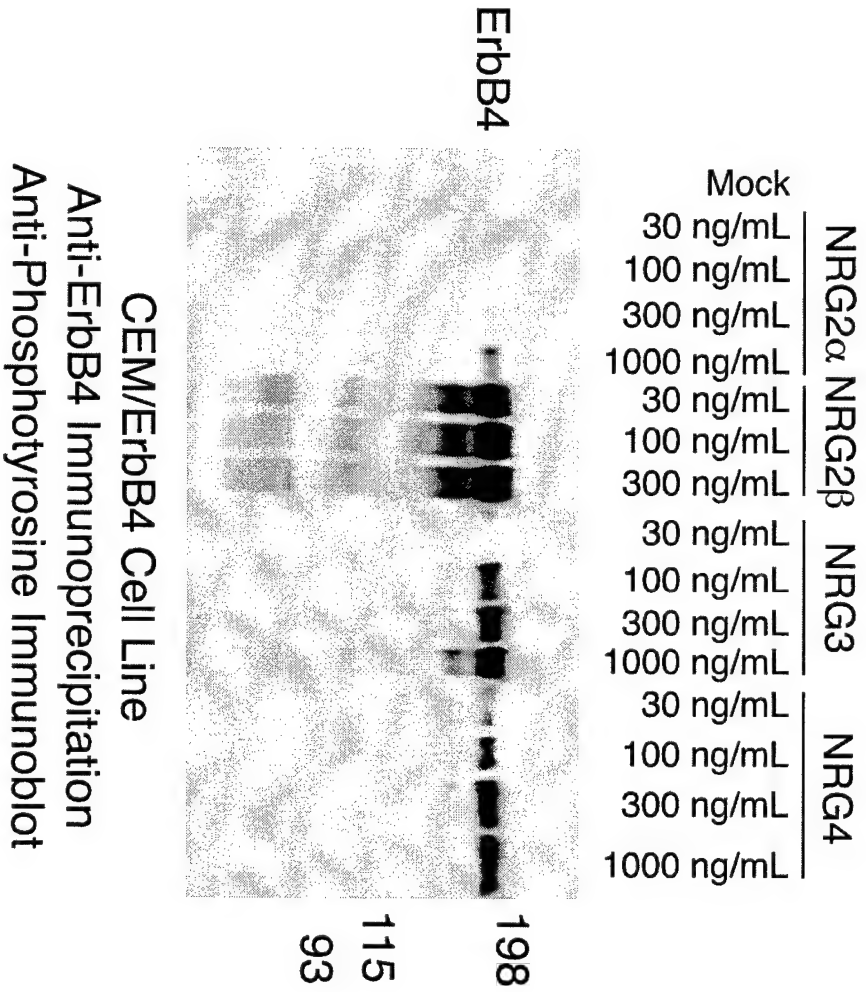

Figure 6. *The recombinant NRGs induce distinct patterns of IL3 independence in BaF3/ErbB2+ErbB3 and BaF3/EGFR+ErbB4 cell lines.* Cells were seeded in 24-well dishes at a density of $1x10^5$ cells/ml in medium lacking interleukin3 (IL3), in medium containing IL3, or in media lacking IL3 but supplemented with the NRGs indicated below (100 ng/mL). Cells were incubated for 96 hours, afterwhich viable cells were counted using a hemacytometer.

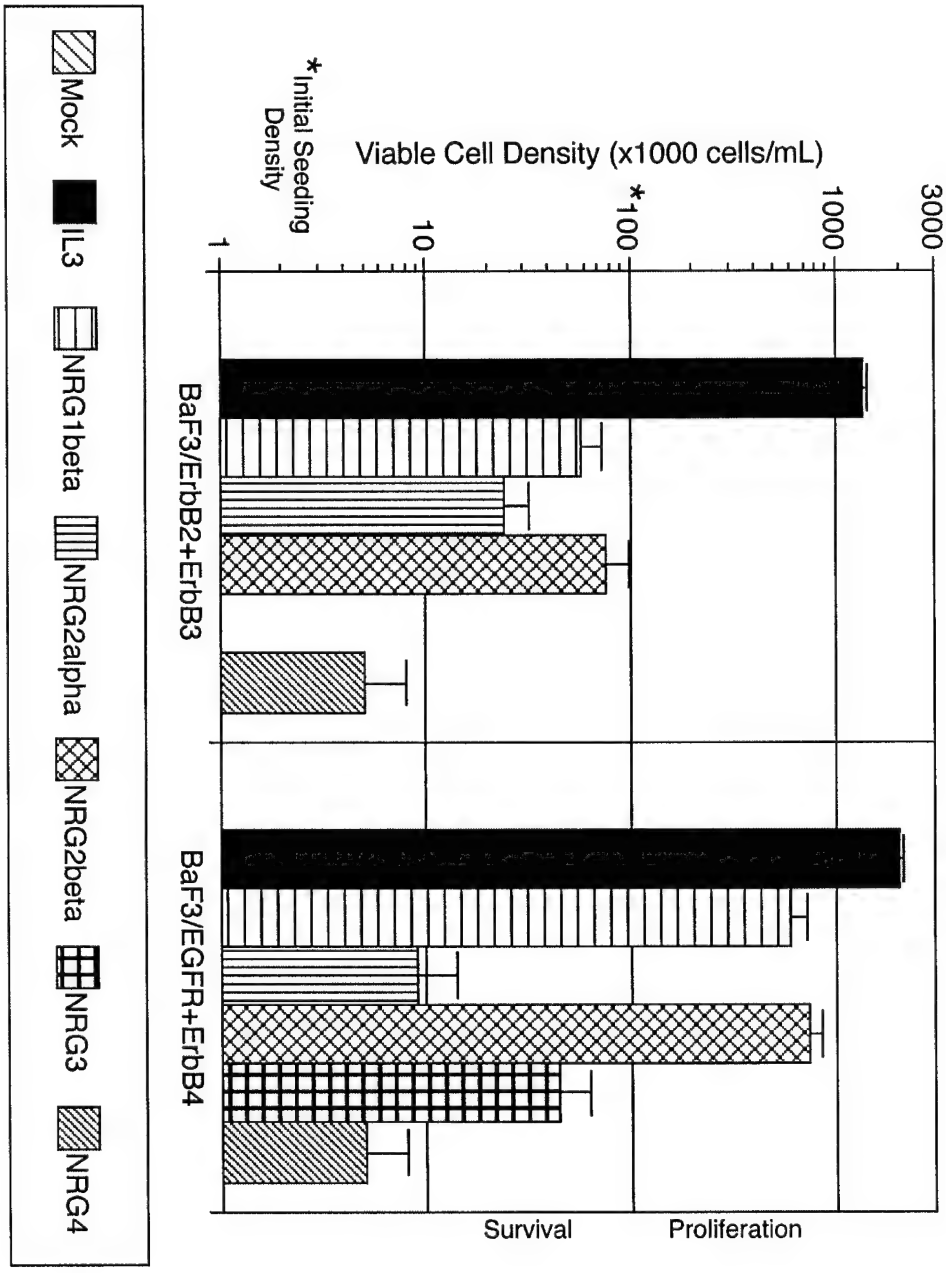

Figure 7. *Different NRG isoforms induce distinct patterns of EGFR and ErbB4 tyrosine phosphorylation in the BaF3/EGFR+ErbB4 cell line.* BaF3/EGFR+ErbB4 cells were stimulated with NRG isoforms (100 ng/mL) as noted below. The NRG solvent (PBS) was used as a negative (mock) control. Cells were lysed and receptors were precipitated using proteinA-sepharose and either an anti-EGFR monoclonal antibody or an anti-ErbB4 rabbit polyclonal antibody. A rabbit anti-mouse secondary antibody was used as a bridge between the anti-EGFR monoclonal antibody and the proteinA sepharose. Precipitates were resolved by SDS-PAGE and the resolved proteins were electroblotted onto nitrocellulose. The blots were probed with an anti-phosphotyrosine monoclonal antibody. Antibody binding was visualized using an HRP-conjugated anti-mouse secondary antibody and chemiluminescence. Positions of molecular weight markers are indicated.

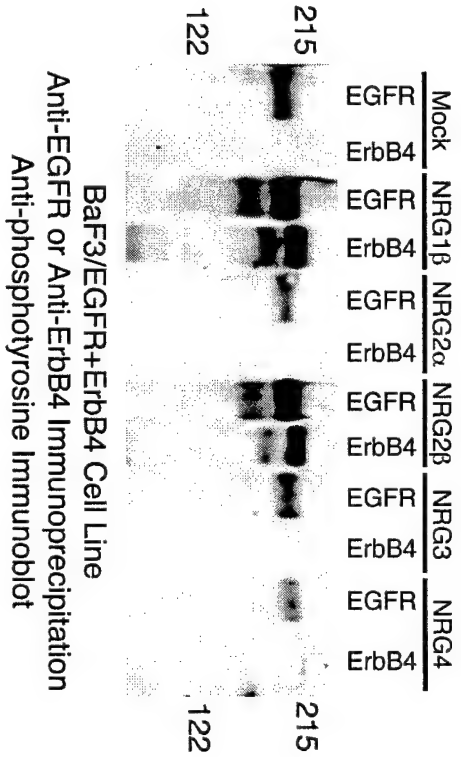

Figure 8. *Increased NRG3 and NRG4 concentrations fail to stimulate EGFR or ErbB4 tyrosine phosphorylation in the BaF3/EGFR+ErbB4 cell line.* BaF3/EGFR+ErbB4 cells were stimulated with NRG isoforms as noted below. The NRG solvent (PBS) was used as a negative (mock) control. Cells were lysed and receptors were precipitated using proteinA-sepharose and either an anti-EGFR monoclonal antibody or an anti-ErbB4 rabbit polyclonal antibody. A rabbit anti-mouse secondary antibody was used as a bridge between the anti-EGFR monoclonal antibody and the proteinA sepharose. Precipitates were resolved by SDS-PAGE and the resolved proteins were electroblotted onto nitrocellulose. The blots were probed with an anti-phosphotyrosine monoclonal antibody. Antibody binding was visualized using an HRP-conjugated anti-mouse secondary antibody and chemiluminescence. Positions of molecular weight markers are indicated.

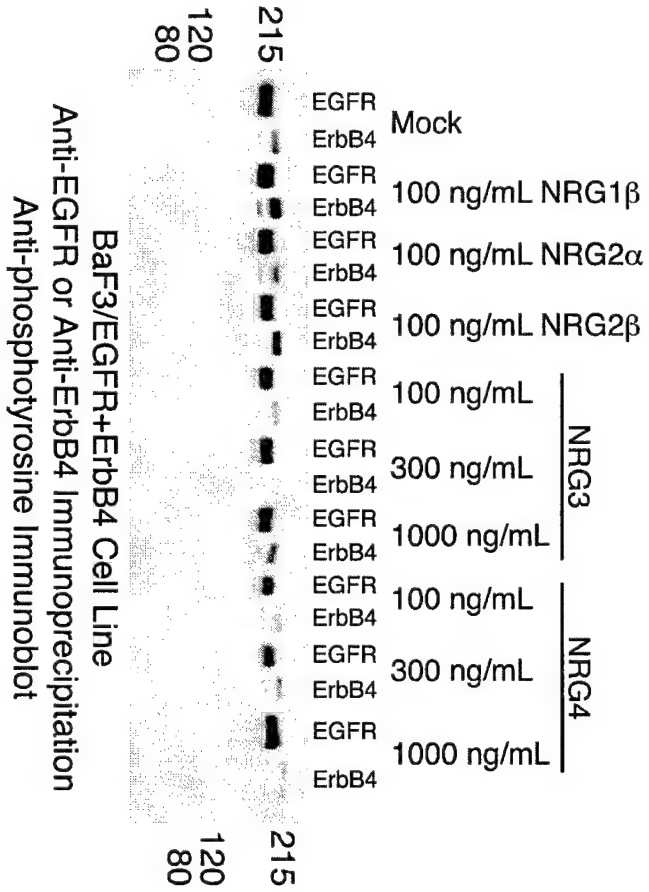

Figure 9. A Venn diagram illustrates the interactions of the four ErbB family receptors with the following EGF family hormones: Transforming Growth Factor alpha (TGFα), Amphiregulin (AR), Heparin-binding Epidermal Growth Factor-like Factor (HB-EGF), Betacellulin (BTC), Epiregulin (EPR), Neregulin1 beta (NRG1β), Neuregulin2 beta (NRG2β), Neuregulin1 alpha (NRG1α), Neuregulin2 alpha (NRG2α), Neuregulin3 (NRG3), and Neuregulin4 (NRG4).

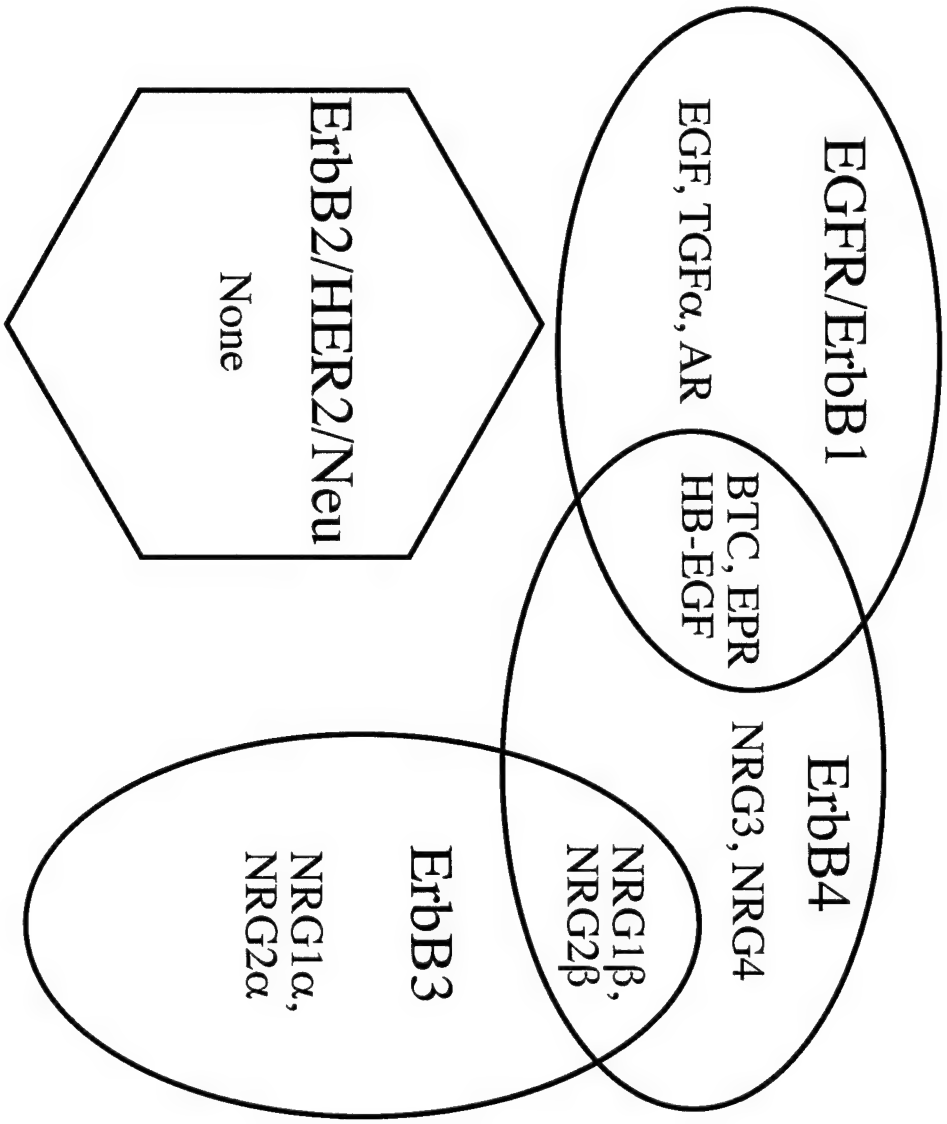

Design, Synthesis, and Biological Evaluation of a Series of Lavendustin A Analogues That Inhibit EGFR and Syk Tyrosine Kinases, as Well as Tubulin Polymerization

Fanrong Mu,† Stephanie L. Coffing,† David J. Riese II,† Robert L. Geahlen,† Pascal Verdier-Pinard,‡ Ernest Hamel,‡ Jill Johnson,§ and Mark Cushman*,†

Department of Medicinal Chemistry and Molecular Pharmacology, School of Pharmacy and Pharmacal Sciences, Purdue University, West Lafayette, Indiana 47907, Screening Technologies Branch, Developmental Therapeutics Program, Division of Cancer Treatment and Diagnosis, National Cancer Institute, Frederick Cancer Research and Development Center, Frederick, Maryland 21702, and Developmental Therapeutics Program, Division of Cancer Treatment and Diagnosis, National Cancer Institute, National Institutes of Health, Rockville, Maryland 20852

Received September 5, 2000

A series of *N*-alkylamide analogues of the lavendustin A pharmacophore were synthesized and tested for inhibition of the epidermal growth factor receptor (EGFR) protein tyrosine kinase and the nonreceptor protein tyrosine kinase Syk. Although several compounds in the series were effective inhibitors of both kinases, it seemed questionable whether their inhibitory effects on these kinases were responsible for the cytotoxic properties observed in a variety of human cancer cell cultures. Accordingly, a COMPARE analysis of the cytotoxicity profile of the most cytotoxic member of the series was performed, and the results indicated that its cytotoxicity profile was similar to that of antitubulin agents. This mechanism of action was supported by demonstrating that most compounds in the series were moderately effective as inhibitors of tubulin polymerization. This suggests that the lavendustin A analogues reported here, as well as some of the previously reported lavendustin A analogues, may be acting as cytotoxic agents by a mechanism involving the inhibition of tubulin polymerization.

Introduction

The protein tyrosine kinases (PTKs) play critical roles in many of the signal transduction processes that control cell growth, differentiation, mitosis, and death. They are therefore important targets for the development of therapeutic agents for the treatment of diseases that are characterized by uncontrolled cell proliferation, such as cancer and psoriasis.[1−3] Fractionation of a butyl acetate culture extract from *Streptomyces griseolavendus* led to the isolation of the novel PTK inhibitor lavendustin A.[4] Structure **1** was proposed for lavendustin A on the basis of ^{1}H and ^{13}C NMR data, and this tentative assignment was confirmed by total synthesis.[4] Lineweaver−Burke analysis carried out in the presence of varying concentrations of ATP and the substrate indicated that the inhibition was competitive with respect to ATP and noncompetitive with respect to the substrate when tested on the epidermal growth factor receptor (EGFR) tyrosine kinase,[4] although subsequent studies showed that lavendustin A can function as a hyperbolic mixed-type inhibitor with respect to both ATP and substrate.[5] It was also determined that the lavendustin A fragment **2** was as potent as the parent compound **1**, suggesting that **2** is the biologically active "pharmacophore" of lavendustin A.

These initial reports have stimulated work on the synthesis of lavendustin A itself and the synthesis and biological investigation of a variety of lavendustin

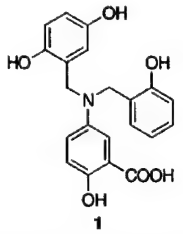

1

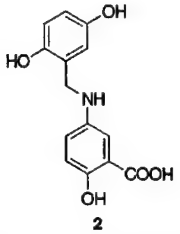

2

analogues.[6−15] The ester derivative **3** and the amide **4** were both found to compare favorably with the lavendustin A pharmacophore **2**. In particular, the ester **3** was as potent as **2** versus the EGFR tyrosine kinase in a cell-free assay, but **3** was more potent than **2** as an inhibitor of EGF-stimulated DNA synthesis in ER 22 cells.[10] Furthermore, the amide **4** was reported to be more potent than **2** as an inhibitor of EGFR tyrosine kinase in a cell-free system.[13] In view of these results, and as an extension of our earlier work on the solid-phase synthesis of lavendustin A and derivatives,[15] we decided to synthesize and evaluate a series of amide derivatives of lavendustin A having the general structure **5**. These compounds have been tested versus both the receptor PTK EGFR in BaF3 mouse lymphoid cells as well as the nonreceptor PTK Syk in a cell-free system. In addition, the new compounds in this series were evaluated as cytotoxic agents using a variety of cultured human cancer cell lines, and the cytotoxicity profile of at least one agent, **13b**, was found to be similar to that of antitubulin drugs when analyzed using the COMPARE algorithm.[16−18] Since the COMPARE program was developed as a predictor of mechanism of action, these results led to the hypothesis that the lavendustin

* To whom correspondence should be addressed. Tel: 765-494-1465. Fax: 765-494-1414. E-mail: cushman@pharmacy.purdue.edu.
† Purdue University.
‡ Frederick Cancer Research and Development Center.
§ National Institutes of Health.

10.1021/jm000387g CCC: $20.00
Published on Web 01/03/2001

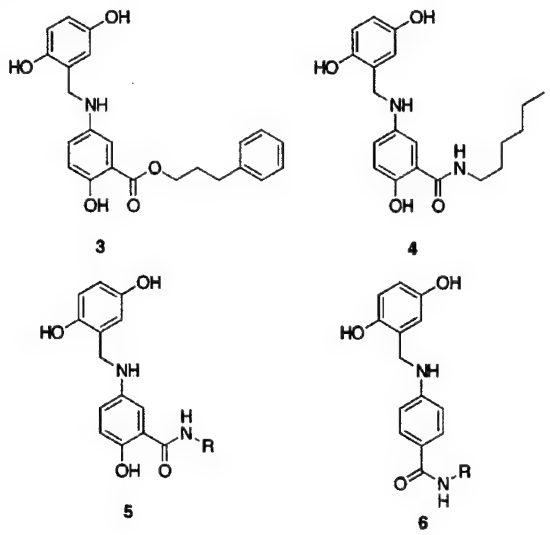

A analogues in our series were functioning as inhibitors of tubulin polymerization, and the appropriate assays were performed to test this hypothesis.

The COMPARE Algorithm

The COMPARE program was developed at the Developmental Therapeutics Program, National Cancer Institute (NCI), to interpret the emerging data from the 60-cell line in vitro human cancer cell cytotoxicity screen and display it in way that would facilitate comparison of the different patterns of dose–response curves produced by different cytotoxic agents. Paull and colleagues developed the "mean graph" representation of the screening data in which the mean concentration affecting all 60 cell lines at three levels of effect (GI_{50} = concentration causing 50% inhibition of growth; TGI = concentration causing total inhibition of growth; LC_{50} = concentration causing 50% cell kill) is plotted in the midline of the graph and the behavior of each individual cell line is represented as a deflection to the left for cells more resistant than the mean and to the right for cells more sensitive than the mean.[17] An important application of this manner of presentation is provided by the richly informative patterns of activity that emerge. Correlations of activity patterns can be quantified using a pattern recognition algorithm named COMPARE.[16] Use of the COMPARE program led to the realization that compounds with the same or similar mechanisms of action often result in cytotoxicity patterns that are similar.[16] This approach has resulted in identification of new tubulin polymerization inhibitors,[19] topoisomerase I and II inhibitors,[20,21] and dihydroorotate dehydrogenase inhibitors.[22] In another example, the use of COMPARE linked the effects of cucurbitacin[23] and jasplakinolide[24] to the actin cytoskeleton. Compounds with unique cytotoxicity profiles, suggesting modes of action not shared with the known clinically active classes of chemotherapeutic agents, have also been identified.[25]

A COMPARE analysis for a test agent can be run against the entire database of more than 77 000 compounds that have been tested in the NCI cell line cytotoxicity assay or against a database of standard agents whose mechanism of cytotoxicity is well-documented or against a single compound. The result of the analysis is a list of compounds in rank order and Pearson correlation coefficients, which provide an indication of the similarity of the patterns of cell line responses. Correlation coefficients of ≥ 0.60 are generally considered to be meaningful. For example, when a COMPARE is performed using paclitaxel as the seed, the correlation coefficient for vinblastine sulfate (another tubulin-interactive agent) is 0.88, whereas the correlation coefficient for phyllanthoside (a topoisomerase II inhibitor) is 0.422. The hypothetical mechanism of action suggested by COMPARE analysis can then be confirmed by laboratory testing. The reason that COMPARE analysis is a predictor of mechanism of action is that biological targets are expressed to a different extent in different cell lines, so that compounds which interact with a single biological target will have similar cytotoxicity patterns when tested in these cell lines.[26]

A COMPARE analysis was performed using **13b** as a seed. The top 20 compounds in the COMPARE analysis included 9 taxanes, 3 colchicine analogues, 2 combretastatins, and vinblastine, all of which interact with tubulin. Representative correlation coefficients between **13b** and various tubulin-interactive drugs were docetaxel, 0.790; vinblastine sulfate, 0.761; paclitaxel, 0.703; and maytansine, 0.701.

Synthesis

The synthesis of the series of lavendustin A analogues **13a–m** is a modification of a previously published route used to prepare a series of lavendustin A hydroxamic acid derivatives (Scheme 1).[10] Treatment of commercially available 5-aminosalicylic acid (**7**) with di-*tert*-butyl dicarbonate and triethylamine in aqueous dioxane afforded the Boc-protected intermediate **8**. Reaction of **8** with the appropriate primary amines **9a–m** in the presence of 1-(3-dimethylaminopropyl)-3-ethylcarbodiimide hydrochloride (EDCI), 1-hydroxybenzyltriazole hydrate (HOBt), and triethylamine in dry DMF yielded the series of amides **10a–m**. Deprotection of the intermediates **10a–m** with a mixture of dichloromethane and trifluoroacetic acid resulted in the formation of the primary amines **11a–m**. Reaction of **11a–m** with 2,5-dihydroxybenzaldehyde (**12**) afforded the corresponding Schiff bases, which were reduced with sodium cyanoborohydride to provide the desired lavendustin A analogues **13a–m**.

As outlined in Scheme 2, a variation of this route was executed in order to obtain the congeners **18a–c**, in which the aniline part of the molecule is substituted in the para position with various amides. Similarly, the lavendustin A analogue **23**, having a β-phenethylamide substituent in the meta position relative to the aniline nitrogen but lacking an adjacent phenolic hydroxyl group, was prepared as shown in Scheme 3.

Biological Results and Discussion

The lavendustin A analogues were examined for antiproliferative activity against the human cancer cell lines in the NCI cytotoxicity screen, in which the activity of each compound was evaluated using approximately 55 different cancer cell lines of diverse tumor origins. The mean-graph midpoint values (MGMs) listed in

Scheme 1

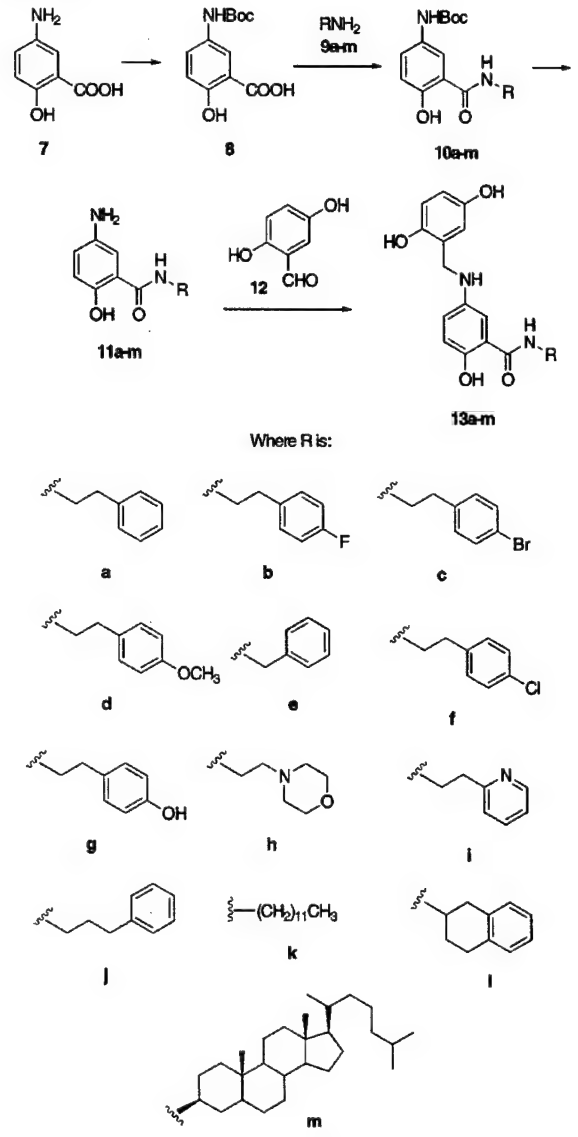

Scheme 2

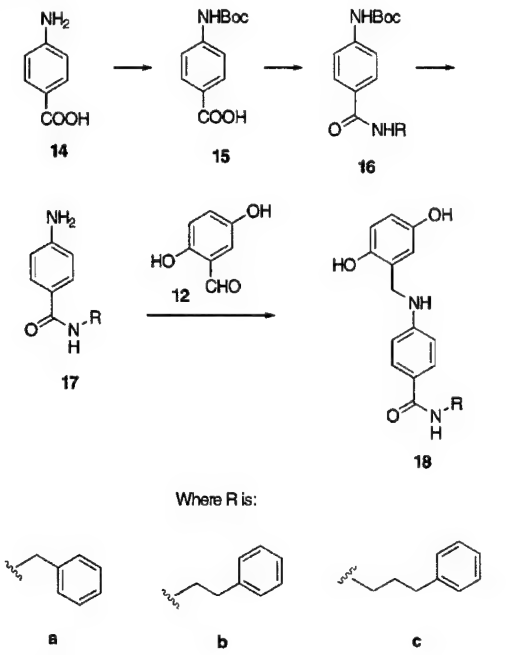

Scheme 3

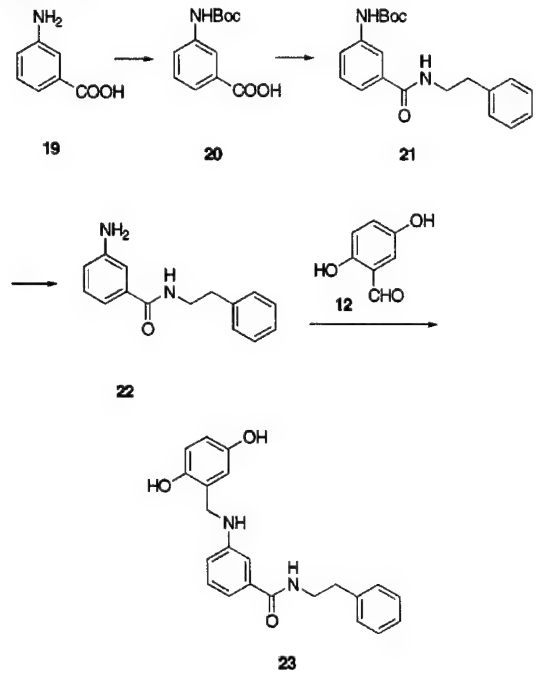

Table 1 are based on a calculation of the average GI_{50} values for all of the cancer cell lines tested (approximately 55) in which GI_{50} values below and above the test range (10^{-4}–10^{-8} M) are taken as the minimum (10^{-8} M) and maximum (10^{-4} M) drug concentrations used in the screening test.[18] A more detailed listing of the cytotoxicities of each compound in eight representative human cancer cell lines is presented in Table 2. With the exception of the cholestane derivative **13m**, all of the compounds in the series were found to be cytotoxic in human cancer cell cultures, with MGM values ranging from 0.35 to 20.4 μM. Starting with the basic β-phenylethylamine **13a**, which had an MGM of 14.8 μM, various substituents were introduced into the para position in order to determine how they affected cytotoxicity. The substituent that resulted in the greatest cytotoxicity was fluorine (**13b**, MGM 0.35 μM), followed by bromine (**13c**, MGM 7.6 μM), chlorine (**13f**, MGM 10.0 μM), methoxy (**13d**, MGM 15.4 μM), and hydroxy (**13g**, MGM 20.4 μM). Lengthening the chain of **13a** by one methylene unit had no appreciable effect on cytotoxicity (**13j**, MGM 13.2 μM), and shortening it by one methylene group also had little effect on cytotoxicity (**13e**, MGM 15.5 μM). The replacement of the benzene ring by a 2-pyridyl substituent (**13i**, MGM 16.0 μM) or a 2-tetralinyl substituent (**13l**, MGM 11.2 μM) did not result in any appreciable change in activity, while replacement of the benzene ring by a morpholine ring caused a slight decrease in cytotoxicity (**13h**, MGM 19.5 μM). The appendage of a long hydrocarbon chain to the amide in **13k** resulted in one of the more cytotoxic compounds (MGM 2.7 μM), but it was not an inhibitor of tubulin polymerization or Syk PTK (see below).

Table 1. Inhibitory Activities of Lavendustin A Analogues

	IC_{50} (μM)					
compd	MGM[a]	tubulin[b]	Syk[c]	EGFR[d]	MCF-7 DNA[e]	MCF-10A DNA[f]
4	8.7 ± 0.4	3.6 ± 0.7	NT[g]	14 ± 10	11 ± 4	14 ± 3
13a	14.8 ± 1.4	3.6 ± 1	5	10 ± 4	9 ± 3	11 ± 3
13b	0.35 ± 0.05	4.0 ± 0.4	5	4 ± 2	12 ± 4	10 ± 1
13c	7.6 ± 2.4	4.2 ± 0.5	45	35 ± 11	7 ± 0	6 ± 1
13d	15.4	4.2 ± 0.8	50	>100	14 ± 0	11 ± 2
13e	15.5	3.2 ± 0.6	25	8 ± 4	17 ± 4	17 ± 4
13f	10.0 ± 0.95	3.2 ± 0.7	25	46 ± 13	13 ± 2	9 ± 1
13g	20.4	4.5 ± 1	5	~300	16 ± 3	15 ± 2
13h	19.5	2.1 ± 0.4	1.5	>50	14 ± 3	16 ± 5
13i	16.0 ± 0.55	3.6 ± 0.3	NT[g]	15 ± 6	11 ± 5	7 ± 0.0
13j	13.2 ± 0.3	5.0 ± 1	28	1 ± 0.4	2 ± 0.2	2 ± 0.0
13k	2.7 ± 0.1	>40	50	35 ± 7	1 ± 0.3	3 ± 0.5
13l	11.2 ± 1.4	5.3 ± 0.9	8	4 ± 1	10 ± 3	6 ± 0.7
13m	>100	>40	NT[g]	*	>50	NT[g]
18a	8.8 ± 1.7	6.2 ± 1	18	>100	16 ± 3	34 ± 9
18b	6.4 ± 1.2	4.9 ± 0.9	5	>200	3 ± 1	7 ± 2
18c	5.3 ± 1.3	5.7 ± 1	35	33 ± 5	0.4 ± 0.1	3 ± 1
23	12.1 ± 0.8	6.9 ± 1	>100	~500	5 ± 1	6 ± 1

[a] Mean graph midpoint for growth inhibition of all human cancer cell lines (approximately 55) successfully tested. [b] IC_{50} values for inhibition of tubulin polymerization. [c] IC_{50} values for in vitro inhibition of Syk PTK. [d] IC_{50} values for inhibition of EGFR phosphorylation in BaF3 mouse lymphoid cells. [e] IC_{50} values for inhibition of DNA synthesis in MCF-7 cells. [f] IC_{50} values for inhibition of DNA synthesis in MCF-10A cells. [g] NT, not tested. * Stimulates EGFR tyrosine phosphorylation.

Table 2. Cytotoxicities of Lavendustin A Analogues in Human Cancer Cell Cultures

	GI_{50} (μM)[a]									
compd	leukemia CCRF-CEM	lung HOP-62	colon HCT-116	CNS SF-539	melanoma UACC-62	ovarian OVCAR-3	renal SN12C	prostate DU-145	breast MDA-MB-435	MGM[b]
4	0.56	19	17	2.3	12	4.0	6.1	15	15	8.7
13a	2.7	20	18	17	14	7.7	18	16	19	14.8
13b	0.29	12	9.2	9.2	7.8	11	7.7	18	13	0.35
13c	NT[c]	18	7.6	15.8	8.6	4.2	6.3	16	10	7.6
13d	3.2	12	23	16	14	5.5	72	21	16	15.4
13e	3.2	23	17	21	15	21	12	16	30	15.5
13f	1.6	17	15	8.4	13	5.9	9.8	16	20	10.0
13g	NT[c]	2.5	16	2.5	18	62	19	17	23	20.4
13h	1.8	NT[c]	20	19	17	87	22	17	13	19.5
13i	1.0	20	17	29	17	17	19	17	13	16.0
13j	2.4	22	24	16	14	6.5	15	8.4	18	13.2
13k	0.34	3.8	2.1	20	3.2	1.9	2.6	11	3.2	2.7
13l	1.4	17	16	2.7	14	7.9	18	17	9.2	11.2
18a	2.7	20	10	9.7	12	6.8	9.7	15	12	8.8
18b	0.59	13	7.4	8.5	9.4	2.7	7.4	14	5.1	6.4
18c	0.83	16	6.4	3.4	7.9	3.0	3.2	13	5.8	5.3
23	4.4	3.8	16	15	13	2.8	13	17	15	12.1

[a] The cytotoxicity GI_{50} values are the concentrations (μM) corresponding to 50% growth inhibition. [b] Mean graph midpoint for growth inhibition of all human cancer cell lines successfully tested. [c] NT, not tested.

Because the hydrocarbon chain in **13k** might be expected to be membrane-interactive, it was replaced by the cholestanyl moiety in **13m**, since that would be expected to bind strongly to biological membranes. However, the resulting compound **13m** proved to be inactive.

A series of analogues **18a–c** was designed by moving the amide to the para position and eliminating the phenolic hydroxyl group. The extension of the amide substituent by consecutive addition of methylene groups led to small increases in cytotoxicity (**18a**, MGM 8.8 μM; **18b**, MGM 6.4 μM; **18c**, MGM 5.3 μM). However, these small differences in cytotoxicity may not be significant based on the standard deviations reported. A final modification in this series involved the elimination of the phenolic hydroxyl group from **13a** (MGM 14.8 μM), resulting in **23** (MGM 12.1). Comparison of **13a** and **23** indicates that the phenolic hydroxyl group of **13a** is not a requirement for cytotoxicity.

Inhibition of EGF-stimulated EGFR phosphorylation by a number of the lavendustin A analogues was tested in BaF3 cells. After addition of inhibitor to the cells, they were stimulated by EGF under conditions which induce abundant receptor phosphorylation but not receptor downregulation or internalization.[27] Immunoprecipitates from the lysed cells were resolved by polyacrylamide gel electrophoresis and electrotransferred onto nitrocellulose. The resulting Western blots were probed with a mouse monoclonal antiphosphotyrosine antibody, and the bound antibody was detected by probing the blot with a horseradish peroxidase-coupled goat anti-mouse antibody. The antibody complexes were visualized by enhanced chemiluminescence. The resulting IC_{50} values for inhibition of EGFR phosphorylation are listed in Table 1. A total of 18 compounds were tested, of which 5 showed appreciable activity (IC_{50} 10 μM or less). The three most potent compounds were **13j** (IC_{50} 1 μM), having a γ-phenyl-

propyl substituent on the amide nitrogen, **13b** (IC_{50} 4 μM), having a *p*-fluoro-β-phenylethyl substituent, and **13l** (IC_{50} 4 μM), having a β-tetralinyl substituent. These three compounds were followed by the benzyl analogue **13e** (IC_{50} 8 μM) and the β-phenylethyl congener **13a** (IC_{50} 10 μM). Each of these values was relatively close to the IC_{50} values for inhibition of DNA synthesis in MCF-7 cells and MCF-10A cells (Table 1). Since MCF-10A cells are EGF-dependent, while MCF-7 cells are not, the fact that the two cell types exhibit similar responses to the lavendustin A analogues is evidence that inhibition of EGFR tyrosine kinase activity is not relevant to the cytotoxic activities of the lavendustin A analogues.[28-31] Compounds **13c,d,f,g**, **18c**, and **23** did not show appreciable activity versus EGFR tyrosine kinase at the concentrations tested.

To assay the new lavendustin A congeners versus a representative nonreceptor PTK, Syk was obtained from lysates of Sf9 cells infected with a baculovirus directing the expression of the full-length enzyme as a fusion protein with glutathione S-transferase. GST-Syk was isolated by affinity chromatography on glutathione-agarose. The activities of the inhibitors were assayed by monitoring the transfer of ^{32}P from [γ-^{32}P]ATP to tyrosyl residues on the immobilized kinase. Reactions were terminated by the addition of EDTA. The immobilized kinase was separated from unreacted [γ-^{32}P]-ATP by centrifugation. The extent of kinase autophosphorylation was determined by liquid scintillation spectrometry. The resulting IC_{50} values are listed in Table 1. In general, IC_{50} values for the inhibition of Syk were comparable to those obtained for the inhibition of EGFR. Four compounds (**13g,h** and **18a,b**), however, did display considerable selectivity for Syk as compared to the EGFR. These IC_{50} values are comparable to that of the Syk-selective inhibitor, piceatannol (**24**), which had an IC_{50} value of 5 μg/mL in this assay.

Whether or not the cytotoxicities of the lavendustin A analogues reported here are due to PTK inhibition is questionable. Since almost all of the EGFR tyrosine kinase activity must be inhibited before effects are seen on cell growth,[27] it is unlikely that the potencies of EGFR inhibitors seen here could possibly be responsible for the effects seen on inhibition of cancer cell growth, since the IC_{50} values for EGFR inhibition are close to the MGMs observed for growth inhibition. The fact that lavendustin A did not inhibit the PTK activity of the mutant protein pp60src^{F527}, but nevertheless did exhibit antiproliferative activity, previously led other investigators to the conclusion that the antiproliferative effects of lavendustin A could be due to actions on cellular targets downstream of pp60src^{F527} or receptors unrelated to the kinase.[11] We therefore also considered other possible targets for the new lavendustin analogues that might be responsible for their inhibitory effects on cancer cell growth.

As stated previously, the COMPARE analysis of **13b** suggested that the lavendustin A analogues in this series might be interacting with tubulin. As shown in Table 1, this turned out to be the case. All of the compounds except **13k,m** inhibited tubulin polymerization with IC_{50} values ranging from 2.1 to 6.9 μM. Under the reaction conditions used here, these values indicate the compounds are moderately active as inhibitors of the polymerization reaction. In previous studies under the same reaction conditions, known potent antimitotic agents such as combretastatin A-4 and dolastatin 10 reproducibly yield IC_{50} values in the 0.5–1.0 μM range. Compounds **4** and **13b,h** were also shown to be weak inhibitors of the binding of [^{3}H]colchicine to tubulin. In an assay with tubulin at 1 μM, [^{3}H]colchicine at 5 μM, and the three agents at 50 μM, the percent inhibitions for these compounds were **13b**, 38 ± 10%; **13h**, 34 ± 20%; and **4**, 45 ± 20%; as compared to 98 ± 2% with 5 μM combretastatin A-4 (**25**) (data not presented).

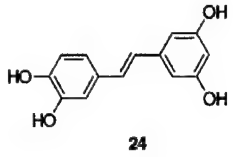

24

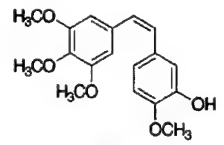

25

The activity of these compounds as inhibitors of tubulin polymerization was unexpected on the basis of prior literature reports, which have indicated that polyhydroxylated *trans*-stilbenes, benzylanilines, and related compounds are inhibitors of the PTKs, while their polymethoxylated *cis*-stilbene analogues and related compounds are inhibitors of tubulin polymerization. For example, in addition to lavendustin A and its analogues, other polyhydroxylated stilbene PTK inhibitors include piceatannol (**24**) and related polyhydroxylated *trans*-stilbenes,[7,32,33] while the polymethoxylated *cis*-stilbene inhibitors of tubulin polymerization include combretastatin A-4 (**25**) and its analogues.[34-37] Polymethoxylated *trans*-stilbenes are much less active as inhibitors of tubulin polymerization and as cytotoxic agents than their cis counterparts.[33] Neussbaumer et al. previously reported that the methylated lavendustin A analogues **26** and **27** have antiproliferative effects and that **27** acts "by blocking the cell cycle at mitosis by perturbing the microtubules of the mitotic spindle apparatus".[12,38] This would basically be in agreement with our prior study which had indicated that the benzylamine **28** and analogous compounds are antimitotic agents that act by inhibition of tubulin polymerization.[37] Furthermore, the methylated lavendustin A analogue **27** did not inhibit EGFR tyrosine kinase in a cell-free system.[38]

However, when we examined human Burkitt lymphoma cells treated with several members (**4**, **13b,c,e,f,k**, and **18a–c**) of this series of compounds for evidence of mitotic arrest (increase in G2/M cells), only **13b** caused such an effect. We thus have evidence for an antitubulin effect at the cellular level only with the most cytotoxic member of the series.

The abilities of the present polyhydroxylated benzylaniline derivatives of lavendustin A to inhibit both receptor and nonreceptor PTKs, as well as tubulin polymerization, is a novel observation which raises the possibility that the antiproliferative effects observed both in this series and in the other series of lavendustin A analogues reported in the literature may actually be due in part to inhibition of tubulin polymerization, rather than any effect on PTK inhibition. The lavendustin A derivatives reported are also unusual tubulin

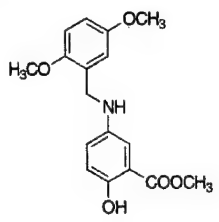

26

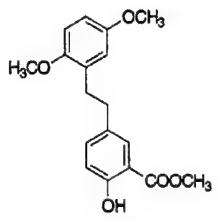

27

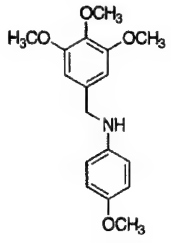

28

polymerization inhibitors, since they are not polymethoxylated *cis*-stilbene or benzylaniline analogues.

Experimental Section

General. Melting points are uncorrected. Nuclear magnetic resonance spectra for proton (^{1}H NMR) were recorded on a 300-MHz spectrometer. The chemical shift values are expressed in ppm (parts per million) relative to tetramethylsilane as internal standard; s = singlet, d = doublet, m = multiplet, bs = broad singlet. Microanalyses were performed at the Purdue Microanalysis Laboratory, and all values were within ±0.4% of the calculated compositions. Column chromatography was carried out using Merck silica gel (230–400 mesh). Analytical thin-layer chromatography (TLC) was performed on silica gel GF (Analtech) glass-coated plates (2.5 × 10 cm with 250 μm layer and prescored), and spots were visualized with UV light at 254 nm. Most chemicals and solvents were analytical grade and used without further purification. Commercial reagents were purchased from Aldrich Chemical Co. (Milwaukee, WI).

Tubulin Assays. Electrophoretically homogeneous tubulin was purified from bovine brain as described previously.[39] The tubulin polymerization and colchicine binding assays were performed as described previously,[40] except that Beckman DU7400/7500 spectrophotometers equipped with "high-performance" temperature controllers were used in the former assay. Unlike the manual control possible with the previously used Gilford spectrophotometers, the polymerization assays required use of programs provided by MDB Analytical Associates, South Plainfield, NJ, since the Beckman instruments are microprocessor-controlled. The Beckman instruments were unable to maintain 0 °C, and the lower temperature in the assays fluctuated between 2 and 4 °C. Temperature changes were, however, more rapid than in the Gilford instruments with the jump from the lower temperature to 30 °C taking about 20 s and the reverse jump about 100 s.

Syk Assays. Preparation of GST-Syk was as described previously.[41] Autophosphorylation reactions contained 50 mM Tris/HCl, pH 7.4, 5 mM $MnCl_2$, 5 μM ATP, 5 μCi [γ-^{32}P]ATP, 1 mM sodium orthovanadate, 5 mM *p*-nitrophenyl phosphate and 1.5% DMSO, which was used as a carrier for the inhibitors. Reactions were terminated by the addition of EDTA to a final concentration of 10 mM. Beads were washed 2 times in 50 mM Tris/HCl, pH 7.4, 1 mM sodium orthovanadate and 10 mM EDTA and counted by liquid scintillation spectrometry. IC_{50} values were determined graphically and represent the concentration of inhibitor that gives half-maximal inhibition as compared to control assays carried out in the absence of inhibitor but in the presence of DMSO carrier.

Cell Lines and Cell Culture. The CEM human T lymphocyte cell line engineered to express ErbB4 (CEM/4) and its culture conditions have been described previously.[42,43] Briefly, these cells were propagated in RPMI supplemented with 10% heat-inactivated fetal bovine serum and 300 μg/mL G418. The BaF3 mouse lymphoid cell lines engineered to express either EGFR (BaF3/EGFR) or ErbB2 and ErbB3 together (BaF3/2+3) and the culture conditions for these cell lines have been described earlier.[27] These cells were propagated in RPMI supplemented with 10% fetal bovine serum, 300 μg/mL G418, and 10% medium conditioned by WeHI cells. This conditioned medium serves as a source for interleukin 3.

MCF-10A human mammary epithelial cells and MCF-7, MDA-MB-231, and MDA-MB-453 human mammary tumor cell lines were obtained from the American Type Culture Collection (ATCC). These lines were propagated according to ATCC recommendations.

Inhibition of Receptor Tyrosine Phosphorylation Assay. The assay for inhibition of ErbB family receptor tyrosine phosphorylation was adapted from a previously described protocol.[27,43] Briefly, 200-mL cultures of CEM/4, BaF3/EGFR, or BaF3/2+3 cells were grown to saturation density (~10^6 cells/mL) and were incubated for 24 h at 37 °C in serum-free medium to reduce basal levels of receptor tyrosine phosphorylation. The cells were collected by centrifugation and resuspended in serum-free medium at a final concentration of ~10^7 cells/mL (~20 mL of cells). Cells were transferred to microcentrifuge tubes in 1-mL aliquots and putative kinase inhibitors were added to the cells. Each tyrosine kinase inhibitor was tested at 3–5 different concentrations. The inhibitors were dissolved in 5 μL of DMSO; hence, cells treated with 5 μL of DMSO were used as a solvent control. Cells were incubated in the presence of inhibitor for 2 h at 37 °C, then were incubated on ice for 20 min. Chilling the cells reduces the amount of ligand-induced receptor downregulation.[27]

Ligand was then added to the appropriate samples at a final concentration of 100 ng/mL and the samples were mixed and incubated on ice for 7 min. Recombinant human EGF (Sigma) was used as the ligand for EGFR, while neuregulin1β (NRG1β; R&D Systems) was used as the ligand for ErbB3 and ErbB4. Note that because ErbB3 lacks kinase activity, ligand-induced ErbB2 and ErbB3 phosphorylation in the BaF3/2+3 cells is the result of ErbB2 kinase activity.[27] Following incubation with ligand, the cells were collected by centrifugation, the supernatant was removed by aspiration, and the cells were resuspended in an isotonic lysis buffer containing 0.5% NP40/Igepal CA-630 (nonionic detergent; Sigma).

The cells were incubated for 20 min on ice to permit lysis. The samples were centrifuged for 10 min at 4 °C to collect the nuclei and cellular debris. The supernatants (cell lysates) were transferred to fresh tubes. Concanavalin A Sepharose (Amersham/Pharmacia) beads were added to each sample (35 μL of a 50% v/v slurry) and the samples were incubated at 4 °C for 30 min. Concanavalin A Sepharose precipitates the cellular glycoproteins, which include ErbB family receptors. The precipitated glycoproteins were washed 3 times with 500 μL of ice-cold lysis buffer, then were eluted by boiling the beads for 5 min in 80 μL of reducing SDS protein sample buffer. The beads were collected by centrifugation and one-half of the eluted glycoproteins (40 μL) were recovered and resolved by SDS/PAGE on a 7.5% acrylamide gel.

The resolved glycoproteins were electroblotted onto nitrocellulose (BiotraceNT; Gelman Sciences). The resulting blot was blocked by incubation for 45 min at room temperature in a solution consisting of 5% bovine serum albumin (Sigma) dissolved in Tris-buffered normal saline (TBS) supplemented with 0.05% Tween-20 (TBS-T). The blot was then probed with a mouse monoclonal antiphosphotyrosine antibody (4G10; Upstate Biotechnology). The blot was washed with TBS-T 5 times for 6 min each, and primary antibody binding was detected by probing the blot with a goat anti-mouse antibody conjugated to horseradish perioxidase (HRP; Pierce). The blot was washed with TBS-T 12 times for 10 min each, after which HRP activity was visualized by enhanced chemiluminescence (ECL; Amersham Pharmacia Biotech). The resulting chemilumigrams were digitized using a Linotype-Hell Jade flatbed

scanner and the amount of receptor tyrosine phosphorylation was quantified using NIH Image software. The amount of receptor tyrosine phosphorylation in samples from cells treated with a putative receptor tyrosine kinase inhibitor were compared to a standard curve generated using samples from cells treated with DMSO solvent control. This enabled us to determine the concentration of a given tyrosine kinase inhibitor that was necessary to cause a 50% reduction in receptor tyrosine phosphorylation. This value is reported as the receptor tyrosine phosphorylation IC_{50} value.

Inhibition of Cellular DNA Synthesis Assay. The assay for inhibition of cellular DNA synthesis was adapted from a previously described protocol.[44] Briefly, human mammary (tumor) cells were seeded in 1-mL aliquots into 24-well culture dishes at a density of 10^5 cells/well. Cells were incubated for 24 h at 37 °C, and a tyrosine kinase inhibitor dissolved in DMSO was added to each well in a volume of 10 μL. Each tyrosine kinase inhibitor was assayed at 3–5 different concentrations and each concentration was assayed using 3–4 wells of cells. Cells treated with 10 μL of DMSO served as the solvent control. Cells were then incubated for 48 h at 37 °C. [^{3}H]Thymidine (1.5 μCi; Amersham Pharmacia Biotech) dissolved in a 1.5 μL of an aqueous solution was added to each well and the cells were incubated for an additional 2 h at 37 °C. The culture medium was aspirated from the wells, and the cells were rinsed once with 1 mL of ice-cold phosphate-buffered saline (PBS) and once with 1 mL of ice-cold 10% trichloroacetic acid (TCA). Incorporated [^{3}H]thymidine was precipitated by incubating the cells for at least 30 min at 4 °C in 1 mL of 10% TCA. Following incubation, the TCA solution was aspirated from each well and the precipitated (incorporated) [^{3}H]thymidine was solubilized by incubating the cells for 30 min at 95 °C in 500 μL of 3% perchloric acid. The perchloric acid samples were transferred to scintillation vials containing 10 mL of Cytoscint scintillation cocktail (ICN). The incorporated [^{3}H]-thymidine was assayed by scintillation counting on a Packard Tricarb scintillation counter. The amount of [^{3}H]thymidine incorporation observed in the cells treated with the solvent control was divided by 2 (two) to determine the amount of half-maximal [^{3}H]thymidine incorporation. Dose–response curves for each combination of putative tyrosine kinase inhibitor and cell line were then constructed using the [^{3}H]thymidine incorporation data. The dose–response curves and the half-maximal [^{3}H]thymidine values were used to calculate the concentration of each inhibitor required to inhibit [^{3}H]thymidine incorporation by 50% in a given cell line. This value is reported as the DNA synthesis IC_{50} value.

5-[*N*-(*tert*-Butoxycarbonyl)amino]salicylic Acid (8). To a mixture of 5-aminosalicylic acid (**7**) (3.0 g, 19.6 mmol) in dioxane (50 mL) and water (25 mL) were added triethylamine (4.0 mL, 29.3 mmol) followed by di-*tert*-butyl dicarbonate (6.4 g, 29.3 mmol). The reaction mixture was stirred at room temperature for 24 h. Solvent was removed by rotary evaporation, and 3 N aqueous hydrochloric acid (30 mL) was added dropwise to the residue. A precipitate was obtained, collected, washed with water, and dried to provide **8** (4.76 g, 96%) as a solid: mp 279–280 °C; ^{1}H NMR (300 MHz, DMSO-d_6) δ 9.29 (s, 1 H), 7.96 (d, J = 1.81 Hz, 1 H), 7.47 (dd, J = 8.93, 2.69 Hz, 1 H), 6.85 (d, J = 8.88 Hz, 1 H), 1.44 (s, 9 H).

5-[*N*-(*tert*-Butoxycarbonyl)amino]-*N*-(β-phenethyl)salicylamide (10a). To a solution of **8** (1.5 g, 5.93 mmol) in dry DMF (15 mL) were added EDCI (1.71 g, 8.92 mmol), HOBt (1.2 g, 8.92 mmol) and triethylamine (1.65 mL, 11.86 mmol). After stirring at room temperature for 24 h, β-phenethylamine **(9a)** (3.7 mL, 29.5 mmol) was added dropwise and the reaction continued for 48 h at room temperature under argon. Water (300 mL) was then added and the mixture stirred for 5 min. The product was then extracted with ethyl acetate (5 × 50 mL). The combined organic extracts were washed with brine (1 × 40 mL), dried over sodium sulfate, filtered, and the solvent removed. Purification was achieved by flash chromatography (silica gel 75 g, ethyl acetate/hexane 1:4 by volume) to yield pure **10a** (1.09 g, 52%) as a white crystalline solid: ^{1}H NMR (300 MHz, $CDCl_3$) δ 12.13 (s, 1 H), 7.74 (s, 1 H), 7.36–7.24 (m, 6 H), 7.00 (dd, J = 8.82, 2.14 Hz, 1 H), 6.90 (d, J = 8.8 Hz, 1 H), 6.60 (bs, 1 H), 6.34 (s, 1 H), 3.68 (q, J = 6.859 Hz, 2 H), 2.93 (t, J = 7.1 Hz, 2 H), 1.51 (s, 9 H).

5-[*N*-(*tert*-Butoxycarbonyl)amino]-*N*-(4-fluoro-β-phenethyl)salicylamide (10b). From compound **8** (0.75 g, 2.9 mmol), EDCI (0.85 g, 4.5 mmol), HOBt (0.6 g, 4.5 mmol), triethylamine (1.65 mL, 11.8 mmol) and 4-fluorophenethylamine **(9b)** (1.2 g, 9.0 mmol), a similar procedure as that described for **10a** gave pure **10b** (0.58 g, 53%) as a white crystalline solid: mp 173–174 °C; ^{1}H NMR (300 MHz, DMSO-d_6) δ 11.68 (s, 1 H), 9.12 (bs, 1 H), 8.70 (t, J = 5.75 Hz, 1 H), 7.87 (s, 1 H), 7.28 (m, 3 H), 7.12 (t, J = 8.79 Hz, 2 H), 6.81 (d, J = 8.83 Hz, 1 H), 3.49 (q, J = 6.92 Hz, 2 H), 2.84 (t, J = 7.35 Hz, 2 H), 1.46 (s, 9 H).

5-[*N*-(*tert*-Butoxycarbonyl)amino]-*N*-(4-bromo-β-phenethyl)salicylamide (10c). From compound **8** (0.66 g, 2.6 mmol), EDCI (0.75 g, 3.9 mmol), HOBt (0.53 g, 3.9 mmol), triethylamine (1.45 mL, 10.4 mmol) and 4-bromophenethylamine **(9c)** (1.0 g, 5.0 mmol), a similar procedure as that described for **10a** gave pure **10c** (0.55 g, 49%) as a white crystalline solid: mp 196–197 °C; ^{1}H NMR (300 MHz, DMSO-d_6) δ 11.66 (s, 1 H), 9.13 (bs, 1 H), 8.71 (t, J = 4.99 Hz, 1 H), 7.81 (s, 1 H), 7.49 (dd, J = 8.20, 1.81 Hz, 1 H), 7.30 (d, J = 8.20 Hz, 2 H), 7.22 (d, J = 8.11 Hz, 2 H), 6.81 (d, J = 9.11 Hz, 1 H), 3.51 (q, J = 6.84 Hz, 2 H), 2.83 (t, J = 7.29 Hz, 2 H), 1.47 (s, 9 H).

5-[*N*-(*tert*-Butoxycarbonyl)amino]-*N*-(4-methoxy-β-phenethyl)salicylamide (10d). From compound **8** (0.74 g, 2.9 mmol), EDCI (0.85 g, 4.5 mmol), HOBt (0.6 g, 4.5 mmol), triethylamine (1.65 mL, 11.8 mmol) and 4-methoxyphenethylamine **(9d)** (1.32 g, 9.0 mmol), a similar procedure as that described for **10a** gave pure **10d** (0.64 g, 55%) as a white crystalline solid: mp 159–160 °C; ^{1}H NMR (300 MHz, DMSO-d_6) δ 11.72 (s, 1 H), 9.12 (bs, 1 H), 8.70 (t, J = 5.01 Hz, 1 H), 7.88 (s, 1 H), 7.29 (dd, J = 8.65, 1.50 Hz, 1 H), 7.16 (d, J = 7.74 Hz, 2 H), 6.86 (d, J = 7.29 Hz, 2 H), 6.81 (d, J = 8.65 Hz, 1 H), 3.72 (s, 3 H), 3.47 (q, J = 6.38 Hz, 2 H), 2.77 (t, J = 8.20 Hz, 2 H), 1.46 (s, 9 H).

5-[*N*-(*tert*-Butoxycarbonyl)amino]-*N*-(benzyl)salicylamide (10e). From compound **8** (0.77 g, 3.0 mmol), EDCI (0.85 g, 4.5 mmol), HOBt (0.6 g, 4.5 mmol), triethylamine (1.65 mL, 11.8 mmol) and benzylamine **(9e)** (0.65 mL, 6.0 mmol), a similar procedure as that described for **10a** gave pure **10e** (0.54 g, 53%) as a white crystalline solid: mp 184–185 °C; ^{1}H NMR (300 MHz, DMSO-d_6) δ 11.74 (s, 1 H), 9.15 (bs, 2 H), 7.94 (s, 1 H), 7.41–7.21 (m, 6 H), 6.84 (d, J = 9.11 Hz, 1 H), 4.51 (d, J = 4.10 Hz, 2 H), 1.46 (s, 9 H).

5-[*N*-(*tert*-Butoxycarbonyl)amino]-*N*-(4-chloro-β-phenethyl)salicylamide (10f). From compound **8** (0.61 g, 2.4 mmol), EDCI (0.69 g, 3.6 mmol), HOBt (0.49 g, 3.6 mmol), triethylamine (1.3 mL, 9.2 mmol) and 4-chlorophenethylamine **(9f)** (1.12 g, 7.2 mmol), a similar procedure as that described for **10a** gave pure **10f** (0.55 g, 58%) as a white crystalline solid: mp 192–193 °C; ^{1}H NMR (300 MHz, $CDCl_3$) δ 11.66 (s, 1 H), 9.13 (bs, 1 H), 8.71 (t, J = 5.42 Hz, 1 H), 7.87 (s, 1 H), 7.31 (d, J = 8.39 Hz, 2 H), 7.29 (d, J = 8.21 Hz, 2 H), 7.27 (dd, J = 8.39, 2.04 Hz, 1 H), 6.80 (d, J = 8.77 Hz, 1 H), 3.52 (q, J = 6.17 Hz, 2 H), 2.84 (t, J = 7.06 Hz, 2 H), 1.47 (s, 9 H).

5-[*N*-(*tert*-Butoxycarbonyl)amino]-*N*-(4-hydroxy-β-phenethyl)salicylamide (10g). From compound **8** (0.61 g, 2.4 mmol), EDCI (0.69 g, 3.6 mmol), HOBt (0.49 g, 3.6 mmol), triethylamine (1.3 mL, 9.3 mmol) and 4-hydroxyphenethylamine **(9g)** (1.2 g, 8.7 mmol), a similar procedure as that described for **10a** gave pure **10g** (0.37 g, 42%) as a white crystalline solid: mp 194–195 °C; ^{1}H NMR (300 MHz, DMSO-d_6) δ 11.73 (s, 1 H), 9.19 (s, 1 H), 9.12 (s, 1 H), 8.69 (t, J = 4.51 Hz, 1 H), 7.88 (s, 1 H), 7.31 (d, J = 9.3 Hz, 1 H), 7.05 (d, J = 8.22 Hz, 2 H), 6.82 (d, J = 8.68 Hz, 1 H), 6.68 (d, J = 7.67 Hz, 2 H), 3.43 (q, J = 8.03 Hz, 2 H), 2.72 (t, J = 7.20 Hz, 2 H), 1.46 (s, 9 H).

5-[*N*-(*tert*-Butoxycarbonyl)amino]-*N*-(2-morpholinoethyl)salicylamide (10h). From compound **8** (0.38 g, 1.5 mmol), EDCI (0.43 g, 2.2 mmol), HOBt (0.30 g, 2.2 mmol), triethylamine (0.87 mL, 6.0 mmol) and 4-(2-aminoethyl)-

morpholine (**9h**) (0.39 mL, 3.0 mmol), a similar procedure as that described for **10a** gave pure **10h** (0.33 g, 56%) as a white crystalline solid: mp 154−155 °C; ^{1}H NMR (300 MHz, $CDCl_3$) δ 11.02 (s, 1 H, OH), 7.83 (bs, 1 H, NH), 7.01 (dd, J = 9.82, 2.14 Hz, 1 H), 6.91 (d, J = 9.9 Hz, 1 H), 6.68 (bs, 1 H), 6.50 (d, J = 2.01 Hz, 1 H), 3.56 (t, J = 4.40 Hz, 4 H), 3.47 (m, 4 H), 2.39 (m, 4 H), 1.43 (s, 9 H).

5-[*N*-(*tert*-Butoxycarbonyl)amino]-*N*-(2-pyridin-2-ylethyl)salicylamide (10i). From compound **8** (0.25 g, 0.99 mmol), EDCI (0.28 g, 1.5 mmol), HOBt (0.26 g, 1.5 mmol), triethylamine (0.3 mL, 2.1 mmol) and 2-(2-aminoethyl)pyridine (**9i**) (0.20 mL, 1.7 mmol), a similar procedure as that described for **10a** gave pure **10i** (0.30 g, 85%) as a white crystalline solid: mp 182−184 °C dec; ^{1}H NMR (300 MHz, DMSO-d_6) δ 11.68 (s, 1 H), 9.13 (s, 1 H), 8.53 (d, J = 4.57 Hz, 1 H), 7.88 (s, 1 H), 7.72 (td, J = 7.67, 1.80 Hz, 1 H), 7.30 (d, J = 7.76 Hz, 1 H), 7.23 (m, 2 H), 6.80 (d, J = 8.78 Hz, 1 H), 3.65 (t, J = 7.17 Hz, 2 H), 3.00 (t, J = 7.10 Hz, 2 H), 1.46 (s, 9 H).

5-[*N*-(*tert*-Butoxycarbonyl)amino]-*N*-(3-phenyl-1-propyl)salicylamide (10j). From compound **8** (0.38 g, 1.5 mmol), EDCI (0.43 g, 2.2 mmol), HOBt (0.30 g, 2.2 mmol), triethylamine (0.87 mL, 6 mmol) and 3-phenyl-1-propylamine (**9j**) (0.43 mL, 3.0 mmol), a similar procedure as that described for **10a** gave pure **10j** (0.45 g, 41%) as a white crystalline solid: mp 111−112 °C; ^{1}H NMR (300 MHz, DMSO-d_6) δ 11.85 (s, 1 H), 9.11 (s, 1 H), 8.72 (s, 1 H), 7.75 (s, 1 H), 7.34−7.14 (m, 6 H), 6.82 (d, J = 8.8 Hz, 1 H), 3.27 (t, J = 6.98 Hz, 2 H), 2.59 (t, J = 7.65 Hz, 2 H), 1.80 (quintet, J = 7.15 Hz, 2 H), 1.43 (s, 9 H).

5-[*N*-(*tert*-Butoxycarbonyl)amino]-*N*-(dodecyl)salicylamide (10k). From compound **8** (0.38 g, 1.5 mmol), EDCI (0.43 g, 2.2 mmol), HOBt (0.30 g, 2.2 mmol), triethylamine (0.87 mL, 6 mmol) and dodecylamine (**9k**) (0.55 g, 3.0 mmol), a similar procedure as that described for **10a** gave pure **10k** (0.35 g, 56%) as a white crystalline solid: mp 104−105 °C; ^{1}H NMR (300 MHz, DMSO-d_6) δ 11.89 (s, 1 H), 9.09 (s, 1 H), 7.86 (s, 1 H), 7.28 (d, J = 7.36 Hz, 1 H), 6.81 (d, J = 8.8 Hz, 1 H), 3.25 (t, J = 6.81 Hz, 2 H), 1.46 (s, 9 H), 1.22 (m, 20 H), 0.84 (t, J = 6.73 Hz, 3 H).

5-[*N*-[(*tert*-Butoxycarbonyl)methyl]amino]-*N*-(1,2,3,4-tetrahydronaphthalen-2-yl)salicylamide (10l). From compound **8** (0.40 g, 1.6 mmol), EDCI (0.46 g, 2.4 mmol), HOBt (0.32 g, 2.4 mmol), triethylamine (0.90 mL, 6.3 mmol) and 1,2,3,4-tetrahydronaphthalen-2-amine hydrochloride (**9l**) (0.43 g, 2.3 mmol), a similar procedure as that described for **10a** gave pure **10l** (0.36 g, 59%) as a white crystalline solid: mp 211−212 °C; ^{1}H NMR (300 MHz, DMSO-d_6) δ 11.62 (s, 1 H, OH), 9.11 (s, 1 H, NH), 8.64 (t, J = 7.14 Hz, 1 H), 7.91 (s, 1 H), 7.34 (d, J = 8.71 Hz, 1 H), 7.10 (m, 4 H), 6.82 (d, J = 8.75 Hz, 1 H), 4.23 (m, 1 H), 3.06 (dd, J = 16.19, 4.99 Hz, 1 H), 2.89−2.77 (m, 3 H), 2.06−1.98 (m, 1 H), 1.88−1.75 (m, 1 H), 1.46 (s, 9 H).

4-[*N*-(*tert*-Butoxycarbonyl)amino]-*N*-(3β-cholestanyl)-salicylamide (10m). From compound **8** (0.20 g, 0.8 mmol), EDCI (0.23 g, 1.2 mmol), HOBt (0.16 g, 1.2 mmol), triethylamine (0.44 mL, 3.2 mmol) and 3β-aminocholestane hydrochloride (**9m**) (0.35 g, 0.82 mmol), a similar procedure as that described for **10a** gave pure **10m** (0.31 g, 62%) as a white crystalline solid: mp 230−231 °C dec; ^{1}H NMR (300 MHz, $CDCl_3$) δ 12.36 (s, 1 H, OH), 7.77 (bs, 1 H, NH), 7.26 (s, 1 H), 7.01 (dd, J = 8.88, 2.92 Hz, 1 H), 6.90 (d, J = 8.75 Hz, 1 H), 6.36 (bs, 1 H, NH), 3.95 (m, 1 H), 1.99−1.67 (m, 3 H), 1.63 (d, J = 2.78 Hz, 4 H), 1.52 (s, 9 H), 1.47−0.99 (m, 9 H), 0.91 (d, J = 6.47 Hz, 3 H), 0.87 (dd, J = 6.59, 1.26 Hz, 6 H), 0.81 (s, 3 H), 0.65 (s, 3 H).

5-Amino-*N*-(β-phenethyl)salicylamide (11a). A solution of **10a** (1.0 g, 2.8 mmol) in 6:1 dichloromethane:trifluoroacetic acid (9 mL) was stirred at room temperature for 2 h. The solvent was evaporated in vacuo, and diethyl ether (20 mL) was added. The precipitate was collected, washed with ether and dried to provide white solid **11a** (0.72 g, 100%): mp 190−191 °C; ^{1}H NMR (300 MHz, DMSO-d_6) δ 8.73 (t, J = 1.8 Hz, 1 H), 7.67 (d, J = 2.74 Hz, 1 H), 7.35−7.20 (m, 6 H), 7.03 (d, J = 8.77 Hz, 1 H), 3.54 (q, J = 6.47 Hz, 2 H), 2.86 (t, J = 7.12 Hz, 2 H).

5-Amino-*N*-(4-fluoro-β-phenethyl)salicylamide (11b). From compound **10b** (0.56 g, 1.5 mmol), a similar procedure as that described for **11a** provided white solid **11b** (0.43 g, 104%): mp 200−202 °C dec; ^{1}H NMR (300 MHz, DMSO-d_6) δ 11.9 (bs, 1 H), 9.83 (bs, 1 H), 8.73 (t, J = 5.50 Hz, 1 H), 7.71 (d, J = 2.54 Hz, 1 H), 7.31−7.26 (m, 2 H), 7.23 (d, J = 2.67 Hz, 1 H), 7.12 (t, J = 8.93 Hz, 1 H), 7.02 (d, J = 8.77 Hz, 1 H), 3.54 (q, J = 6.90 Hz, 2 H), 2.84 (t, J = 7.15 Hz, 2 H).

5-Amino-*N*-(4-bromo-β-phenethyl)salicylamide (11c). From compound **10c** (0.54 g, 1.2 mmol), a similar procedure as that described for **11a** provided white solid **11c** (0.41 g, 101%): mp 201−202 °C dec; ^{1}H NMR (300 MHz, DMSO-d_6) δ 12.48 (bs, 1 H), 9.27 (bs, 2 H), 8.73 (t, J = 5.78 Hz, 1 H), 7.77 (d, J = 2.90 Hz, 1 H), 7.49 (d, J = 8.35 Hz, 2 H), 7.27 (dd, J = 9.08, 2.54 Hz, 1 H), 7.23 (d, J = 8.36 Hz, 2 H), 7.00 (d, J = 8.72 Hz, 1 H), 3.55 (q, J = 6.18 Hz, 2 H), 2.84 (t, J = 7.26 Hz, 2 H).

5-Amino-*N*-(4-methoxyphenethyl)salicylamide (11d). From compound **10d** (0.64 g, 1.65 mmol), a similar procedure as that described for **11a** provided white solid **11d** (0.48 g, 100%): mp 196−198 °C dec; ^{1}H NMR (300 MHz, DMSO-d_6) δ 12.03 (bs, 1 H), 9.40 (bs, 2 H), 8.74 (t, J = 5.73 Hz, 1 H), 7.74 (d, J = 2.86 Hz, 1 H), 7.28 (dd, J = 9.06, 2.87 Hz, 1 H), 7.18 (d, J = 8.58 Hz, 2 H), 7.00 (d, J = 8.59 Hz, 1 H), 6.87 (d, J = 8.58 Hz, 2 H), 3.73 (s, 3 H), 3.52 (q, J = 6.19 Hz, 2 H), 2.79 (t, J = 7.63 Hz, 2 H).

5-Amino-*N*-(benzyl)salicylamide (11e). From compound **10e** (0.53 g, 1.55 mmol), a similar procedure as that described for **11a** provided white solid **11e** (0.38 g, 101%): mp 202−204 °C dec; ^{1}H NMR (300 MHz, DMSO-d_6) δ 12.27 (bs, 1 H), 9.40 (m, 2 H), 9.18 (t, J = 5.80 Hz, 1 H), 7.73 (s, 1 H), 7.35 (d, J = 1.78 Hz, 1 H), 7.37−7.20 (m, 5 H), 7.00 (d, J = 8.46 Hz, 1 H), 4.54 (d, J = 5.79 Hz, 2 H).

5-Amino-*N*-(4-chloro-β-phenethyl)salicylamide (11f). From compound **10f** (0.46 g, 1.18 mmol), a similar procedure as that described for **11a** provided white solid **11f** (0.34 g, 100%): mp 199−200 °C dec; ^{1}H NMR (300 MHz, DMSO-d_6) δ 12.48 (bs, 1 H), 9.33 (bs, 2 H), 8.73 (t, J = 5.01 Hz, 1 H), 7.70 (d, J = 2.80 Hz, 1 H), 7.36 (d, J = 8.19 Hz, 2 H), 7.28 (d, J = 8.09 Hz, 2 H), 7.26 (dd, J = 9.21, 2.51 Hz, 1 H), 6.98 (d, J = 8.68 Hz, 1 H), 3.54 (q, J = 6.10 Hz, 2 H), 2.85 (t, J = 7.00 Hz, 2 H).

5-Amino-*N*-(4-hydroxy-β-phenethyl)salicylamide (11g). From compound **10g** (0.35 g, 0.94 mmol), a similar procedure as that described for **11a** provided white solid **11g** (0.25 g, 100%): mp 139−140 °C dec; ^{1}H NMR (300 MHz, CD_3OD) δ 7.82 (d, J = 2.65 Hz, 1 H), 7.34 (dd, J = 8.71, 2.69 Hz, 1 H), 7.08 (d, J = 8.02 Hz, 2 H), 7.02 (d, J = 8.76 Hz, 1 H), 3.60 (t, J = 7.13 Hz, 2 H), 2.81 (t, J = 7.02 Hz, 2 H).

5-Amino-*N*-(2-morpholinoethyl)salicylamide (11h). From compound **10h** (0.30 g, 0.82 mmol), a similar procedure as that described for **11a** provided white solid **11h** (0.21 g, 100%): ^{1}H NMR (300 MHz, $CDCl_3$) δ 10.82 (s, 1 H, OH), 7.83 (bs, 1 H, NH), 7.01 (dd, J = 8.90, 2.14 Hz, 1 H), 6.98 (d, J = 9.01 Hz, 1 H), 6.50 (d, J = 2.01 Hz, 1 H), 3.56 (t, J = 4.20 Hz, 4 H), 3.47 (m, 4 H), 2.39 (m, 4 H).

5-Amino-*N*-(2-pyridin-2-ylethyl)salicylamide (11i). From compound **10i** (0.29 g, 0.81 mmol), a similar procedure as that described for **11a** provided white solid **11i** (0.21 g, 100%): mp 163−165 °C; ^{1}H NMR (300 MHz, DMSO-d_6) δ 12.08 (s, 1 H), 8.85 (t, J = 5.57 Hz, 1 H), 8.69 (d, J = 5.13 Hz, 1 H), 8.11 (td, J = 7.66, 1.67 Hz, 1 H), 7.75 (d, J = 2.67 Hz, 1 H), 7.63 (d, J = 7.92, 1 H), 7.58 (t, J = 6.41 Hz, 1 H), 7.33 (dd, J = 8.71, 2.76 Hz, 1 H), 7.03 (d, J = 8.72 Hz, 1 H), 3.73 (q, J = 5.82 Hz, 2 H), 3.15 (t, J = 6.66 Hz, 2 H).

5-Amino-*N*-(3-phenyl-1-propyl)salicylamide (11j). From compound **10j** (0.35 g, 0.95 mmol), a similar procedure as that described for **11a** provided white solid **11j** (0.23 g, 90%): mp 162−164 °C; ^{1}H NMR (300 MHz, DMSO-d_6) δ 12.10 (bs, 1 H), 8.76 (t, J = 5.52 Hz, 1 H), 7.74 (d, J = 2.69 Hz, 1 H), 7.31−7.02 (m, 6 H), 7.00 (d, J = 8.71 Hz, 1 H), 3.70 (bs, 1 H), 3.32

(q, J = 5.71 Hz, 2 H), 2.63 (t, J = 7.35 Hz, 2 H), 1.84 (quintet, J = 7.37 Hz, 2 H).

5-Amino-*N*-(dodecyl)salicylamide (11k). From compound **10k** (0.35 g, 0.83 mmol), a similar procedure as that described for **11a** provided white solid **11k** (0.27 g, 101%): mp 158–160 °C; ^{1}H NMR (300 MHz, DMSO-d_6) δ 8.70 (s, 1 H), 7.76 (d, J = 2.43 Hz, 1 H), 7.35 (dd, J = 8.72, 2.65 Hz, 1 H), 7.06 (d, J = 8.74 Hz, 1 H), 3.30 (t, J = 6.8 Hz, 2 H), 1.25 (m, 20 H), 0.85 (t, J = 6.64 Hz, 3 H).

5-Amino-*N*-(1,2,3,4-tetrahydronaphthalen-2-yl)salicylamide (11l). From compound **10l** (0.35 g, 0.91 mmol), a similar procedure as that described for **11a** provided white solid **11l** (0.25 g, 98%): mp 208–209 °C dec; ^{1}H NMR (300 MHz, DMSO-d_6) δ 8.67 (d, J = 7.54 Hz, 1 H), 7.75 (d, J = 2.51 Hz, 1 H), 7.25 (dd, J = 8.69, 2.56 Hz, 1 H), 7.10 (m, 4 H), 6.98 (d, J = 8.72 Hz, 1 H), 4.25 (m, 1 H), 3.09 (dd, J = 16.46, 5.29 Hz, 1 H), 2.89–2.76 (m, 3 H), 2.03 (m, 1 H), 1.89–1.79 (m, 1 H).

5-Amino-*N*-(3β-cholestanyl)salicylamide (11m). From compound **10m** (0.29 g, 0.46 mmol), a similar procedure as that described for **11a** provided white solid **11m** (0.21 g, 87%): mp 200–202 °C dec; ^{1}H NMR (300 MHz, DMSO-d_6) δ 12.18 (bs, 1 H, OH), 8.51 (d, J = 7.73 Hz, 1 H), 7.73 (d, J = 2.46 Hz, 1 H), 7.26 (dd, J = 8.72, 2.56 Hz, 1 H), 6.98 (d, J = 8.74 Hz, 1 H), 1.94–0.98 (m, 20 H), 0.88 (d, J = 6.35 Hz, 3 H), 0.83 (d, J = 6.65 Hz, 6 H), 0.80 (s, 3 H), 0.62 (s, 3 H).

5-[*N*-[(2,5-Dihydroxyphenyl)methyl]amino]-*N*-(phenethyl)salicylamide (13a). 2,5-Dihydroxybenzaldehyde **(12)** (0.21 g, 1.40 mmol) was added to **11a** (0.35 g, 1.40 mmol) in benzene (40 mL), and the mixture was heated to reflux under argon for 24 h, using a Dean–Stark trap. The reaction mixture was then concentrated to remove the benzene completely, and the residue was redissolved in methanol (15 mL). While stirring, sodium cyanoborohydride $NaBH_3CN$ (0.18 g, 2.81 mmol) was added in three portions during 30 min, and the reaction mixture was stirred at room temperature for an additional 1 h. To the reaction mixture was then added a saturated solution of NaCl (100 mL) containing 37% HCl (0.28 g, 2.8 mmol). The reaction mixture was extracted with ethyl acetate (3 × 50 mL). The combined organic layers were washed with brine (10 mL), dried over sodium sulfate and concentrated to furnish the crude product, which was further purified by flash chromatography (silica gel 40 g, ethyl acetate:hexane 1:1). The product **13a** (0.37 g, 71.4%) was isolated as a light yellow solid: mp 175–177 °C; ^{1}H NMR (300 MHz, DMSO-d_6) δ 11.43 (s, 1 H, OH), 8.76 (m, 2 H, OH, NH), 8.58 (s, 1 H, OH), 7.35–7.20 (m, 5 H), 7.05 (d, J = 2.51, 1 H), 6.74 (dd, J = 2.28, 8.79 Hz, 1 H), 6.68 (d, J = 8.97 Hz, 1 H), 6.66 (d, J = 3.53 Hz, 1 H), 6.63 (d, J = 8.56 Hz, 1 H), 6.46 (dd, J = 2.75, 8.58 Hz, 1 H), 5.43 (bs, 1 H, NH), 4.11 (s, 2 H), 3.52 (q, J = 6.52 Hz, 2 H), 2.86 (t, J = 7.19 Hz, 2 H); FABMS (Gly) m/z 379 (MH^+). Anal. ($C_{22}H_{22}N_2O_4$) C, H, N.

5-[*N*-[(2,5-Dihydroxyphenyl)methyl]amino]-*N*-(4-fluorophenethyl)salicylamide (13b). From compounds **11b** (0.56 g, 2.0 mmol), **12** (0.35 g, 2.5 mmol), and $NaBH_3CN$ (0.26 g, 4.1 mmol), a similar procedure as that described for **13a** gave pure **13b** (0.34 g, 42%) as a slightly yellow crystalline solid: mp 154–156 °C; ^{1}H NMR (300 MHz, $CDCl_3$) δ 11.37 (s, 1 H), 8.77 (s, 1 H), 8.72 (t, J = 5.33 Hz, 1 H), 8.56 (s, 1 H), 7.27 (t, J = 7.07 Hz, 2 H), 7.10 (t, J = 8.92 Hz, 2 H), 7.00 (d, J = 2.78 Hz, 1 H), 6.74 (dd, J = 8.68, 2.61 Hz, 1 H), 6.67 (d, J = 9.09 Hz, 1 H), 6.62 (s, 1 H), 6.59 (d, J = 8.62 Hz, 1 H), 6.42 (dd, J = 8.44, 2.85 Hz, 1 H), 5.42 (bs, 1 H, NH), 4.09 (d, J = 3.88 Hz. 2 H), 3.47 (q, J = 5.92 Hz, 2 H), 2.82 (t, J = 7.08 Hz, 2 H); ESMS m/z 419 (MNa^+), 397 (MH^+). Anal. ($C_{22}H_{21}FN_2O_4$) C, H, N, F.

5-[*N*-[(2,5-Dihydroxyphenyl)methyl]amino]-*N*-(4-bromo-β-phenethyl)salicylamide (13c). From compounds **11c** (0.48 g, 1.4 mmol), **12** (0.24 g, 1.4 mmol) and $NaBH_3CN$ (0.20 g, 2.9 mmol), a similar procedure as that described for **13a** gave pure **13c** (0.42 g, 64%) as a white crystalline solid: mp 179–180 °C; ^{1}H NMR (300 MHz, $CDCl_3$) δ 11.35 (s, 1 H), 8.77 (s, 1 H), 8.71 (t, J = 2.44 Hz, 1 H), 8.56 (s, 1 H), 7.48 (d, J = 8.20 Hz, 2 H), 7.21 (d, J = 8.28 Hz, 2 H), 7.00 (d, J = 2.87, 1 H), 6.72 (dd, J = 8.55, 2.40 Hz, 1 H), 6.67 (d, J = 9.37 Hz, 1 H), 6.60 (s, 1 H), 6.61 (d, J = 9.76 Hz, 1 H), 6.44 (dd, J = 8.40, 2.65 Hz, 1 H), 5.43 (bs, 1 H, NH), 4.09 (d, J = 4.68 Hz, 2 H), 3.49 (q, J = 7.22 Hz, 2 H), 2.81 (t, J = 7.15 Hz, 2 H); ESMS m/z 458 (M^+ + 2), 457 (M^+ + 1), 456 (M^+). Anal. ($C_{22}H_{21}BrN_2O_4$) C, H, N, Br.

5-[*N*-[(2,5-Dihydroxyphenyl)methyl]amino]-*N*-(4-methoxy-β-phenethyl)salicylamide (13d). From compounds **11d** (0.60 g, 2.0 mmol), **12** (0.35 g, 2.5 mmol) and $NaBH_3CN$ (0.25 g, 4.0 mmol), a similar procedure as that described for **13a** gave pure **13d** (0.50 g, 61%) as a white crystalline solid: mp 173–174 °C dec; ^{1}H NMR (300 MHz, DMSO-d_6) δ 11.42 (s, 1 H, OH), 8.78 (s, 1 H, OH), 8.71 (t, J = 5.42 Hz, 1 H, NH), 8.57 (s, 1 H, OH), 7.15 (d, J = 8.60, 2 H), 7.02 (d, J = 2.41 Hz, 1 H), 6.85 (d, J = 8.64 Hz, 2 H), 6.72 (dd, J = 8.76, 2.57 Hz, 1 H), 6.65 (d, J = 8.88 Hz, 1 H), 6.63 (d, J = 3.03 Hz, 1 H), 6.60 (d, J = 8.53 Hz, 1 H), 6.44 (dd, J = 8.48, 2.88 Hz, 1 H), 5.42 (t, J = 5.68 Hz, 1 H, NH), 4.10 (d, J = 4.82 Hz, 2 H), 3.72 (s, 3 H), 3.46 (q, J = 6.91 Hz, 2 H), 2.76 (t, J = 7.02 Hz, 2 H); ESMS m/z 431 (MNa^+), 409 (MH^+). Anal. ($C_{23}H_{24}N_2O_5$) C, H, N.

5-[*N*-[(2,5-Dihydroxyphenyl)methyl]amino]-*N*-(benzyl)salicylamide (13e). From compounds **12** (0.38 g, 2.6 mmol), **11e** (0.54 g, 2.2 mmol) and $NaBH_3CN$ (0.14 g, 2.2 mmol), a similar procedure as that described for **13a** gave pure **13e** (0.55 g, 69%) as a white crystalline solid: mp 195–196 °C; ^{1}H NMR (300 MHz, DMSO-d_6) δ 11.43 (s, 1 H), 9.18 (t, J = 6.24 Hz, 1 H), 8.75 (s, 1 H), 8.56 (s, 1 H), 7.38–7.20 (m, 5 H), 7.09 (d, J = 2.69 Hz, 1 H), 6.76 (dd, J = 8.46, 2.66 Hz, 1 H), 6.68 (d, J = 8.91 Hz, 1 H), 6.65 (d, J = 3.11 Hz, 1 H), 6.60 (d, J = 8.46 Hz, 1 H), 6.43 (dd, J = 8.46, 3.12 Hz, 1 H), 5.41 (t, J = 5.41 Hz, 1 H), 4.49 (d, J = 5.79, 2 H), 4.09 (d, J = 5.35 Hz, 2 H); CIMS m/z 379 (MH^+). Anal. ($C_{21}H_{20}N_2O_4$) C, H, N.

5-[*N*-[(2,5-Dihydroxyphenyl)methyl]amino]-*N*-(4-chloro-β-phenethyl)salicylamide (13f). From compounds **11f** (0.34 g, 1.2 mmol), **12** (0.16 g, 1.2 mmol) and $NaBH_3CN$ (0.15 g, 2.4 mmol), a similar procedure as that described for **13a** gave pure **13f** (0.34 g, 69%) as a light yellow crystalline solid: mp 158–160 °C; ^{1}H NMR (300 MHz, DMSO-d_6) δ 11.35 (s, 1 H, OH), 8.77 (s, 1 H, OH), 8.71 (t, J = 5.31 Hz, 1 H, NH), 8.56 (s, 1 H, OH), 7.48 (d, J = 8.20 Hz, 2 H), 7.21 (d, J = 8.28 Hz, 2 H), 7.00 (d, J = 2.87, 1 H), 6.72 (dd, J = 8.55, 2.40 Hz, 1 H), 6.67 (d, J = 9.37 Hz, 1 H), 6.60 (s, 1 H), 6.61 (d, J = 9.76 Hz, 1 H), 6.44 (dd, J = 8.40, 2.65 Hz, 1 H), 5.44 (t, J = 5.29 Hz, 1 H, NH), 4.09 (d, J = 4.68 Hz, 2 H), 3.49 (q, J = 7.22 Hz, 2 H), 2.81 (t, J = 7.15 Hz, 2 H); ESMS m/z 414 (M^+ + 2), 412 (M^+). Anal. ($C_{22}H_{21}ClN_2O_4$) C, H, N, Cl.

5-[*N*-[(2,5-Dihydroxyphenyl)methyl]amino]-*N*-(4-hydroxyphenethyl)salicylamide (13g). From compounds **11g** (0.22 g, 0.81 mmol), **12** (0.14 g, 0.97 mmol) and $NaBH_3CN$ (0.15 g, 2.3 mmol), a similar procedure as that described for **13a** gave pure **13g** (0.18 g, 55%) as a slightly yellow crystalline solid: mp 175–176 °C; ^{1}H NMR (300 MHz, DMSO-d_6) δ 11.38 (s, 1 H, OH), 9.87 (s, 1 H, OH), 8.76 (s, 1 H, OH), 8.68 (t, J = 5.33 Hz, 1 H, NH), 8.56 (s, 1 H, OH), 7.30 (t, J = 7.07 Hz, 2 H), 7.10 (t, J = 8.92 Hz, 1 H), 7.00 (d, J = 2.78 Hz, 1 H), 6.73 (dd, J = 8.68, 2.61 Hz, 1 H), 6.67 (d, J = 9.09 Hz, 2 H), 6.62 (d, J = 2.50 Hz, 1 H), 6.59 (d, J = 8.62 Hz, 1 H), 6.42 (dd, J = 8.44, 2.85 Hz, 1 H), 5.40 (bs, 1 H, NH), 4.11 (d, J = 3.88 Hz, 2 H), 3.47 (q, J = 5.92 Hz, 2 H), 2.82 (t, J = 7.08 Hz, 2 H); ESMS m/z 417 (MNa^+), 395 (MH^+). Anal. ($C_{22}H_{22}N_2O_5$) C, H, N.

5-[*N*-[(2,5-Dihydroxyphenyl)methyl]amino]-*N*-(2-morpholinoethyl)salicylamide (13h). From compounds **12** (0.12 g, 0.80 mmol), **11h** (0.20 g, 0.75 mmol) and $NaBH_3CN$ (0.19 g, 3.0 mmol), a similar procedure as that described for **13a** gave pure **13h** (0.18 g, 55%) as a yellow crystalline solid: mp 184–186 °C dec; ^{1}H NMR (300 MHz, DMSO-d_6) δ 11.25 (s, 1 H, OH), 8.77 (s, 1 H, OH), 8.66 (t, J = 4.39 Hz, 1 H, NH), 8.55 (s, 1 H, OH), 7.02 (d, J = 2.21 Hz, 1 H), 6.74 (dd, J = 8.80, 2.55 Hz, 1 H), 6.67 (d, J = 8.00 Hz, 1 H), 6.63 (d, J = 2.87 Hz, 1 H), 6.60 (d, J = 8.66 Hz,1 H), 6.43 (dd, J = 8.42, 2.85 Hz, 1 H), 5.45 (s, 1 H, NH), 4.08 (s, 2 H), 3.56 (t, J = 4.42 Hz, 4 H), 3.38 (m, 4 H), 2.43 (m, 4 H); ESMS m/z 388 (MH^+). Anal. ($C_{20}H_{25}N_5O_5$) C, H, N.

5-[*N*-[(2,5-Dihydroxyphenyl)methyl]amino]-*N*-(2-pyridin-2-ylethyl)salicylamide (13i). From compounds **11i** (0.24 g, 0.93 mmol), **12** (0.17 g, 1.2 mmol) and $NaBH_3CN$ (0.25 g, 4.0 mmol), a similar procedure as that described for **13a** gave pure **13i** (0.18 g, 51%) as a white solid: mp 114−116 °C dec; ^1H NMR (300 MHz, DMSO-d_6) δ 11.68 (s, 1 H, OH), 9.13 (s, 1 H, OH), 8.79 (m, 2 H), 8.62 (t, J = 2.12 Hz, 1 H, NH), 8.59 (s, 1 H, OH), 8.53 (d, J = 4.67 Hz, 1 H), 7.72 (td, J = 7.67, 1.80 Hz, 1 H), 7.01 (d, J = 2.51 Hz, 1 H), 6.74 (dd, J = 8.87, 2.31 Hz, 1 H), 6.69 (d, J = 8.83 Hz, 1 H), 6.65 (d, J = 2.53 Hz, 1 H), 6.61 (d, J = 8.94 Hz, 1 H), 6.46 (dd, J = 8.61, 2.77 Hz, 1 H), 5.39 (t, J = 1.98 Hz, 1 H, NH), 4.08 (s, 2 H), 3.65 (t, J = 7.20 Hz, 2 H), 3.05 (t, J = 7.31 Hz, 2 H); ESMS m/z 380 (MH^+). Anal. ($C_{21}H_{21}N_3O_4$) C, H, N.

5-[*N*-[(2,5-Dihydroxyphenyl)methyl]amino]-*N*-(3-phenyl-1-propyl)salicylamide (13j). From compounds **12** (0.13 g, 0.98 mmol) **11j** (0.22 g, 0.81 mmol) and $NaBH_3CN$ (0.2 g, 3.1 mmol), a similar procedure as that described for **13a** gave pure **13j** (0.19 g, 60%) as a white crystalline solid: mp 152−154 °C; ^1H NMR (300 MHz, DMSO-d_6) δ 11.56 (s, 1 H, OH), 8.77 (s, 1 H, OH), 8.69 (t, J = 4.58 Hz, 1 H, NH), 8.56 (s, 1 H, OH), 7.32−7.16 (m, 5 H), 7.03 (d, J = 2.42 Hz, 1 H), 6.75 (dd, J = 8.82, 2.53 Hz, 1 H), 6.68 (d, J = 8.80 Hz, 1 H), 6.64 (d, J = 2.90 Hz, 1 H), 6.62 (d, J = 8.59 Hz, 1 H), 6.45 (dd, J = 8.53, 2.94 Hz, 1 H), 5.40 (t, J = 5.78 Hz, 1 H, NH), 4.10 (d, J = 4.51 Hz, 2 H), 3.29 (q, J = 4.87 Hz, 2 H), 2.62 (t, J = 7.53 Hz, 2 H), 1.83 (quintet, J = 7.26 Hz, 2 H); CIMS m/z 393 (MH^+). Anal. ($C_{23}H_{24}N_2O_4$) C, H, N.

5-[*N*-[(2,5-Dihydroxyphenyl)methyl]amino]-*N*-(dodecyl)-salicylamide (13k). From compounds **11k** (0.30 g, 0.93 mmol), **12** (0.14 g, 1.0 mmol) and $NaBH_3CN$ (0.13 g, 2.0 mmol), a similar procedure as that described for **13a** gave pure **13k** (0.23 g, 56%) as a slightly yellow crystalline solid: mp 126−128 °C; ^1H NMR (300 MHz, DMSO-d_6) δ 11.59 (s, 1 H, OH), 8.77 (s, 1 H, OH), 8.62 (t, J = 2.12 Hz, 1 H, NH), 8.56 (s, 1 H, OH), 7.01 (d, J = 2.51 Hz, 1 H), 6.74 (dd, J = 8.87, 2.31 Hz, 1 H), 6.69 (d, J = 8.83 Hz, 1 H), 6.65 (d, J = 2.53 Hz, 1 H), 6.61 (d, J = 8.94 Hz, 1 H), 6.46 (dd, J = 8.61, 2.77 Hz, 1 H), 5.39 (t, J = 1.98 Hz, 1 H, NH), 4.09 (s, 2 H), 3.25 (t, J = 7.90 Hz, 2 H), 1.50 (m, 2 H), 1.20 (s, 18 H), 0.88 (t, J = 6.87 Hz, 3 H); CIMS m/z 443 (MH^+). Anal. ($C_{26}H_{38}N_2O_4$) C, H, N.

5-[*N*-[(2,5-Dihydroxyphenyl)methyl]amino]-*N*-(1,2,3,4-tetrahydronaphthalen-2-yl)salicylamide (13l). From compounds **11l** (0.32 g, 1.13 mmol), **12** (0.19 g, 1.36 mmol) and $NaBH_3CN$ (0.3 g, 4.7 mmol), a similar procedure as that described for **13a** gave pure **13l** (0.28 g, 61%) as a yellow crystalline solid: mp 159−161 °C; ^1H NMR (300 MHz, DMSO-d_6) δ 11.30 (s, 1 H, OH), 8.79 (s, 1 H, OH), 8.62 (t, J = 4.58, 1 H, NH), 8.58 (s, 1 H, OH), 7.11 (m, 5 H), 6.74 (dd, J = 8.83, 2.41 Hz, 1 H), 6.67 (d, J = 8.87 Hz, 1 H), 6.65 (d, J = 2.82 Hz, 1 H), 6.60 (d, J = 8.49 Hz, 1 H), 6.45 (dd, J = 8.44, 2.84 Hz, 1 H), 5.45 (t, J = 5.30 Hz, 1 H, NH), 4.22 (m, 1 H), 4.11 (d, J = 4.51 Hz, 2 H), 3.07 (dd, J = 16.34, 5.10 Hz, 1 H), 2.89−2.76 (m, 3 H), 2.03 (m, 1 H), 1.80 (m, 1 H); CIMS m/z 405 (MH^+). Anal. ($C_{24}H_{24}N_2O_4$) C, H, N.

5-[*N*-[(2,5-Dihydroxyphenyl)methyl]amino]-*N*-(3β-cholestanyl)salicylamide (13m). From compounds **11m** (0.15 g, 0.28 mmol), **12** (0.05 g, 0.35 mmol) and $NaBH_3CN$ (0.14 g, 2.2 mmol), a similar procedure as that described for **13a** gave pure **13m** (0.08 g, 44%) as a yellow solid: mp 202−204 °C dec; ^1H NMR (300 MHz, DMSO-d_6) δ 11.65 (s, 1 H, OH), 8.79 (s, 1 H, OH), 8.58 (s, 1 H, OH), 8.38 (d, 1 H, NH), 7.04 (d, J = 2.16 Hz, 1 H), 6.72 (dd, J = 8.81, 2.18 Hz, 1 H), 6.66−6.64 (m, 2 H), 6.59 (d, J = 8.56 Hz, 1 H), 6.45 (dd, J = 8.50, 2.70 Hz, 1 H), 5.35 (bs, 1 H, NH), 4.09 (s, 2 H), 3.81 (m, 1 H), 1.95−1.00 (m, 21 H), 0.90 (d, J = 6.34 Hz, 3 H), 0.86 (dd, J = 6.66, 1.17 Hz, 6 H), 0.82 (s, 3 H), 0.63 (s, 3 H); CIMS m/z 646 (MH^+). Anal. ($C_{41}H_{60}N_2O_4$) C, H, N.

4-[(*tert*-Butoxycarbonyl)amino]benzoic Acid (15). From 4-aminobenzoic acid (**14**) (0.5 g, 3.65 mmol), triethylamine (1.02 mL, 7.30 mmol) and di-*tert*-butyl dicarbonate (1.59 g, 7.30 mmol), a similar procedure as that described for **8** provided pure **15** (0.86 g, 100%) as a white solid: mp 191−192 °C; ^1H NMR (300 MHz, DMSO-d_6) δ 9.71 (s, 1 H), 7.82 (d, J = 8.64 Hz, 2 H), 7.54 (d, J = 8.68 Hz, 2 H), 1.47 (s, 9 H).

4-[*N*-(*tert*-Butoxycarbonyl)amino]-*N*-(benzyl)benzamide (16a). From compound **15** (0.38 g, 1.5 mmol), EDCI (0.43 g, 2.2 mmol), HOBt (0.30 g, 2.2 mmol), triethylamine (0.87 mL, 6.0 mmol) and benzylamine (**9e**) (0.33 mL, 3.0 mmol), a similar procedure as that described for **10a** gave pure **16a** (0.34 g, 69%) as a white crystalline solid: mp 198−199 °C; ^1H NMR (300 MHz, $CDCl_3$) δ 7.74 (d, J = 8.58 Hz, 2 H), 7.43 (d, J = 8.55 Hz, 2 H), 7.37−7.26 (m, 5 H), 4.64 (d, J = 5.63 Hz, 2 H), 1.52 (s, 9 H).

4-[*N*-(*tert*-Butoxycarbonyl)amino]-*N*-(β-phenethyl)benzamide (16b). From compound **15** (0.278 g, 1.16 mmol), EDCI (0.45 g, 2.34 mmol), HOBt (0.32 g, 2.34 mmol), triethylamine (0.36 mL, 4.68 mmol) and β-phenethylamine (**9a**) (1.0 mL, 11.7 mmol), a similar procedure as that described for **10a** gave pure **16b** (0.23 g, 58%) as a white crystalline solid: mp 210−211 °C; ^1H NMR (300 MHz, $CDCl_3$) δ 7.64 (d, J = 8.69 Hz, 2 H), 7.40 (d, J = 8.65 Hz, 2 H), 7.36−7.22 (m, 5 H), 6.62 (s, 1 H), 6.05 (t, J = 6.5 Hz, 1 H), 3.71 (q, J = 6.8 Hz, 2 H), 2.93 (t, J = 6.9 Hz, 2 H), 1.52 (s, 9 H).

4-[*N*-(*tert*-Butoxycarbonyl)amino]-*N*-(3-phenyl-1-propyl)benzamide (16c). From compound **15** (0.38 g, 1.5 mmol), EDCI (0.43 g, 2.2 mmol), HOBt (0.30 g, 2.2 mmol), triethylamine (0.87 mL, 6.0 mmol) and 3-phenyl-1-propylamine (**9j**) (0.43 mL, 3.0 mmol), a similar procedure as that described for **10a** gave pure **16c** (0.43 g, 81%) as a white crystalline solid: mp 178−180 °C; ^1H NMR (300 MHz, $CDCl_3$) δ 7.61 (d, J = 8.69 Hz, 2 H), 7.42 (d, J = 8.70 Hz, 2 H), 7.33−7.19 (m, 5 H), 4.69 (q, J = 6.19 Hz, 2 H), 2.73 (t, J = 7.28 Hz, 2 H), 1.97 (quint, J = 7.47 Hz, 2 H), 1.53 (s, 9 H).

4-Amino-*N*-(benzyl)benzamide (17a). From compound **16a** (0.30 g, 0.92 mmol), a similar procedure as that described for **11a** provided white solid **17a** (0.20 g, 100%): mp 199−200 °C dec; ^1H NMR (300 MHz, DMSO-d_6) δ 8.67 (t, J = 5.66 Hz, 1 H, NH), 7.70 (d, J = 8.57 Hz, 2 H), 7.34−7.20 (m, 5 H), 6.71 (d, J = 8.52 Hz, 2 H), 5.11 (bs, 2 H, NH_2), 4.44 (d, J = 4.22 Hz, 2 H).

4-Amino-*N*-(β-phenethyl)benzamide (17b). From compound **16b** (0.066 g, 0.19 mmol), a similar procedure as that described for **11a** provided **17b** (0.045 g, 98.6%) as a white solid: ^1H NMR (300 MHz, $CDCl_3$) δ 7.54 (d, J = 8.51 Hz, 2 H), 7.35−7.24 (m, 5 H), 6.65 (d, J = 8.44 Hz, 2 H), 6.15 (bs, 1 H), 4.46 (bs, 2 H), 3.68 (q, J = 6.32 Hz, 2 H), 2.92 (t, J = 6.80 Hz, 2 H).

4-Amino-*N*-(3-phenyl-1-propyl)benzamide (17c). From compound **16c** (0.43 g, 0.92 mmol), a similar procedure as that described for **11a** provided **17c** (0.23 g, 100%) as a white solid: mp 126−128 °C; ^1H NMR (300 MHz, DMSO-d_6) δ 8.11 (t, J = 5.25 Hz, 1 H, NH), 7.64 (d, J = 8.59 Hz, 2 H), 7.30−7.17 (m, 5 H), 6.71 (d, J = 8.55 Hz, 2 H), 5.51 (bs, 2 H, NH_2), 3.23 (q, J = 7.04 Hz, 2 H), 2.60 (t, J = 7.39 Hz, 2 H), 1.81 (quint, J = 7.21 Hz, 2 H).

4-[*N*-[(2,5-Dihydroxyphenyl)methyl]amino]-*N*-(benzyl)benzamide (18a). From compounds **12** (0.17 g, 1.25 mmol), **17a** (0.34 g, 1.04 mmol) and $NaBH_3CN$ (0.26 g, 4.2 mmol), a similar procedure as that described for **13a** gave pure **18a** (0.28 g, 77%) as a slightly yellow crystalline solid: mp 204−205 °C; ^1H NMR (300 MHz, DMSO-d_6) δ 8.81 (s, 1 H, OH), 8.57 (t, J = 3.79 Hz, 1 H, NH), 8.57 (s, 1 H, OH), 7.65 (d, J = 8.72 Hz, 2 H), 7.32−7.18 (m, 6 H), 6.63 (d, J = 8.37 Hz, 1 H), 6.58 (d, J = 2.76 Hz, 1 H), 6.55 (d, J = 8.72 Hz, 2 H), 6.44 (dd, J = 8.46, 2.81 Hz, 1 H), 4.43 (d, J = 5.88 Hz, 2 H), 4.16 (s, 2 H); CIMS m/z 349 (MH^+). Anal. ($C_{21}H_{20}ClN_2O_3$) C, H, N.

4-[*N*-[(2,5-Dihydroxyphenyl)methyl]amino]-*N*-(β-phenethyl)benzamide (18b). From compounds **12** (0.031 g, 0.22 mmol), **17b** (0.045 g, 0.22 mmol) and $NaBH_3CN$ (0.03 g, 0.47 mmol), a similar procedure as that described for **13a** gave pure **18b** (0.040 g, 59%) as a yellow solid: mp 154−156 °C; ^1H NMR (300 MHz, DMSO-d_6) δ 8.81 (s, 1 H, OH), 8.57 (s, 1 H, OH), 8.10 (t, J = 5.38 Hz, 1 H, NH), 7.58 (d, J = 8.41 Hz, 2 H), 7.33−7.17 (m, 6 H), 6.63 (d, J = 8.47 Hz, 1 H), 6.58 (d, J = 2.74 Hz, 1 H), 6.54 (d, J = 8.48 Hz, 2 H), 6.45 (dd, J = 8.47, 2.83 Hz, 1 H), 4.17 (d, J = 4.56 Hz, 2 H), 3.41 (q, J = 8.15 Hz,

2 H), 2.80 (t, J = 7.89 Hz, 2 H); CIMS m/z 363 (MH^+). Anal. ($C_{22}H_{22}N_2O_3$) C, H, N.

4-[*N*-[(2,5-Dihydroxyphenyl)methyl]amino]-*N*-(3-phenyl-1-propyl)benzamide (18c). From compounds **12** (0.17 g, 0.85 mmol), **17c** (0.20 g, 0.8 mmol) and $NaBH_3CN$ (0.21 g, 3.2 mmol), a similar procedure as that described for **13a** gave pure **18c** (0.22 g, 73%) as a slightly yellow crystalline solid: mp 133–134 °C; ^1H NMR (300 MHz, DMSO-d_6) δ 8.80 (s, 1 H, OH), 8.57 (s, 1 H, OH), 8.00 (t, J = 5.49 Hz, 1 H, NH), 7.58 (d, J = 8.69 Hz, 2 H), 7.30–7.14 (m, 6 H), 6.62 (d, J = 8.54 Hz, 1 H), 6.57 (d, J = 2.76 Hz, 1 H), 6.53 (d, J = 8.70 Hz, 2 H), 6.42 (dd, J = 8.50, 2.90 Hz, 1 H), 4.15 (s, 2 H), 3.21 (q, J = 6.60 Hz, 2 H), 2.59 (t, J = 7.84 Hz, 2 H), 1.79 (quint, J = 7.55 Hz, 2 H); CIMS m/z 377 (MH^+). Anal. ($C_{23}H_{24}N_2O_3$) C, H, N.

3-[*N*-(*tert*-Butoxycarbonyl)amino]benzoic Acid (20). From 3-aminobenzoic acid (**14**) (0.75 g, 5.47 mmol), triethylamine (1.5 mL, 8.20 mmol) and di-*tert*-butyl dicarbonate (1.78 g, 8.20 mmol), a similar procedure as that described for **8** provided pure **20** (1.3 g, 100%) as a white solid: mp 189–190 °C; ^1H NMR (DMSO-d_6) δ 9.53 (s, 1 H), 8.13 (s, 1 H), 7.61 (d, J = 7.66 Hz, 1 H), 7.53 (d, J = 7.52 Hz, 1 H), 7.35 (t, J = 7.91 Hz, 1 H), 1.47 (s, 9 H).

3-[*N*-(*tert*-Butoxycarbonyl)amino]-*N*-(β-phenethyl)benzoylamide (21). From compound **20** (0.48 g, 2.03 mmol), EDCI (0.45 g, 2.34 mmol), HOBt (0.33 g, 2.34 mmol), triethylamine (0.37 mL, 4.68 mmol) and β-phenethylamine (**9a**), a similar procedure as that described for **10a** gave pure **21** (0.35 g, 51%) as a white solid: mp 186–188 °C; ^1H NMR (300 MHz, $CDCl_3$) δ 7.51 (t, J = 4.86 Hz, 1 H), 7.36–7.31 (m, 4 H), 7.24 (d, J = 4.08 Hz, 1 H), 7.22 (d, J = 2.3 Hz, 1 H), 6.61 (s, 1 H), 6.22 (bs, 1 H), 3.71 (q, J = 6.9 Hz, 2 H), 2.93 (t, J = 7.0 Hz, 2 H), 1.53 (s, 9 H).

3-Amino-*N*-(β-phenethyl)benzamide (22). From compound **21** (0.23 g, 0.66 mmol), a similar procedure as that described for **11a** provided white solid **22** (0.16 g, 100%): mp 137–139 °C; ^1H NMR (300 MHz, DMSO-d_6) δ 8.47 (t, 1 H), 7.35–7.18 (m, 7 H), 6.99 (s, 2 H), 3.46 (q, J = 7.00 Hz, 2 H), 2.83 (t, J = 7.06 Hz, 2 H).

3-[*N*-[(2,5-Dihydroxyphenyl)methyl]amino]-*N*-(β-phenethyl)benzamide (23). From compounds **12** (0.25 g, 1.77 mmol), **22** (0.38 g, 1.58 mmol) and $NaBH_3CN$ (0.2 g, 3.16 mmol), a similar procedure as that described for **13a** gave pure **23** (0.42 g, 73%) as a light yellow solid: mp 124–126 °C; ^1H NMR (300 MHz, DMSO-d_6) δ 8.81 (s, 1 H, OH), 8.58 (s, 1 H, OH), 8.35 (t, J = 4.93 Hz, 1 H, NH), 7.33–7.19 (m, 5 H), 7.11 (t, J = 7.74 Hz, 1 H), 7.03 (d, J = 2.11 Hz, 1 H), 6.95 (d, J = 7.61 Hz, 1 H), 6.69 (dd, J = 2.24, 8.24 Hz, 1 H), 6.64 (d, J = 8.40 Hz, 1 H), 6.24 (s, 1 H), 6.45 (dd, J = 2.91, 8.28 Hz, 1 H), 6.20 (t, J = 4.56 Hz, 1 H, NH), 4.17 (d, J = 5.46 Hz, 2 H), 3.48 (q, J = 6.55 Hz, 2 H), 2.83 (t, J = 7.67 Hz, 2 H); CIMS m/z 363 (MH^+). Anal. ($C_{22}H_{22}N_2O_3$) C, H, N.

Acknowledgment. This research was made possible by grants from the Showalter Trust, Purdue Research Foundation, National Institutes of Health (CA37372 and CA80770), and American Chemical Society (IRG 58-006-40).

Supporting Information Available: Elemental analyses for compounds **13a–m**, **18a–c**, and **23**. This material is available free of charge via the Internet at http://pubs.acs.org.

References

(1) Levitzki, A. Protein Tyrosine Kinase Inhibitors as Novel Therapeutic Agents. *Pharmacol. Ther.* **1999**, *82*, 231–239.
(2) Traxler, P.; Furet, R. Strategies Toward the Design of Novel and Selective Protein Tyrosine Kinase Inhibitors. *Pharmacol. Ther.* **1999**, *82*, 195–206.
(3) Hamby, J. M.; Showalter, H. D. Small Molecule Inhibitors of Tumor-Promoted Angiogenesis, Including Protein Tyrosine Kinase Inhibitors. *Pharmacol. Ther.* **1999**, *82*, 169–193.
(4) Onoda, T.; Iinuma, H.; Sasaki, Y.; Hamada, M.; Isshiki, K.; Naganawa, H.; Takeuchi, T. Isolation of a Novel Tyrosine Kinase Inhibitor, Lavendustin A, from *Streptomyces griseolavendus*. *J. Nat. Prod.* **1989**, *52*, 1252–1257.
(5) Hsu, C.-Y. J.; Persons, P. E.; Spada, A. P.; Bednar, R. A.; Levitzki, A.; Zilberstein, A. Kinetic Analysis of the Inhibition of the Epidermal Growth Factor Receptor Tyrosine Kinase by Lavendustin A and Its Analogue. *J. Biol. Chem.* **1991**, *266*, 21105–21112.
(6) Imoto, M.; Sujikai, I.; Ui, H.; Umezawa, K. Involvement of Tyrosine Kinase in Growth Factor-Induced Phospholipase C Activation in NIH3T3 Cells. *Biochim. Biophys. Acta* **1993**, *1166*, 188–192.
(7) Smyth, M. S.; Stefanova, I.; Hartman, F.; Horad, I. D.; Osherov, N.; Levitzki, A. Non-Amine Based Analogues of Lavendustin A as Protein-Tyrosine Kinase Inhibitors. *J. Med. Chem.* **1993**, *36*, 3010–3014.
(8) Smyth, M. S.; Stefanova, I.; Horak, I. D.; Burke, T. R. J. Hydroxylated 2-(5′-Salicyl)naphthalenes as Protein-Tyrosine Kinase Inhibitors. *J. Med. Chem.* **1993**, *36*, 3015–3020.
(9) Chen, H.; Boiziau, J.; Parker, F.; Maroun, R.; Tocque, B.; Roques, B. P.; Garbay-Jaureguiberry, C. Synthesis and Structure–Activity Studies of a Series of [(Hydroxybenzyl)amino]salicylates as Inhibitors of EGF Receptor-Associated Tyrosine Kinase Activity. *J. Med. Chem.* **1993**, *36*, 4094–4098.
(10) Chen, H.; Boiziau, J.; Parker, F.; Mailliet, P.; Commerçon, A.; Tocque, B.; Le Pecq, J.-B.; Roques, B.-P.; Garbay, C. Structure–Activity Relationships in a Series of 5-[(2,5-Dihydroxybenzyl)-amino]salicylate Inhibitors of EGF–Receptor-Associated Tyrosine Kinase: Importance of Additional Hydrophobic Aromatic Interactions. *J. Med. Chem.* **1994**, *37*, 845–859.
(11) Agbotounou, W. K.; Umezawa, K.; Jacuemin-Sablon, A.; Pierre, J. Inhibition by Two Lavendustins of the Tyrosine Kinase Activity of $pp60^{F527}$ In Vitro and in Intact Cells. *Eur. J. Pharmacol.* **1994**, *269*, 1–8.
(12) Nussbaumer, P.; Winiski, A. P.; Cammisuli, S.; Hiestand, P.; Weckbecker, G.; Stütz, A. Novel Antiproliferative Agents Derived from Lavendustin A. *J. Med. Chem.* **1994**, *37*, 4079–4084.
(13) Liu, T.; Shirai, R.; Matsui, T.; Umezawa, K.; Iwasaki, S. Synthesis and Biological Activity of 5-[2,5-Dihydroxybenzyl)-amino]salicylic Acid Analogues as Inhibitors of EGF Receptor-Associated Protein Tyrosine Kinase. *Bioorg. Med. Chem. Lett.* **1997**, *7*, 365–368.
(14) Green, J. Solid-Phase Synthesis of Lavendustin A and Analogues. *J. Org. Chem.* **1995**, *60*, 4287–4290.
(15) Devraj, R.; Cushman, M. A Versatile Solid Phase Synthesis of Lavendustin A and Certain Biologically Active Analogues. *J. Org. Chem.* **1996**, *61*, 9368–9373.
(16) Paull, K. D.; Hamel, E.; Malspeis, L. *Prediction of Biochemical Mechanism of Action from the In Vitro Antitumor Screen of the National Cancer Institute*; American Chemical Society: Washington, DC, 1995.
(17) Paull, K. D.; Shoemaker, R. H.; Hodes, L.; Monks, A.; Scudiero, D. A.; Rubinstein, L.; Plowman, J.; Boyd, M. R. Display and Analysis of Patterns of Differential Activity of Drugs Against Human Tumor Cell Lines: Development of Mean Graph and COMPARE Algorithm. *J. Natl. Cancer Inst.* **1989**, *81*, 1088–1092.
(18) Boyd, M. R.; Paull, K. D. Some Practical Considerations and Applications of the National Cancer Institute In Vitro Anticancer Drug Discovery Screen. *Drug Dev. Res.* **1995**, *34*, 91–109.
(19) Paull, K. D.; Lin, C. M.; Malspeis, L.; Hamel, E. Identification of Novel Antimitotic Agents Acting at the Tubulin Level by Computer-assisted Evaluation of Differential Cytotoxicity Data. *Cancer Res.* **1992**, *52*, 3892–3900.
(20) Kohlhagen, G.; Paull, K.; Cushman, M.; Nagafuji, P.; Pommier, Y. Protein-Linked DNA Strand Breaks Induced by NSC 314622, a Novel Noncamptothecin Topoisomerase I Poison. *Mol. Pharmacol.* **1998**, *54*, 50–58.
(21) Leteurtre, F.; Kohlhagen, G.; Paull, K. D.; Pommier, Y. Topoisomerase II Inhibition and Cytotoxicity of the Anthrapyrazoles DuP 937 and DuP 941 (Losaxantrone) in the National Cancer Institute Preclinical Antitumor Drug Discovery Screen. *J. Natl. Cancer Inst.* **1994**, *86*, 1239–1244.
(22) Cleaveland, E. S.; Monks, A.; Vaigro-Wolff, A.; Zaharevitz, D. W.; Paull, K.; Ardalan, K.; Cooney, D. A.; Ford, H. J. Site of Action of Two Pyrimidine Biosynthesis Inhibitors Accurately Predicted by the COMPARE Program. *Biochem. Pharmacol.* **1995**, *49*, 947–954.
(23) Duncan, K. K.; Duncan, M. D.; Alley, M. C.; Sausville, E. A. Cucurbitacin E-Induced Disruption of the Actin and Vimentin Cytoskeleton in Prostate Carcinoma Cells. *Biochem. Pharmacol.* **1996**, *52*, 1553–1560.
(24) Bubb, M. R.; Senderowicz, A. M.; Sauville, E. A.; Duncan, K. K.; Korn, E. D. Jasplakinolide, a Cytotoxic Natural Product, Induces Actin Polymerization and Competitively Inhibits the Binding of Phalloidin to F-Actin. *J. Biol. Chem.* **1994**, *269*, 14869–14871.
(25) Bradshaw, T. D.; Wrigley, S.; Shi, D.-F.; Schultz, R. J.; Paull, K. D.; Stevens, M. F. G. 2-(4-Aminophenyl)benzothiazoles: Novel Agents with Selective Profiles of In Vitro Antitumor Activity. *Br. J. Cancer* **1998**, *77*, 745–752.

(26) Wosikowski, K.; Schuurhuis, D.; Johnson, K.; Paull, K. D.; Myers, T. G.; Weinstein, J. N.; Bates, S. E. Identification of Epidermal Growth Factor Receptor and C-erb-B2 Pathway Inhibitors by Correlation with Gene Expression Patterns. *J. Natl. Cancer Inst.* **1997**, *89*, 1505−1515.
(27) Riese, D. J. I.; van Raaij, T. M.; Plowman, G. D.; Andrews, G. C.; Stern, D. F. The Cellular Response to Neuregulins is Governed by Complex Interactions of the ErbB Receptor Family. *Mol. Cell. Biol.* **1995**, *15*, 5770−5776.
(28) Normanno, N.; Selvam, M. P.; Qi, C.-F.; Saeki, T.; Johnson, G.; Kim, N.; Ciardiello, F.; Shoyab, M.; Plowman, G.; Brandt, R.; Todaro, G.; Salomon, D. S. Amphiregulin as an Autocrine Growth Factor for C-Ha-*ras*- and c-*erbB-2*-Transformed Human Mammary Epithelial Cells. *Proc. Natl. Acad. Sci. U.S.A.* **1994**, *91*, 2790−2794.
(29) Soule, H. D.; Maloney, T. M.; Wolman, S. R.; Peterson, W. D. J.; Brenz, R.; McGrath, C. M.; Russo, J.; Pauley, R. J.; Jones, R. F.; Brooks, S. C. Isolation and Characterization of a Spontaneously Immortalized Human Breast Epithelial Cell Line, MCF-10. *Cancer Res.* **1990**, *50*, 6075−6086.
(30) Dickstein, B.; Valverius, E. M.; Wosikowski, K.; Saceda, M.; Pearson, J. W.; Martin, M. B.; Bates, S. E. Increased Epidermal Growth Factor Receptor in an Estrogen-responsive, Adriamycin-resistant MCF-7 Cell Line. *J. Cell. Physiol.* **1993**, *157*, 110−118.
(31) Dong, X. F.; Berthois, Y.; Colomb, E.; Martin, P. M. Cell Cycle Phase Dependence of Estrogen and Epidermal Growth Factor (EGF) Receptor Expression in MCF-7 Cells. *Endocrinology* **1991**, *129*, 2719−2728.
(32) Geahlen, R. L.; McLaughlin, J. L. Piceatannol (3,4,3′,5′-Tetrahydroxy-*trans*-stilbene) is a Naturally Occurring Protein Tyrosine Kinase Inhibitor. *Biochem. Biophys. Res. Commun.* **1989**, *165*, 241−245.
(33) Thakkar, K.; Geahlen, R. L.; Cushman, M. Synthesis and Protein-Tyrosine Kinase Inhibitory Activity of Polyhydroxylated Stilbene Analogues of Piceatannol. *J. Med. Chem.* **1993**, *36*, 2950−2955.
(34) Lin, C. M.; Singh, S. B.; Chu, P. S.; Dempcy, R. O.; Schmidt, J. M.; Pettit, G. R.; Hamel, E. Interactions of Tubulin with Potent Natural and Synthetic Analogues of the Antimitotic Agent Combretastatin: a Structure−Activity Study. *Mol. Pharmacol.* **1988**, *34*, 200−208.
(35) Cushman, M.; Nagarathnam, D.; Gopal, D.; Chakraborti, A. K.; Lin, C. M.; Hamel, E. Synthesis and Evaluation of Stilbene and Dihydrostilbene Derivatives as Potential Anticancer Agents that Inhibit Tubulin Polymerization. *J. Med. Chem.* **1991**, *34*, 2579−2588.
(36) Cushman, M.; Nagarathnam, D.; Gopal, D.; He, H.-M.; Lin, C. M.; Hamel, E. Synthesis and Evaluation of Analogues of (Z)-1-(4-Methoxyphenyl)-2-(3,4,5-trimethoxyphenyl)ethene as Potential Cytotoxic and Antimitotic Agents. *J. Med. Chem.* **1992**, *35*, 2293−2306.
(37) Cushman, M.; He, H.-M.; Lin, C. M.; Hamel, E. Synthesis and Evaluation of a Series of Benzylaniline Hydrochlorides as Potential Cytotoxic and Antimitotic Agents Acting by Inhibition of Tubulin Polymerization. *J. Med. Chem.* **1993**, *36*, 2817−2821.
(38) Cammisuli, S.; Winiski, A.; Nussbaumer, P.; Hiestand, P.; Stutz, A.; Weckbecker, G. SDZ 281-977: a Modified Partial Structure of Lavendustin A that Exerts Potent and Selective Antiproliferative Activities In Vitro and In Vivo. *Int. J. Cancer* **1996**, *65*, 351−359.
(39) Hamel, E.; Lin, C. M. Separation of Active Tubulin and Microtubule-Associated Proteins by Ultracentrifugation and Isolation of a Component Causing the Formation of Microtubule Bundles. *Biochemistry* **1984**, *23*, 4173−4184.
(40) Verdier-Pinard, P.; Lai, J. Y.; Yoo, H.-D.; Yu, J.; Marquez, B.; Nagle, D. G.; Nambu, M.; White, J. D.; Falck, J. R.; Gerwick, W. H.; Day, B. W.; Hamel, E. Structure−Activity Analysis of the Interaction of Curacin A, the Potent Colchicine Site Antimitotic Agent, with Tubulin and Effects of Analogues of the Growth of MCF-7 Breast Cancer Cells. *Mol. Pharmacol.* **1998**, *53*, 62−76.
(41) Peters, J. D.; Furlong, M. T.; Asai, D. J.; Harrison, M. L.; Geahlen, R. L. Syk, Activated by Cross-linking the B-cell Antigen Receptor Localizes to the Cytosol Where It Interacts with and Phosphorylates α-Tubulin on Tyrosine. *J. Biol. Chem.* **1996**, *271*, 4755−4762.
(42) Plowman, G. D.; Green, J. M.; Culouscou, J.-M.; Carlton, G. W.; Rothwell, V. M.; Buckley, S. Heregulin Induces Tyrosine Phosphorylation of HER4/p180erbB4. *Nature* **1993**, *366*, 473−475.
(43) Riese, D. J. I.; Komurasaki, T.; Plowman, G. D.; Stern, D. F. Activation of ErbB4 by the Bifunctional EGF Family Hormone Epiregulin is Regulated by ErbB2. *J. Biol. Chem.* **1998**, *273*, 11288−11294.
(44) Hwang, E.-S.; Riese, D. J. I.; Settleman, J.; Nilson, L. A.; Honig, J.; Flynn, S.; DiMaio, D. Inhibition of Cervival Carcinoma Cell Line Proliferation by the Introduction of a Bovine Papillomavirus Regulatory Gene. *J. Virol.* **1993**, *67*, 3720−3729.

JM000387G

Constitutively Active ErbB4 and ErbB2 Mutants Exhibit Distinct Biological Activities[1]

Desi J. Penington, Ianthe Bryant, and David J. Riese II[2]

Department of Medicinal Chemistry and Molecular Pharmacology, Purdue University, West Lafayette, Indiana 47907-1333

Abstract

ErbB4 is a member of the epidermal growth factor receptor (EGFR) family of tyrosine kinases, which includes EGFR/ErbB1, ErbB2/HER2/Neu, and ErbB3/HER3. These receptors play important roles both in normal development and in neoplasia. For example, deregulated signaling by ErbB1 and ErbB2 is observed in many human malignancies. In contrast, the roles that ErbB4 plays in tumorigenesis and normal biological processes have not been clearly defined. To identify the biological responses that are coupled to ErbB4, we have constructed three constitutively active ErbB4 mutants. Unlike a constitutively active ErbB2 mutant, the ErbB4 mutants are not coupled to increased cell proliferation, loss of contact inhibition, or anchorage independence in a rodent fibroblast cell line. This suggests that ErbB2 and ErbB4 may play distinct roles in tumorigenesis *in vivo*.

Introduction

ErbB4 (HER4/p180^{erbB4}) is a member of the EGFR[3] (EGFR/ErbB) family of receptor tyrosine kinases. These receptors play important roles in the embryonic development of heart, lung, and nervous tissues (1–4), and they have been implicated in the progression of metastatic disease. For example, EGFR/ErbB1 is overexpressed, amplified, or mutated in a number of human malignancies including breast, ovary, prostate, and lung cancers (5–7). ErbB2 overexpression correlates with tumor aggressiveness and poor prognosis in node-positive breast cancer patients (reviewed in Ref. 8). Finally, ErbB3 overexpression is observed in a subset of human mammary and gastric cancers (9, 10).

Some reports indicate that increased ErbB4 expression or signaling is associated with tumorigenesis. ErbB4 overexpression has been observed in a variety of cancers, including tumors of the thyroid, breast, and gastrointestinal tract (11–14). However, the prognostic significance of ErbB4 expression in tumors may also depend on which ErbB family members are coexpressed with ErbB4. In the case of childhood medulloblastoma (one of the most common solid tumors of childhood), patients with tumors overexpressing both ErbB2 and ErbB4 have a significantly worse prognosis than patients with tumors that overexpress either receptor alone (15).

Other reports indicate that increased ErbB4 expression or signaling correlates with tumor cell differentiation and reduced aggressiveness. ErbB4 overexpression in breast tumors is associated with progesterone receptor and estrogen receptor expression and a more favorable prognosis (16–17). In contrast, ErbB2 overexpression varies inversely with progesterone receptor and estrogen receptor levels and indicates tumors that are more likely to be metastatic and fatal (18). In one survey of common solid human cancers, the loss of ErbB4 expression is seen in a significant percentage of breast, prostate, and head and neck malignancies (19). These findings raise the intriguing possibility that ErbB4 is unique to the ErbB family of receptors in that ErbB4 expression and signaling may couple to reduced tumorigenesis or tumor cell proliferation. However, in the face of the conflicting evidence we have summarized here, it remains unclear what general or specific roles ErbB4 plays in differentiation, tumor suppression, or proliferation.

Efforts to elucidate ErbB4 function have been hampered by many factors. There are no known agonists or antagonists specific to the ErbB4 receptor. All of the peptide hormones of the EGF family that are capable of binding ErbB4 also bind at least one other ErbB family member. For example, epiregulin and betacellulin bind and activate both ErbB1 and ErbB4 (20, 21). Furthermore, ligands that do not bind an ErbB family receptor can still activate signaling by that receptor in *trans* through ligand-induced receptor heterodimerization (reviewed in Refs. 22, 23). For example, EGF stimulates ErbB2 tyrosine phosphorylation when ErbB2 is coexpressed with ErbB1, whereas EGF will not stimulate ErbB2 tyrosine phosphorylation in the absence of ErbB1 (24). Consequently, ligands that bind and directly activate ErbB4 (neuregulin, betacellulin, and epiregulin) also stimulate ErbB1, ErbB2, and ErbB3 signaling (Refs. 20, 21, 25, 26; reviewed in Refs. 22, 23). Therefore, in most contexts it is virtually impossible to use an EGF family hormone to study the functional consequences of ErbB4 signaling.

Received 9/11/01; revised 5/8/02; accepted 5/10/02.

The costs of publication of this article were defrayed in part by the payment of page charges. This article must therefore be hereby marked *advertisement* in accordance with 18 U.S.C. Section 1734 solely to indicate this fact.

[1] Supported in part by Purdue University Graduate Opportunities Minority Student Fellowship (to D. J. P.), a MARC-AIM Minority Undergraduate Research Fellowship (to I. B.), an American Society for Microbiology Undergraduate Research Fellowship (to I. B.), American Cancer Society Institutional Grant IRG-58-006 to the Purdue Cancer Research Center, and grants from the Purdue Cancer Research Center (to D. J. R.), the Showalter Trust (to D. J. R.), the Indiana Elks Foundation (to D. J. R.), the United States Army Medical Research and Materiel Command Breast Cancer Research Program Contracts DAMD17-00-1-0415 and DAMD17-00-1-0416 (to D. J. R.), and National Cancer Institute Grant CA80770 (to D. J. R.).

[2] To whom requests for reprints should be addressed, at Department of Medicinal Chemistry and Molecular Pharmacology, Purdue University, 1333 RHPH, Room 224D, West Lafayette, IN 47907-1333. Phone: (765) 494-6091; Fax: (765) 494-1414; E-mail: driese@purdue.edu.

[3] The abbreviations used are: EGFR, epidermal growth factor receptor; cfu, colony-forming unit(s); FR3T3, Fischer rat 3T3; LMP, low melting point; LTR, long terminal repeat.

To study ErbB4 function, we have opted to generate ErbB4 mutants that contain a cysteine substitution in the extracellular domain. This is predicted to result in constitutively dimerized and constitutively active ErbB4 mutants. Introducing cysteine residues to form covalently linked, dimeric, constitutively active receptor tyrosine kinases is not novel. This strategy has been used to generate dimeric, constitutively active mutants of EGFR/ErbB1 and ErbB2 (27, 28). Cysteine substitutions also lead to constitutively active mutants of the fibroblast growth factor receptors 2 and 3 (29, 30).

Here we report the generation and characterization of three constitutively active ErbB4 mutants. These mutants were generated through the introduction of a cysteine residue in the extracellular region of ErbB4. These mutants exhibit increased ligand-independent ErbB4 tyrosine phosphorylation, dimerization, and kinase activity. However, these constitutively active ErbB4 mutants do not induce increased proliferation, loss of contact inhibition, or anchorage-independent growth in FR3T3 fibroblasts. In contrast, a constitutively active ErbB2 mutant does induce increased proliferation, loss of contact inhibition, and anchorage-independent growth in FR3T3 fibroblasts. These results suggest that ErbB4 and ErbB2 couple to different signaling pathways and biological responses. These results also suggest that ErbB4 and ErbB2 may play distinct roles in tumorigenesis *in vivo*.

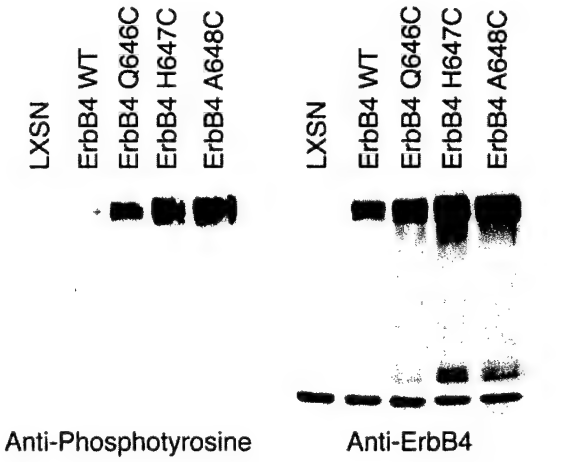

Fig. 1. ErbB4 mutants are constitutively tyrosine phosphorylated. ErbB4 expression and tyrosine phosphorylation were assayed in PA317 cells infected with retroviruses that direct the expression of wild-type ErbB4 or the ErbB4 mutants. Cells infected with the LXSN recombinant retrovirus vector control served as the negative control. Lysates were prepared from each of the cell lines, and ErbB4 was immunoprecipitated from 1000 μg of each lysate. Samples were resolved by SDS-PAGE, electroblotted to nitrocellulose, and immunoblotted with an anti-phosphotyrosine antibody (*left panel*). The blot was then stripped and probed with an anti-ErbB4 rabbit polyclonal antibody (*right panel*). The band at the *top* of the blots represents ErbB4.

Results

ErbB4 Mutants Are Constitutively Tyrosine Phosphorylated. We substituted a single cysteine for amino acids Pro-645, Gln-646, His-647, Ala-648, and Arg-649 in the juxtamembrane region of the ErbB4 extracellular domain. These ErbB4 mutants (P645C, Q646C, H647C, A648C, and R649C) were generated in the context of the pLXSN-ErbB4 recombinant retroviral expression vector (26). Because these cysteine substitutions might cause inappropriate protein folding and decreased protein stability, we assayed the ErbB4 mutants for stable expression. We transfected the recombinant retroviral vectors containing the ErbB4 mutant constructs into the Ψ2 ecotropic retrovirus packaging cell line, selected for stable transformants, and generated pooled cell lines. We harvested low-titer ecotropic retrovirus stocks from these cell lines, and we analyzed the expression and tyrosine phosphorylation of the ErbB4 mutants in these cell lines. Three ErbB4 mutants (Q646C, H647C, and A648C) exhibit abundant expression and ligand-independent tyrosine phosphorylation (data not shown). However, the R649C ErbB4 mutant is not efficiently expressed, and the P645C mutant does not display ligand-independent tyrosine phosphorylation (data not shown).

Previous studies indicate that transfection and subsequent overexpression of ErbB family receptors lead to ligand-independent receptor tyrosine phosphorylation (31–33). Consequently, we were concerned that the ligand-independent phosphorylation of the Q646C, H647C, and A648C ErbB4 mutants in the transfected Ψ2 cells was a consequence of overexpression. Therefore, we infected the PA317 amphotropic retrovirus packaging cell line with the ErbB4 mutant recombinant ecotropic retroviruses at low multiplicities of infection (<0.1), selected for infected cells, and generated pooled cell lines. Because these cell lines were generated by infection at low multiplicities of infection, it is likely that each cell contains only one or two copies of the ErbB4 expression construct. This reduces the likelihood of ErbB4 overexpression in these cell lines.

We analyzed ErbB4 expression and tyrosine phosphorylation in the PA317 cell lines by anti-ErbB4 immunoprecipitation and either anti-ErbB4 (Fig. 1, *right panel*) or anti-phosphotyrosine (Fig. 1, *left panel*) immunoblotting. As expected, cells infected with the LXSN vector control retrovirus do not exhibit ErbB4 expression (Fig. 1, *right panel*) or tyrosine phosphorylation (Fig. 1, *left panel*). Cells infected with the wild-type or mutant ErbB4 retroviruses exhibit ErbB4 expression (Fig. 1, *right panel*). However, cells infected with the mutant ErbB4 retroviruses exhibit abundant ErbB4 tyrosine phosphorylation, whereas cells infected with the wild-type ErbB4 retrovirus exhibit minimal ErbB4 tyrosine phosphorylation (Fig. 1, *left panel*).

Quantification of the chemilumigrams shown in Fig. 1 suggests that the expression levels of the three ErbB4 mutants is less than three times greater than the amount of wild-type ErbB4 expression (Table 1). In contrast, the amounts of tyrosine phosphorylation of the three ErbB4 mutants appear to be much greater than the amount of wild-type ErbB4 tyrosine phosphorylation. Moreover, the ratios of ErbB4 tyrosine phosphorylation to ErbB4 expression for the three ErbB4 mutants appear to be at least four times greater than the ratio for wild-type ErbB4. These data suggest that the three ErbB4 mutants exhibit greater amounts of tyrosine phosphorylation on a per-molecule basis than does wild-type ErbB4. Consequently, these data indicate that the Q646C, H647C, and A648C ErbB4 mutants are constitutively active for signaling.

Table 1 The Q646C, H647C, and A648C ErbB4 mutants exhibit increased normalized tyrosine phosphorylation

Cell line	ErbB4 tyrosine phosphorylation	ErbB4 expression	Ratio
Wild-type ErbB4	210000	1800000	0.12
ErbB4 Q646C	1900000	3300000	0.58
ErbB4 H647C	2900000	4700000	0.62
ErbB4 A648C	4000000	4500000	0.89

ErbB4 Mutants Have Increased *in Vitro* Kinase Activity. Next, we assessed whether the increased tyrosine phosphorylation of the three ErbB4 mutants correlates with increased kinase activity. Equal amounts of the same lysates used for the experiments described in Fig. 1 were immunoprecipitated with an anti-ErbB4 polyclonal antibody. Kinase reactions were performed on the immunoprecipitates in the presence of [γ-^{32}P]ATP. The reaction products were resolved by SDS-PAGE on a 7.5% acrylamide gel. The gel was dried, and the reaction products were visualized by autoradiography.

In Fig. 2, we show that PA317 cells infected with the LXSN vector control retrovirus lack detectable ErbB4 kinase activity. Moreover, PA317 cells that express the three constitutively active ErbB4 mutants exhibit greater ErbB4 tyrosine kinase activity than cells that express wild-type ErbB4. Quantification of the bands on the autoradiogram indicates that the Q646C and H647C ErbB4 mutants exhibit approximately five times more kinase activity than does wild-type ErbB4, whereas the A648C ErbB4 mutant exhibits approximately nine times more kinase activity than does wild-type ErbB4. Given that the expression of the ErbB4 mutants (in these same lysates) is somewhat greater than the expression of wild-type ErbB4 (Fig. 1 and Table 1), it appears that the intrinsic kinase activity of the three ErbB4 mutants is three to four times greater than the intrinsic kinase activity of wild-type ErbB4.

Constitutively Active ErbB4 Mutants Do Not Induce a Loss of Contact Inhibition. Once we determined that the Q646C, H647C, and A648C ErbB4 mutants are constitutively active for signaling, we performed experiments using these mutants to identify the biological events coupled to ErbB4 signaling. A common assay for genes that encode growth control or signaling proteins involves introducing the gene into an established rodent fibroblast cell line and assaying for foci of piled-up cells. These foci indicate a loss of contact inhibition, a common attribute of malignant cells. Thus, this gene transfer assay is commonly used to identify genes that encode proteins that are coupled to malignant growth transformation.

Conflicting results have been obtained from assays for growth transformation by ErbB4. Transfection and consequent overexpression of ErbB4 induces foci (loss of contact inhibition) in NIH 3T3 clone 7 cells in the absence of ligand. Moreover, in these cells focus formation was stimulated by the ErbB4 ligand neuregulin 2β. In contrast, NIH 3T3 clone 7d cells (which lack EGFR expression) transfected with wild-type ErbB4 did not form foci in the presence or absence of neuregulin 1β; however, ErbB4 cotransfected with EGFR/ErbB1 or ErbB2 does induce foci in these cells (32, 33). One possible explanation is that ErbB4 lacks intrinsic transforming activity but does permit EGFR/ErbB1 or ErbB2 signaling and coupling to growth transformation in the presence of an ErbB4 ligand.

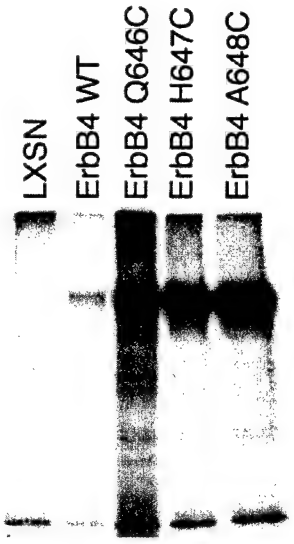

Fig. 2. Q646C, H647C, and A648C mutants exhibit increased *in vitro* kinase activity. Equal amounts of protein lysates (1000 μg) from PA317 cells that stably express wild-type ErbB4 or the ErbB4 mutants (Q646C, H647C, and A648C) were immunoprecipitated with an anti-ErbB4 rabbit polyclonal antibody. Lysates from PA317 cells that express the LXSN vector served as the negative control. Kinase reactions were performed on the immunoprecipitates in the presence of [γ-^{32}P]ATP. The products were resolved by SDS-PAGE. The gel was dried overnight and exposed to X-ray film for ~20 h to visualize the products of the kinase reactions.

To test whether ErbB4 signaling is sufficient to transform the growth of cultured rodent fibroblasts, FR3T3 fibroblasts were infected with 200 cfu of the ErbB4 mutant recombinant ecotropic retrovirus stocks and assayed for focus formation. Cells infected with 200 cfu of the LXSN vector control recombinant ecotropic retrovirus and with 200 cfu of the wild-type ErbB4 recombinant ecotropic retrovirus served as negative controls. Cells infected with 200 cfu of the constitutively active (V664E transmembrane domain) mutant ErbB2* retrovirus served as a positive control.

FR3T3 cells infected with the ErbB2* retrovirus had formed foci within 9 days after infection, whereas cells infected with the vector control retrovirus had not (Fig. 3). Furthermore, cells infected with the wild-type or mutant ErbB4 retroviruses had not formed foci within 9 days after infection. Within 18 days after infection, the foci arising from FR3T3 cells infected with the ErbB2* retrovirus had completely covered the surface of the tissue culture plate and had began to detach from the surface of the plate (data not shown). Within 18 days after infection, FR3T3 cells infected with the mutant ErbB4 retroviruses had formed relatively high-density clumps (data not shown). These high-density clumps did not exhibit the overlapping cell processes characteristic of foci (data not shown). The cells comprising these clumps were cloned and expanded into cell lines, as were cells from less dense regions of the cell monolayers. The cells from the clumps are morphologically indistinguishable from cells derived from the

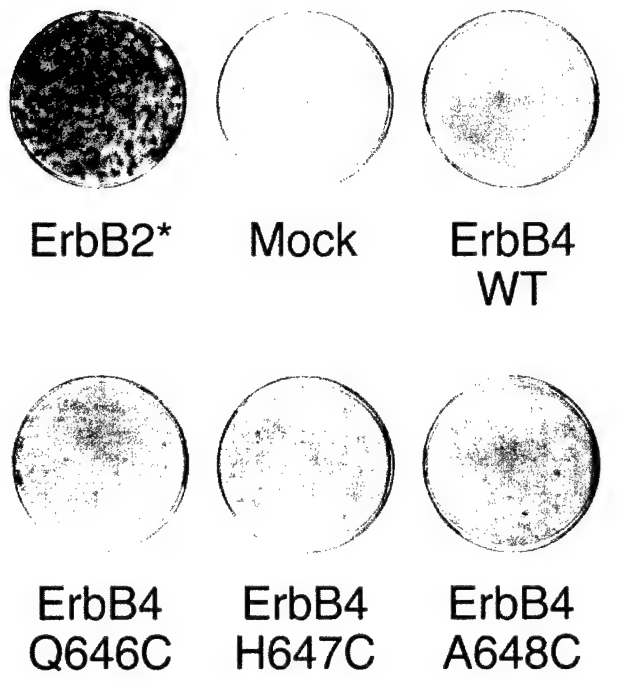

Fig. 3. Constitutively active ErbB4 receptors do not induce a loss of contact inhibition. FR3T3 fibroblasts infected with the LXSN (vector control) retrovirus, the wild-type ErbB4 retrovirus, the constitutively active ErbB2* retrovirus, or the constitutively active ErbB4 mutant retroviruses were assayed for loss of contact inhibition (focus formation).

less dense regions of the plates and are morphologically indistinguishable from cells that express wild-type ErbB4 or cells infected with the vector control retrovirus (data not shown). Again, this suggests that the constitutively active ErbB4 mutants do not transform the growth of FR3T3 fibroblasts.

We were concerned that the apparent failure of the constitutively active ErbB4 mutants to transform the growth of FR3T3 fibroblasts might be specific to this cell type. Consequently, we performed similar experiments with mouse C127 fibroblasts. Infection with the ErbB2* retrovirus resulted in numerous foci, whereas infection with the constitutively active ErbB4 mutant retroviruses did not (data not shown). Thus, again, whereas the constitutively active ErbB2* mutant readily induces foci in fibroblasts, the constitutively active ErbB4 mutants do not. This suggests that ErbB2 and ErbB4 couple to distinct cellular signaling pathways and biological events.

Constitutively Active ErbB4 Mutants Do Not Induce Anchorage-independent Growth. Next, we assayed FR3T3 cells that express the constitutively active ErbB4 mutants for growth while suspended in semisolid medium. Because anchorage-independent growth is another characteristic attribute of tumor cells *in vivo*, this assay is another way to determine whether ErbB4 signaling is coupled to malignant growth transformation.

FR3T3 cells were infected with the ErbB4 mutant recombinant ecotropic retroviruses at a low multiplicity of infection, and infected cells were selected using G418. Drug-resistant colonies of cells were pooled and expanded into cell lines. Control cell lines were generated through infection of FR3T3 cells with the wild-type ErbB4 retrovirus, the constitutively active ErbB2 retrovirus, and with the LXSN vector control retrovirus. These cell lines were seeded at a density of 2×10^4 cells/ml in 60-mm dishes in semisolid medium containing 0.3% LMP-agarose. Fresh medium containing LMP-agarose was added every 3 days. Photographs were taken of representative fields after 10 days.

FR3T3 cells that express the constitutively active ErbB2* mutant exhibit anchorage-independent growth (Fig. 4). In contrast, cells that were infected with the LXSN recombinant retroviral vector control and cells that express wild-type ErbB4 or the ErbB4 mutants do not exhibit anchorage-independent growth. The results of this assay are consistent with the results of the focus formation assay; both assays indicate that ErbB4 signaling is distinct from ErbB2 signaling in that ErbB4 signaling is not coupled to malignant growth transformation in FR3T3 fibroblasts.

Constitutively Active ErbB4 Mutants Do Not Increase the Growth Rate or Saturation Density. Another characteristic of malignantly transformed fibroblasts is that their growth rates and saturation densities are higher than those of their nontransformed counterparts. Indeed, constitutive ErbB2 signaling is coupled to increased growth rates (reviewed in Ref. 8). Thus, we assessed whether the constitutively active ErbB4 mutants affected the growth rate or saturation density of FR3T3 fibroblasts. The FR3T3 cell lines described earlier were seeded in 60-mm dishes at a density of 2×10^4 cells/dish (700 cells/cm^2). Cells were incubated for 10 days to permit proliferation. During this period, cells were counted every 24 h.

The growth rate of the cells that express ErbB2* is slightly greater than the growth rates of the other cell lines (Fig. 5). Note that the growth rates of the cells that express the constitutively active ErbB4 mutants are indistinguishable from the growth rates of cell lines that express wild-type ErbB4 or the vector control. The growth curves in Fig. 5 were used to determine the saturation densities for the six cell lines (Table 2). Note that the saturation density of the cell line that expresses ErbB2* is higher than the saturation densities of the other cell lines. Moreover, the saturation densities of the cell lines that express the ErbB4 mutants are not markedly higher than the saturation densities of the vector control cell line or the cell line that expresses wild-type ErbB4. Once again, these data suggest that constitutive ErbB4 signaling is not coupled to malignant growth transformation in fibroblasts. Thus, the signaling pathways and biological responses that are coupled to ErbB4 are distinct from those that are coupled to ErbB2.

The Constitutively Active ErbB4 Mutants Are Expressed and Are Constitutively Tyrosine Phosphorylated in FR3T3 Cells. We were concerned that the apparent failure of the constitutively active ErbB4 mutants to transform the growth of FR3T3 fibroblasts might be attributable to the absence of ErbB4 expression or constitutive tyrosine phosphorylation in these cells. In parallel with the infections described in Fig. 3, we infected FR3T3 cells with 200 cfu of the constitutively active mutant ErbB4 recombinant retroviruses

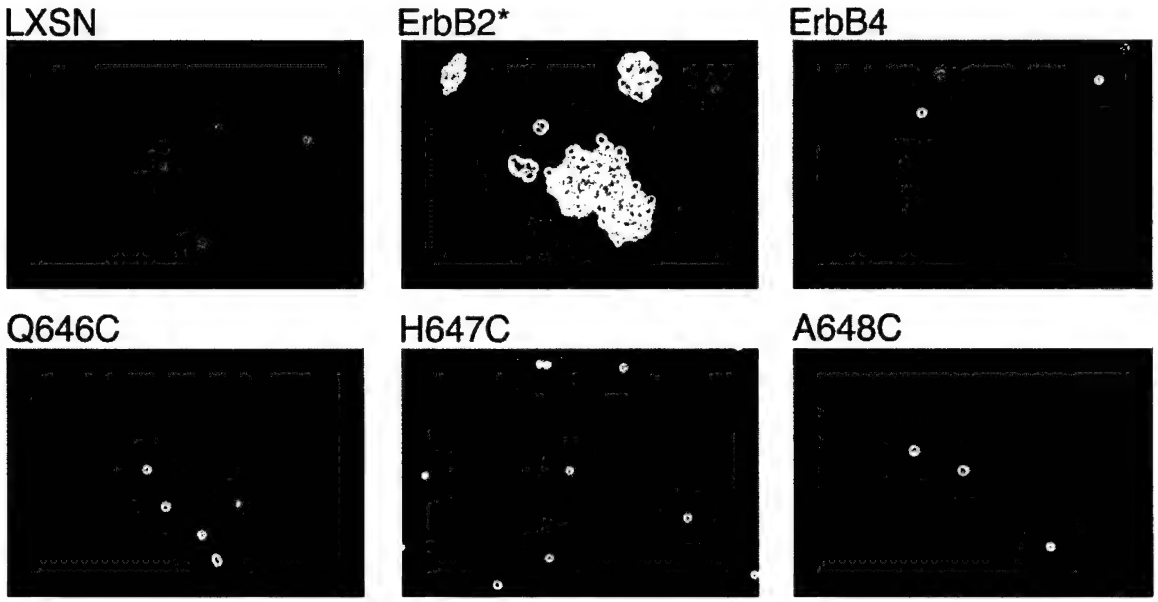

Fig. 4. Constitutively active ErbB4 receptors do not induce growth in semisolid medium. FR3T3 cells that stably express the LXSN vector control, the constitutively active ErbB2 mutant (ErbB2*), wild-type ErbB4, or the constitutively active ErbB4 mutants (Q646C, H647C, and A648C) were seeded in semisolid medium at a density of 2×10^4 cells/ml in 60-mm dishes. The cells were incubated for 10 days, after which images were recorded by photomicroscopy. Images shown are representative of those obtained in three independent experiments.

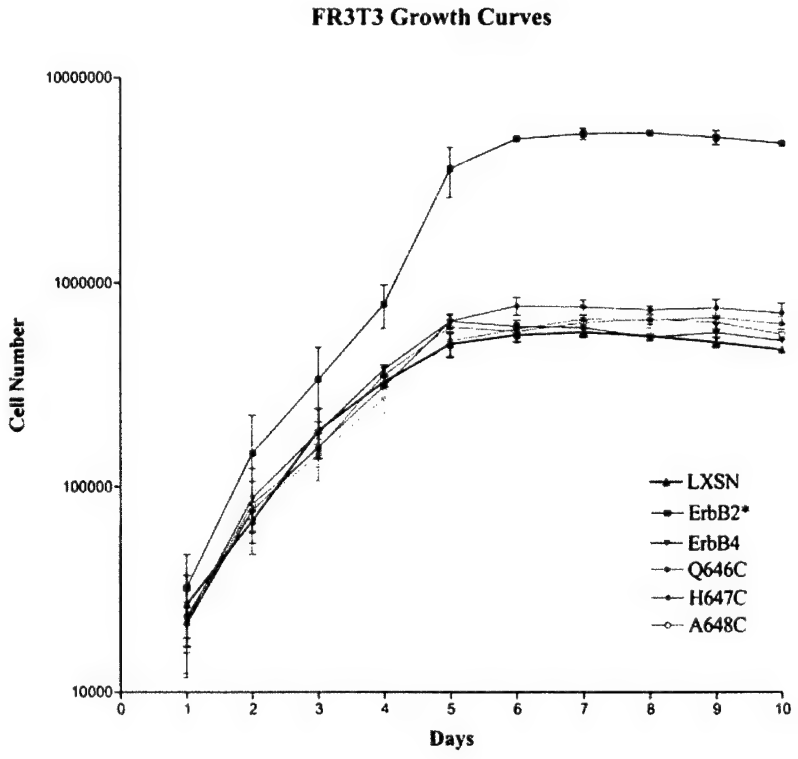

Fig. 5. Constitutively active ErbB4 mutants do not increase the growth rate of FR3T3 fibroblasts. FR3T3 cells that express the LXSN vector control, the constitutively active ErbB2* mutant, wild-type ErbB4, or the constitutively active ErbB4 mutants (Q646C, H647C, and A648C) were plated at a density of 2×10^4 cells in 60-mm dishes (700 cells/cm^2) and were incubated for 1–10 days. Cells were counted daily to assess growth rates and saturation densities. The means for three independent experiments; *bars,* SE.

and selected for stable infection using G418. As controls, we also infected FR3T3 cells with 200 cfu of the vector control retrovirus, 200 cfu of the ErbB2* retrovirus, and with 200 cfu of the wild-type ErbB4 retrovirus. Drug-resistant colonies were pooled and expanded into stable cell lines. The cell lines were starved of serum in the presence of 500 μM Na_3VO_4 (34) to decrease the background level of tyrosine phosphorylation and to increase the phosphorylation of the

Table 2 Constitutively active ErbB4 mutants do not increase the saturation density of FR3T3 fibroblasts

	Saturation Densities
LXSN	$5.8 \pm 0.3 \times 10^5$
ErbB2*	$5.4 \pm 0.1 \times 10^6$
ErbB4	$6.1 \pm 0.5 \times 10^5$
Q646C	$6.6 \pm 0.6 \times 10^5$
H647C	$7.6 \pm 0.7 \times 10^5$
A648C	$6.6 \pm 0.4 \times 10^5$

constitutively active ErbB4 mutants. We prepared lysates and analyzed ErbB4 expression and tyrosine phosphorylation by precipitation with an anti-ErbB4 antibody and sequential anti-phosphotyrosine and anti-ErbB4 immunoblotting.

In Fig. 6, *lower panel*, we show that ErbB4 expression is detectable in the FR3T3 cell lines infected with the wild-type ErbB4 retrovirus or the constitutively active ErbB4 mutant retroviruses. However, ErbB4 tyrosine phosphorylation is observed only in the FR3T3 cell lines infected with the constitutively active ErbB4 mutant retroviruses (Fig. 6, *upper panel*). The amount of phosphorylation exhibited by the ErbB4 mutants is less than the amount of phosphorylation exhibited by the constitutively active ErbB2 mutant. Furthermore, the expression of wild-type ErbB4 appears to be less than the expression of the ErbB4 mutants. Nonetheless, these data suggest that the apparent failure of the constitutively active ErbB4 mutants to transform the growth of FR3T3 fibroblasts is not attributable to an absence of expression and tyrosine phosphorylation of these mutants in these cells.

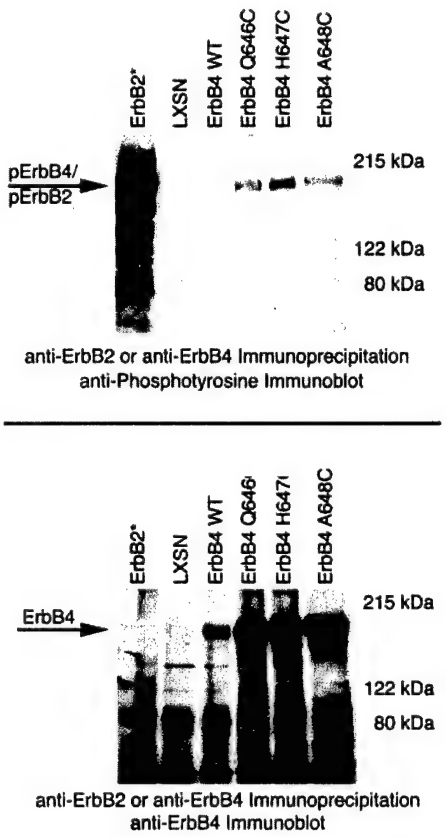

Fig. 6. Constitutively active ErbB4 mutants are expressed and are constitutively tyrosine phosphorylated in FR3T3 cells. ErbB4 expression and tyrosine phosphorylation were assayed in FR3T3 cells infected with retroviruses that direct the expression of wild-type ErbB4 or the ErbB4 mutants. Cells infected with the LXSN recombinant retrovirus vector control or with the ErbB2* retrovirus served as controls. Lysates were prepared from each of the cell lines, and ErbB receptors were precipitated from 1.5 mg of each lysate using protein A-Sepharose and either an anti-ErbB4 rabbit polyclonal antibody or an anti-ErbB2 rabbit polyclonal antibody. Samples were resolved by SDS-PAGE, electroblotted to nitrocellulose, and immunoblotted with an anti-phosphotyrosine antibody (*upper panel*). The blot was then stripped and probed with an anti-ErbB4 rabbit polyclonal antibody (*lower panel*). *Arrows*, positions of ErbB2 and ErbB4 on the blots.

Discussion

In this report, we describe the construction and initial characterization of three constitutively active ErbB4 mutants. These mutants display increased dimerization (data not shown) and ligand-independent tyrosine phosphorylation and kinase activity. In these respects, the ErbB4 mutants resemble constitutively active mutants of ErbB2 or EGFR. However, unlike constitutively active ErbB2 mutants, these mutants are not coupled to malignant growth transformation in FR3T3 fibroblasts; they do not induce foci, anchorage-independent growth, or increases in the growth rate or saturation density. These data suggest that ErbB2 and ErbB4 play distinct roles in tumorigenesis *in vivo*. This conclusion is supported by the observation that NIH3T3 clone 7d cells do not form foci after ErbB4 transfection and treatment with the ErbB4 ligand neuregulin but do form foci after ErbB2 and ErbB4 cotransfection and neuregulin treatment (32, 33).

Of course, another potential explanation is that the amounts of tyrosine phosphorylation displayed by the three constitutively active ErbB4 mutants are insufficient to couple to malignant growth transformation in fibroblasts. This is consistent with the observation that the three constitutively active ErbB4 mutants are less phosphorylated than the constitutively active ErbB2 mutant (Fig. 6). However, anti-phosphotyrosine immunoblotting is not a sensitive method for assessing ErbB family receptor signaling and coupling to biological responses. Indeed, the neuregulin concentration required for maximal ErbB4 tyrosine phosphorylation is ~10-fold greater than the neuregulin concentration sufficient for maximal ErbB family receptor coupling to biological responses. Furthermore, the neuregulin concentration sufficient for maximal ErbB family receptor coupling to biological responses stimulates, at most, only modest amounts of ErbB4 tyrosine phosphorylation (26). Thus, it is not likely that the failure of the constitutively active ErbB4 mutants to couple to malignant growth transformation in fibroblasts is attributable to insufficient ErbB4 tyrosine phosphorylation.

Clearly, additional work is necessary to define the roles that ErbB4 plays in tumorigenesis and in regulating cellular functions *in vivo*. However, important clues have emerged to guide these future studies. In a significant percentage of breast tumor samples, ErbB4 expression correlates with estrogen receptor expression, which indicates a favorable prognosis (16–17). Furthermore, ErbB4 expression is fre-

quently lost in tumors of the breast and prostate (19). Finally, ligands for ErbB4 can induce terminal differentiation and growth arrest of some mammary tumor cell lines (35–37). These data indicate that ErbB4 signaling may be coupled to differentiation, growth arrest, and tumor suppression. The ErbB4 mutants described in this study will enable us to evaluate this hypothesis. Indeed, preliminary data from our laboratory indicate that the Q646C ErbB4 mutant causes reduced colony formation in plastic dishes by a number of cultured human breast and prostate tumor cell lines.

We will also perform additional studies to characterize the biochemistry of signaling by the three ErbB4 mutants. Whereas these mutants exhibit greater ligand-independent tyrosine phosphorylation and autokinase activity than the wild-type receptor, it is unclear whether this is attributable to increased intrinsic kinase activity or attributable to increased availability of the substrate. Additional experiments are warranted to distinguish between these two possibilities.

Another area of future study will focus on identifying the mechanisms by which ErbB4 is coupled to biological responses. Initial studies will identify the sites of ErbB4 tyrosine phosphorylation for these mutants. If our preliminary studies indicating that the Q646C ErbB4 mutant is coupled to prostate and mammary tumor cell growth arrest hold true, then we will use genetic strategies to identify the sites of ErbB4 tyrosine phosphorylation that are sufficient and necessary to couple the Q646C ErbB4 mutant to this biological response. A similar strategy has been used to identify the sites of ErbB2 and platelet-derived growth factor receptor tyrosine phosphorylation that are critical for coupling these receptors to biological responses (38, 39).

Once we have identified the site(s) of tyrosine phosphorylation that is sufficient for coupling to biological responses, we will identify signaling proteins that bind this phosphorylation site and couple it to biological responses. Using this strategy, we will begin to characterize the ErbB4 signaling pathway. Our prediction is that the three constitutively active ErbB4 mutants are phosphorylated on different tyrosine residues and that these mutants differentially couple to biological responses. We have shown previously that different ErbB4 ligands cause phosphorylation on different sites on ErbB4 and differential coupling to biological responses (40). Moreover, one cysteine substitution mutation in the rat ErbB2 extracellular domain (V656C) results in low amounts of constitutive receptor tyrosine phosphorylation and efficient coupling to malignant growth transformation in rodent fibroblasts. In contrast, another rat ErbB2 extracellular domain cysteine substitution mutant (T657C) exhibits very high levels of constitutive receptor tyrosine phosphorylation but a relatively low amount of coupling to malignant growth transformation in rodent fibroblasts (28).

We were somewhat surprised to discover that the three constitutively active ErbB4 mutants failed to couple to malignant growth transformation in a rodent fibroblast cell line. Nonetheless, these mutants will enable us to assess ErbB4 function in a wide variety of cell, tissue, and organismal contexts. Given that ErbB4 appears to regulate diverse functions in a number of distinct contexts, much work remains to complete this story.

Materials and Methods

Cell Lines, Cell Culture, and Antibodies. The Ψ2, PA317, C127, and FR3T3 cell lines were generous gifts from Daniel DiMaio (Yale University New Haven, CT). All cell lines were propagated in DMEM supplemented with 10% FBS, 50 IU/ml penicillin, 50 μg/ml streptomycin (Mediatech), and 0.25 μg/ml Fungizone (Amphotericin B; Life Technologies, Inc.). Recombinant cell lines generated in the course of the experiments described in this report were propagated in the medium described above supplemented with 200 μg/ml G418 (Mediatech).

The anti-ErbB4 mouse monoclonal (SC-8050), anti-ErbB4 rabbit polyclonal (SC-283), and anti-ErbB2 rabbit polyclonal (C-18) antibodies were purchased from Santa Cruz Biotechnology. Goat antimouse and goat antirabbit horseradish peroxidase-conjugated antibodies were purchased from Pierce. Enhanced chemiluminescence (ECL) Western blotting reagents, Redivue adenosine 5′-[γ-^{32}P]triphosphate, and Protein-A Sepharose (CL-4B) were purchased from Amersham Pharmacia Biotech. The 4G10 anti-phosphotyrosine mouse monoclonal antibody was purchased from Upstate Biotechnology.

Plasmids. The recombinant retroviral vector pLXSN (41) was obtained from Daniel DiMaio (Yale University). This construct contains two recombinant LTRs derived from the Maloney murine leukemia virus and the Maloney murine sarcoma virus. These LTRs flank the Ψ packaging signal and the aminoglycoside 3′-phosphotransferase (*Neo*^{R}) gene under the transcriptional control of the SV40 early promoter. The *Neo*^{R} gene confers resistance to the aminoglycoside antibiotic G418 (geneticin; Life Technologies, Inc.).

The recombinant retroviral construct pLXSN-ErbB4 (26) was generated by subcloning the human ErbB4 cDNA into pLXSN. In this construct, the ErbB4 cDNA is under the transcriptional control of the upstream LTR. The recombinant retroviral construct pLXSN-ErbB2* (42) was a gift of Lisa Petti (Albany Medical College, Albany, NY). It was generated by subcloning the cDNA encoding the constitutively active rat ErbB2 mutant (V664E transmembrane domain mutant, ErbB2*) into pLXSN. In this construct, the ErbB2* cDNA is under the transcriptional control of the upstream LTR.

ErbB4 Mutagenesis. The plasmid pLXSN-ErbB4 was used as the template for site-directed mutagenesis (QuikChange Site Directed Mutagenesis kit; Stratagene) to construct the putative constitutively active ErbB4 mutants. The mutants were constructed by introducing mutations that substitute a cysteine residue for proline 645, glutamine 646, histidine 647, alanine 648, or arginine 649 in the ErbB4 extracellular juxtamembrane domain. These mutants are denoted as follows: P645C, Q646C, H647C, A648C, and R649C. A new restriction enzyme site was also engineered in each mutant to facilitate the identification of the mutants. The following primers were used for mutagenesis. "T" denotes the upper primer, whereas "B" denotes the lower primer. The novel cysteine codons and anticodons are indicated by bold type, the point mutations that create the novel cysteine residues are double underlined, and the novel restriction enzyme sites are singly underlined.

P645CT:5′-ATTTACTACCCATGGACCGGTCATTCCACTT
TATGCCAACATGCTAGAACTCCC-3′
P645CB:5′-GGGAGTTCTAGCATGTTGGCATAAAGTGGA
ATGACCGGTCCATGGGTAGTAAAT-3′
Q646CT:5′-TACTACCCATGGACCGGTCATTCCACTTTAC
CATGCCATGCTAGAACTCCCCTG-3′
Q646CB:5′-CAGGGGAGTTCTAGCATGGCATGGTAAAGT
GGAATGACCGGTCCATGGGTAGTA-3′
H647CT:5′-CATTTACTACCCATGGACCGGTCATTCCACT
TTACCACAATGTGCTAGAACTCCCCT-3′
H647CB:5′-AGGGGAGTTCTAGCACATTGTGGTAAAGTG
GAATGACCGGTCCATGGGTAGTAAATG-3′
A648CT:5′-TCCACTTTACCACAACATTGTAGAACTCCTC
TGATTGCAGCTGGA-3′
A648CB:5′-TCCAGCTGCAATCAGAGGAGTTCTACAATG
TTGTGGTAAAGTGGA-3′
R649CT:5′-ACTTTACCACAACATGCTTGCACTCCTCTGA
TTGCAGCTGGA-3′
R649CB:5′-TCCAGCTGCAATCAGAGGAGTGCAAGCATG
TTGTGGTAAAGT-3′

The site-directed mutagenesis reactions were performed according to the manufacturer's instructions. Standard techniques (43) were used for bacterial transformations, small-scale plasmid DNA preparations, restriction enzyme analysis of the clones, and large-scale plasmid DNA preparations. Positive clones were sequenced by the University of Wisconsin-Madison Biotechnology Center to confirm their identity.

Production of Recombinant Retroviruses and Retroviral Infections. The ErbB4 mutant constructs were transfected using standard techniques (44, 45) into the $\psi 2$ ecotropic retrovirus packaging cell line (46) to generate cell lines that express the ErbB4 mutants and to package the constructs into low-titer ecotropic retrovirus particles (44, 45). $\psi 2$ cells were transfected with the pLXSN vector control plasmid, pLXSN-ErbB4, and pLXSN-ErbB2* to generate control cell lines and recombinant ecotropic retroviruses. The PA317 amphotropic packaging cell line (47) and the FR3T3 rat fibroblast cell line were infected with the ecotropic recombinant retroviruses using standard techniques (44, 45) to generate additional cell lines that express the ErbB4 mutants.

Immunoblot Assays for Receptor Tyrosine Phosphorylation and Expression. The analysis of ErbB4 and ErbB2 tyrosine phosphorylation by immunoprecipitation and anti-phosphotyrosine immunoblotting has been described previously (21, 26). Briefly, cell lysates were generated, and protein content was quantified using a Coomassie Protein Assay Reagent (Ref. 48; Pierce Chemical). ErbB2 or ErbB4 was immunoprecipitated from equal amounts of protein using specific antibodies. The immunoprecipitates were resolved by SDS-PAGE on a 7.5% acrylamide gel and were electrotransferred onto nitrocellulose. The blots were probed with the anti-phosphotyrosine monoclonal antibody 4G10. Antibody binding was detected and visualized using a goat antimouse horseradish peroxidase-coupled antibody and enhanced chemiluminescence. The blots were then stripped and probed with the anti-ErbB4 polyclonal antibody to assess ErbB4 expression levels. Antibody binding was detected and visualized using a goat antimouse horseradish peroxidase-coupled antibody and enhanced chemiluminescence.

The amounts of receptor tyrosine phosphorylation and expression were quantified by digitizing the chemilumigrams using a Linotype-Hell Jade two-dimensional scanning densitometer set at 600-dpi resolution. The bands on the images were quantified using NIH Image for Macintosh v1.6 software. Values are expressed as arbitrary units. Background levels were computed using the vector control lanes and were subtracted from the gross values to produce net receptor expression and tyrosine phosphorylation values. The digitized images were also cropped and annotated using Adobe Photoshop for Macintosh v3.0.5 software.

***In Vitro* Kinase Assay.** ErbB2 and ErbB4 were immunoprecipitated from protein extracts from PA317 cells as described previously (26). Immune complex kinase reactions were performed as described previously (31). Briefly, 35 μl of protein A-Sepharose and 5 μl of anti-ErbB2 or anti-ErbB4 rabbit polyclonal antibodies were used to immunoprecipitate the receptors from lysates containing the same amount of protein (1000 μg). Immunoprecipitates were washed five times in 500 μl of kinase buffer [20 mM Tris-HCl (pH 7.4), 5 mM $MgCl_2$, and 3 mM $MnCl_2$]. After the last wash, the samples were resuspended in 100 μl of kinase buffer supplemented with 10 μCi of [γ-^{32}P]ATP and were incubated for 10 min at room temperature to permit the kinase reaction to occur. The beads were then washed two times in NET-N buffer (49) and boiled for 5 min in SDS-PAGE protein sample buffer. The samples were resolved by SDS-PAGE on a 7.5% acrylamide gel. The gels were dried overnight and exposed to X-ray film for ~20 h. The autoradiograms were digitized using a Linotype-Hell Jade two-dimensional scanning densitometer set at 600-dpi resolution. The bands on the images were quantified using NIH Image for Macintosh v1.6 software. Values are expressed as arbitrary units. Background levels were computed using the vector control lanes and were subtracted from the gross values to produce net kinase activity values. The digitized images were also cropped and annotated using Adobe Photoshop for Macintosh v3.0.5 software.

Focus Formation Assay for Loss of Contact Inhibition. FR3T3 and C127 cells were infected with recombinant ecotropic retroviruses as described earlier and in reports published previously (44, 45). Briefly, 60-mm dishes of cells at ~70% confluence were infected with ecotropic retrovirus stocks. Approximately 24 h after infection, cells were passaged into three 60-mm dishes. Cells were maintained in DMEM supplemented with 10% FBS until foci appeared. During this period, the medium was changed every 3 days. Once robust foci appeared, cells were fixed in 100% methanol and stained with Giemsa (Fisher) to visualize the foci. The plates were digitized using a Linotype-Hell Jade two-dimensional scanning densitometer set at 600-dpi resolution. The digitized images were cropped and annotated using Adobe Photoshop for Macintosh v3.0.5 software.

Assay for Anchorage Independence. FR3T3 cells were seeded at a density of 2×10^4 cells in 60-mm dishes containing 2.5 ml of 0.3% LMP-agarose (Life Technologies, Inc.)

as described previously (50). Every 3 days, DMEM supplemented with 10% FBS and 0.3% LMP-agarose was added to each plate. The cells were incubated at 37°C for 10 days, and fields were photographed with an Olympus OM-10 camera attached to an Olympus CK-2 phase-contrast inverted microscope. The images were digitized by the photofinisher. These images were cropped and annotated using Adobe Photoshop for Macintosh v3.0.5 software. Images are representative of three independent experiments.

Growth Rate/Saturation Density Assay. Stable FR3T3 cell lines expressing the wild-type ErbB4 receptor, ErbB2*, or the ErbB4 mutants (Q646C, H647C, and A648C) were plated in 10 60-mm dishes at a density of 2×10^4 cells/dish. Cells were incubated from 1 to 10 days at 37°C. Cells were counted (Coulter Counter ZM) each day for a total of 10 days. The mean and SE are representative of three independent experiments.

Acknowledgments

We thank Gar Park, Roberto Ricardo, and Fernando Cruz-Guilloty for their preliminary studies that led to these experiments.

References

1. Miettinen, P. J., Berger, J. E., Meneses, J., Werb, Z., and Derynck, R. Epithelial immaturity and multiorgan failure in mice lacking epidermal growth factor receptor. Nature (Lond.), *376:* 337–344, 1995.

2. Lee, K., Simon, H., Chen, H., Bates, B., Hung, M., and Hauser, C. Requirement for neuregulin receptor ErbB2 in neuronal and cardiac development. Nature (Lond.), *378:* 394–398, 1995.

3. Riethmacher, D., Sonnenberg-Riethmacher, E., Brinkmann, V., Yamaai, T., Lewin, G. R., and Birchmeier, C. Severe neuropathies in mice with targeted mutations in the ErbB3 receptor. Nature (Lond.), *389:* 725–730, 1997.

4. Gassmann, M., Casagranda, F., Orioli, D., Simon, H., Lai, C., Klein, R., and Lemke, G. Aberrant neuronal and cardiac development in mice lacking the ErbB4 neuregulin receptor. Nature (Lond.), *378:* 390–394, 1995.

5. Wong, A. J., Ruppert, J. M., Bigner, S. H., Grzeschik, C. H., Humphrey, P. A., Bigner, D. S., and Vogelstein, B. Structural alterations of the epidermal growth factor receptor gene in human gliomas. Proc. Natl. Acad. Sci. USA, *89:* 2965–2969, 1992.

6. Moscatello, D. K., Holgado-Madruga, M., Godwin, A. K., Ramirez, G., Gunn, G., Zoltick, P. W., Biegel, J. A., Hayes, R. L., and Wong, A. J. Frequent expression of a mutant epidermal growth factor receptor in multiple human tumors. Cancer Res., *55:* 5536–5539, 1995.

7. Gorgoulis, V., Aninos, D., Mikou, P., Kanavaros, P., Karameris, A., Joardanoglou, J., Rasidakis, A., Veslemes, M., Ozanne, B., and Spandidos, D. A. Expression of EGF, TGF-α, and EGFR in squamous cell lung carcinoma. Anticancer Res., *12:* 1183–1187, 1992.

8. Hynes, N. E., and Stern, D. F. The biology of ErbB-2/Neu/HER-2 and its role in cancer. Biochem. Biophys. Acta, *1198:* 165–184, 1994.

9. Kraus, M. H., Issing, W., Miki, T., Popescu, N. C., and Aaronson, S. A. Isolation and characterization of ERBB3, a third member of the ERBB/epidermal growth factor receptor family: evidence for overexpression in a subset of human mammary tumors. Proc. Natl. Acad. Sci. USA, *86:* 9193–9197, 1989.

10. Sanidas, E. E., Filipe, M. I., Linehean, J., Lemoine, N. R., Gullick, W. J., Rajkumar, T., and Levinson, D. A. Expression of the c-ErbB-3 gene product in gastric cancer. Int. J. Cancer, *54:* 935–940, 1993.

11. Haugen, D. R., Akslen, L. A., Varhaug, J. E., and Lillehaug, J. R. Expression of c-erbB-3 and c-erbB-4 proteins in papillary thyroid carcinomas. Cancer Res., *56:* 1184–1188, 1996.

12. Kew, T. Y., Bell, J. A., Pinder, S. E., Denley, H., Srinivasan, R., Gullick, W. J., Nicholson, R. I., Blamey, R. W., and Ellis, I. O. c-ErbB-4 protein expression in human breast cancer. Br. J. Cancer, *82:* 1163–1170, 2000.

13. Kato, T. Expression of mRNA for heregulin and its receptor, ErbB-3 and ErbB-4, in human upper gastrointestinal mucosa. Life Sci., *63:* 553–564, 1998.

14. Bacus, S. S, Zelnick, C. R., Plowman, G., and Yarden, Y. Expression of the ErbB-2 family of growth factor receptors and their ligands in breast cancer: implications for tumor biology and clinical behavior. Am. J. Clin. Pathol., *102:* S13–S24, 1994.

15. Gilbertson, R. J., Perry, R. H., Kelly, P. J., Pearson, A. D. J., and Lunec, J. Prognostic significance of HER2 and HER4 coexpression in childhood medulloblastoma. Cancer Res., *57:* 3272–3280, 1997.

16. Knowlden, J. M., Gee, J. W., Seery, L. T., Farrow, L., Gullick, W. J., Ellis, I. O., Blamey, R. W., Robertson, J. R., and Nicholson, R. I. c-ErbB3 and c-ErbB4 expression is a feature of the endocrine responsive phenotype in clinical cancer. Oncogene, *17:* 1949–1957, 1998.

17. Bacus, S. S., Chin, D., Yarden, Y., Zelnick, C. R., and Stern, D. F. Type 1 receptor tyrosine kinases are differentially phosphorylated in mammary carcinoma and differentially associated with steroid receptors. Am. J. Pathol., *148:* 549–558, 1996.

18. Borg. A., Tandon, A. K., Sigurdsson, H., Clark, G. M., Ferno, M., Fuqua, S. A. W., Killander, D., and McGuire, W. L. HER-2/neu amplification predicts poor survival in node-positive breast cancer. Cancer Res., *50:* 4332–4337, 1990.

19. Srinivasan, R., Poulsom, R., Hurst, H. C., and Gullick, W. J. Expression of the c-erbB4/HER4 protein and mRNA in normal human fetal and adult tissues and in a survey of nine solid tumor types. J. Pathol., *185:* 236–245, 1998.

20. Riese, D. J., II, Bermingham, Y., van Raaij, T. M., Buckley, S., Plowman, G. D., and Stern, D. F. Betacellulin activates the epidermal growth factor receptor and erbB-4 and induces cellular response patterns distinct from those stimulated by epidermal growth factor or neuregulin-β. Oncogene, *12:* 345–353, 1996.

21. Riese, D. J., II, Komurasaki, T., Plowman, G. D., and Stern, D. F. Activation of ErbB4 by the bifunctional epidermal growth factor family hormone epiregulin is regulated by ErbB2*. J. Biol. Chem., *273:* 11288–11294, 1998.

22. Alroy, I., and Yarden, Y. The ErbB signaling network in embryogenesis and oncogenesis: signal diversification through combinatorial ligand-receptor interactions. FEBS Lett., *410:* 83–86, 1997.

23. Riese, D. J., II, and Stern, D. F. Specificity within the EGF family/ErbB receptor family signaling network. Bioessays, *20:* 41–48, 1998.

24. Stern, D. F., and Kamps, M. EGF-stimulated tyrosine phosphorylation of p185neu: a potential model for receptor interactions. EMBO J., *7:* 995–1001, 1988.

25. Riese, D. J., II, Kim, E. D., Elenius, K., Buckley, S., Klagsbrun, M., Plowman, G. D., and Stern, D. F. The epidermal growth factor receptor couples transforming growth factor-α, heparin-binding epidermal growth factor-like factor, and amphiregulin to Neu, ErbB-3, and ErbB-4. J. Biol. Chem., *271:* 20047–20052, 1996.

26. Riese, D. J., II, Van Raaij, T. M., Plowman, G. D., Andrews, G. C., and Stern, D. F. The cellular response to neuregulins is governed by complex interactions of the erbB receptor family. Mol. Cell. Biol., *15:* 5770–5776, 1995.

27. Moriki, T., Maruyama, H., and Maruyama, I. N. Activation of preformed EGF receptor dimers by ligand-induced rotation of the transmembrane domain. J. Mol. Biol., *311:* 1011–1025, 2001.

28. Burke, C. L., and Stern, D. F. Activation of Neu (ErbB-2) mediated by disulfide bond-induced dimerization reveals a receptor tyrosine kinase dimer interface. Mol. Cell. Biol., *18:* 5371–5379, 1998.

29. d'Avis, P. Y., Robertson, S. C., Meyer, A. N., Bardwell, W. M., Webster, M. K., and Donoghue, D. J. Constitutive activation of fibroblast growth factor receptor 3 by mutations responsible for the lethal skeletal dysplasia thanatophoric dysplasia type I. Cell Growth Differ., *9:* 71–78, 1998.

30. Galvin, B. D., Hart, K. C., Meyer, A. N., Webster, M. K., and Donoghue, D. J. Constitutive receptor activation by Crouzon syndrome mutations in fibroblasts growth factor receptor (FGFR) 2 and FGFR2/Neu chimeras. Proc. Natl. Acad. Sci. USA, *93:* 7894–7899, 1996.

31. Cohen, B. D., Green, J. M., Foy, L., and Fell, H. P. HER4 mediated biological and biochemical properties in NIH 3T3 cells. J. Biol. Chem., *271:* 4813–4818, 1996.

32. Cohen, B. D., Kiener, P. A., Green, J. M., Foy, L., Perry Fell, H., and Zhang, K. The relationship between human epidermal growth-like factor receptor expression and cellular transformation in NIH3T3 cells. J. Biol. Chem., *271:* 30897–30903, 1996.

33. Zang, K., Sun, J., Liu, N., Wen, D., Chang, D., Thomason, A., and Yoshinaga, S. K. Transformation of NIH3T3 cells by HER3 or HER4 receptors requires the presence of HER1 or HER2*. J. Biol. Chem., *271:* 3884–3890, 1996.

34. DiGiovanna, M. P., and Stern, D. F. Activation state-specific monoclonal antibody detects tyrosine phosphorylated $p185^{neu/erbB2}$ in a subset of human breast tumors overexpressing this receptor. Cancer Res., *55:* 1946–1955, 1995.

35. Peles, E., Bacus, S. S., Koski, R. A., Lu, H. S., Wen, D., Ogden, S. G., Ben Levy, R., and Yarden, Y. Isolation of the Neu/HER-2 stimulatory ligand: a 44 Kd glycoprotein that induces differentiation of mammary tumor cells. Cell, *69:* 205–216, 1992.

36. Jones, F. E., Jerry, D. J., Guarino, B. C., Andrews, G. C., and Stern, D. F. Heregulin induces *in vivo* proliferation and differentiation of mammary epithelium into secretory lobuloalveoli. Cell Growth Differ., *7:* 1031–1038, 1996.

37. Sartor, C. I., Zhou, H., Kozlowska, E., Guttridge, K., Kawata, E., Caskey, L., Harrelson, J., Hynes, N., Ethier, S., Calvo, B., and Earp, H. S., III. HER4 mediates ligand-dependent antiproliferative and differentiation responses in human breast cancer cells. Mol. Cell. Biol., *21:* 4265–4275, 2001.

38. Dankort, D. L., Wang, Z., Blackmore, V., Moran, M. F., and Muller, W. J. Distinct tyrosine autophosphorylation sites negatively and positively modulate Neu-mediated transformation. Mol. Cell. Biol., *17:* 5410–5425, 1997.

39. Drummond-Barbosa, D., Vaillancourt, R. R., Kazlauskas, A., and DiMaio, D. Ligand-independent activation of the platelet-derived growth factor β receptor: requirements for bovine papillomavirus E5-induced mitogenic signaling. Mol. Cell. Biol., *15:* 2570–2581, 1995.

40. Sweeney, C., Lai, C., Riese, D. J., II, Diamonti, A. J., Cantley, L. C., and Carraway, K. L., III. Ligand discrimination in signaling through an ErbB4 receptor homodimer. J. Biol. Chem., *275:* 19803–19807, 2000.

41. Miller, D. A., and Rosman, G. J. Improved retroviral vectors for gene transfer and expression. BioTechniques, *7:* 980–990, 1989.

42. Petti, L. M., and Ray, F. A. Transformation of mortal human fibroblasts and activation of a growth inhibitory pathway by the bovine papillomavirus E5 oncoprotein. Cell Growth Differ., *11:* 395–408, 2000.

43. Sambrook, J., and Russell, D. W. Molecular Cloning: A Laboratory Manual, pp. 1.31–1.170. Cold Spring Harbor, NY: Cold Spring Harbor Laboratory, 2001.

44. Leptak, C., Ramon y Cajal, S., Kulke, R., Horwitz, B. H., Riese, D. J., II, Dotto, G. P., and DiMaio, D. Tumorigenic transformation of murine keratinocytes by the *E5* genes of bovine papillomavirus type I and human papillomavirus type 16. J. Virol., *65:* 7078–7083, 1991.

45. Riese, D. J., II, and DiMaio, D. An intact PDGF signaling pathway is required for efficient growth transformation of mouse C127 cells by the bovine papillomavirus E5 protein. Oncogene, *10:* 1431–1439, 1999.

46. Mann, R., Mulligan, R. C., and Baltimore, D. Construction of a retrovirus packaging mutant and its use to produce helper-free defective retrovirus. Cell, *33:* 153–159, 1983.

47. Miller, D. A., and Buttimore, C. Redesign of retrovirus packaging cell lines to avoid recombination leading to helper virus production. Mol. Cell. Biol., *6:* 2895–2902, 1986.

48. Bradford, M. A rapid and sensitive method for the quantification of microgram quantities of protein utilizing the principle of protein dye-binding. Anal. Biochem., *72:* 248–254, 1976.

49. Petti, L., Nilson, L. A., and DiMaio, D. Activation of the platelet-derived growth factor receptor by the bovine papillomavirus E5 transforming protein. EMBO J., *10:* 845–855, 1991.

50. Hwang, E., Riese, D. J., II, Settleman, J., Nilson, L. A., Honig, J., Flynn, S., and Dimaio, D. Inhibition of cervical carcinoma cell line proliferation by the introduction of a bovine papillomavirus regulatory gene. J. Virol., *67:* 3720–3729, 1993.